

Four Generations of High-Dimensional Neural Network Potentials

Jörg Behler*

Cite This: <https://doi.org/10.1021/acs.chemrev.0c00868>

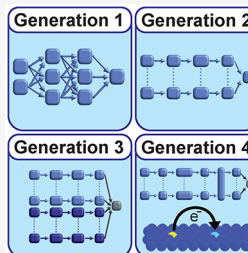
Read Online

ACCESS |

Metrics & More

Article Recommendations

ABSTRACT: Since their introduction about 25 years ago, machine learning (ML) potentials have become an important tool in the field of atomistic simulations. After the initial decade, in which neural networks were successfully used to construct potentials for rather small molecular systems, the development of high-dimensional neural network potentials (HDNNPs) in 2007 opened the way for the application of ML potentials in simulations of large systems containing thousands of atoms. To date, many other types of ML potentials have been proposed continuously increasing the range of problems that can be studied. In this review, the methodology of the family of HDNNPs including new recent developments will be discussed using a classification scheme into four generations of potentials, which is also applicable to many other types of ML potentials. The first generation is formed by early neural network potentials designed for low-dimensional systems. High-dimensional neural network potentials established the second generation and are based on three key steps: first, the expression of the total energy as a sum of environment-dependent atomic energy contributions; second, the description of the atomic environments by atom-centered symmetry functions as descriptors fulfilling the requirements of rotational, translational, and permutation invariance; and third, the iterative construction of the reference electronic structure data sets by active learning. In third-generation HDNNPs, in addition, long-range interactions are included employing environment-dependent partial charges expressed by atomic neural networks. In fourth-generation HDNNPs, which are just emerging, in addition, nonlocal phenomena such as long-range charge transfer can be included. The applicability and remaining limitations of HDNNPs are discussed along with an outlook at possible future developments.



CONTENTS

1. Introduction	A
2. First-Generation Neural Network Potentials	C
3. Second-Generation Neural Network Potentials	E
3.1. General Structure and Energy Expression	E
3.2. The Challenge of the Descriptor	F
3.3. Atom-Centered Symmetry Functions	H
3.4. Discussion of ACSFs	J
3.5. Forces and Stress	L
4. Third-Generation Neural Network Potentials	M
4.1. Structure and Energy Expression	M
4.2. Electrostatic Forces	N
5. Fourth-Generation Neural Network Potentials	O
5.1. The Challenge of Nonlocality	O
5.2. The CENT Approach	Q
5.3. Becke Population Neural Networks	R
5.4. 4G-HDNNPs	S
6. Construction of High-Dimensional Neural Network Potentials	T
6.1. General Strategy	T
6.2. Construction of the Reference Data Set	T
6.3. Training	U
6.4. Validation	V
7. Discussion	Y
7.1. Applicability and Applications	Y
7.2. Outlook	AA
8. Summary	AB

Author Information

Corresponding Author	AB
Notes	AB
Biography	AB
Acknowledgments	AB
Abbreviations	AB
References	AB

1. INTRODUCTION

Computer simulations are becoming increasingly important in chemistry and materials science and are about to reach eye-level with experiment. This poses severe challenges to theory as the systems are becoming more and more complex in terms of system size, composition, and quantities of interest. Consequently, a compromise has to be found taking into account the chosen model systems, target properties, and the affordable accuracy as illustrated in Figure 1 for the example of water and aqueous systems.

Special Issue: Machine Learning at the Atomic Scale

Received: August 14, 2020

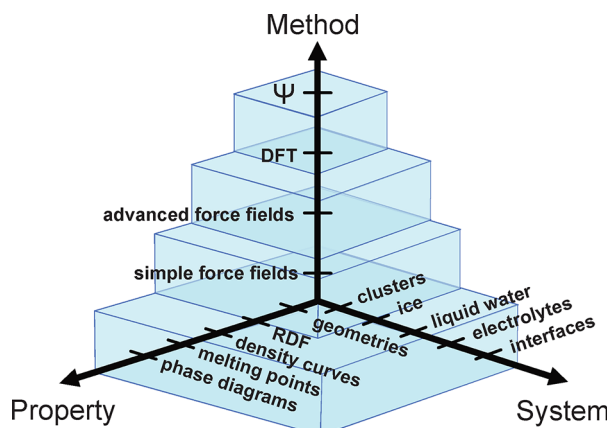


Figure 1. Pyramid of potentials for atomistic simulations illustrated for the example of water and aqueous systems. Using high-level wave function-based methods as represented by Ψ only the geometries of small systems such as water clusters in vacuum are accessible, while density-functional theory (DFT) is the standard method to determine simple properties such as radial distribution functions (RDF) of liquid water in ab initio molecular dynamics simulations. Very large-scale simulations of complex systems such as electrolytes or solid–liquid interfaces, or the determination of complex thermodynamic properties, can only be carried out using atomistic potentials such as force fields. Also machine learning potentials allow the study of these systems.

A key step in computer simulations is the determination of the potential energies and forces of given atomic configurations. While electronic structure methods are the best and obvious choice for systems of moderate size, the costs quickly become prohibitive. Hence, even if efficient methods such as density-functional theory (DFT) are used, which are at the heart of ab initio molecular dynamics (MD) simulations,¹ most questions cannot directly be answered using first-principle methods.

A possible solution to this problem is offered by atomistic potentials, which avoid solving the Schrödinger equation explicitly by providing a direct functional relation between the atomic positions and the potential energy. The resulting multidimensional potential energy surface (PES) can be evaluated with little effort enabling the simulation of complex systems on extended time scales.

There is a long list of requirements that should be met by atomistic potentials, making the construction very challenging. They should be very accurate, efficient to evaluate, generally applicable to many types of systems, transferable between different chemical situations, easy to construct, to validate, and to improve, and they should be able to describe the making and breaking of bonds.

Two main approaches can be distinguished to construct atomistic potentials, depending on if they rely on physical approximations or on purely mathematical fitting procedures. To date, physical potentials, which necessarily have a limited accuracy but often show a very good transferability, have dominated the literature, and countless potentials of very different form and complexity have been proposed. Typical examples range from simple classical force fields in the realms of organic molecules and biochemistry,^{2–6} via reactive empirical potentials used in materials science^{7–12} to approximate electronic structure methods, which even include basic quantum mechanical concepts.^{13–17}

Mathematical potentials, which are constructed by fitting very general functional forms to high-level electronic structure data and aim for the highest possible numerical accuracy, have an equally long history. However, high-dimensional systems have remained a substantial challenge for this class of potentials for a long time, although methods such as splines,¹⁸ Taylor expansions,^{19,20} and the combination of simple functions by genetic programming²¹ have been applied with great success to low-dimensional systems. With the advent of modern machine learning (ML) methods,^{22–24} new players have entered the stage, which in recent years have revolutionized the construction of mathematical potentials and substantially extended their applicability.

ML methods are nowadays routinely used in many fields of chemistry, physics, and materials science.^{25–29} Starting with the seminal work of Doren and co-workers published in 1995,³⁰ they became a tool for the construction of atomistic potentials by exploiting their capabilities to approximate unknown functions, and many reviews can be found in the literature on ML potentials and their applications in computer simulations.^{31–43}

A ML potential may be defined by the following three criteria:

1. A ML potential is an analytic expression of the potential-energy surface providing the potential energy and its analytic derivatives as a function of the atomic positions using a ML algorithm.
2. A ML potential is constructed using a consistent set of reference electronic structure data.
3. A ML potential does not contain any ad hoc assumptions about the functional form apart from the approximations implicitly included in the chosen reference electronic structure method.

In recent years an increasing number of ML potentials has been published, including a variety of neural network potentials (NNPs),^{30,44–56} Gaussian approximation potentials (GAP),^{57,58} moment tensor potentials (MTP),⁵⁹ spectral neighbor analysis potentials (SNAP),^{60,61} atomic cluster expansion,⁶² graph networks,⁶³ kernel ridge regression methods,⁶⁴ gradient-domain machine learning (GDML),^{65,66} support vector machines (SVM)⁶⁷ and many others.

Most of today's ML potentials are applicable to high-dimensional systems, but it should be noted that the term "high-dimensional" is used in very different meanings throughout the literature. Here, we will refer to a ML potential as being high-dimensional, if the following criteria apply:⁴⁰

- The ML potential should be applicable to a very large numbers of atoms, typically in the order of tens of thousands, while fulfilling the required translational, rotational, and permutational invariances of the PES exactly.
- The ML potential should explicitly depend on all degrees of freedom of the system.

Obviously, other equally valid definitions are possible, and irrespective of the specific definition high-dimensional ML potentials are also applicable if certain degrees of freedom are frozen.

There are numerous border cases, which may or may not be considered as ML potentials, because they meet these criteria at least to some extent. An example is permutation invariant polynomials, which have been used very successfully for the construction of accurate PESs of low-dimensional molecular

systems for about 15 years.^{68,69} They share many important challenges with current ML potentials, and the invariance of the PES with respect to the permutation of chemically equivalent atoms, which has plagued first-generation ML potentials for many years, has first been solved in a very general way for permutation invariant polynomials. For high-dimensional condensed systems the situation is less ambiguous since in this field mathematical potentials nowadays typically rely on well-established machine learning methods such as neural networks (NN) or kernel ridge regression (KRR), which allow performing simulations of very large numbers of atoms.

The use of ML methods for the construction of interatomic potentials offers many advantages. Their nonlinear functional form is very general and flexible allowing a very accurate representation of reference data from electronic structure calculations; they are very efficient and can be computed many orders of magnitude faster than even relatively fast electronic structure methods such as DFT; and they do not require any knowledge or approximations concerning the functional form such that all types of atomic interactions can be described without bias at the same level of accuracy. For instance, for the case of feed-forward neural networks, it has been proven independently by several groups that they are universal approximators being able to approximate any multidimensional real-valued function—such as PESs—with in principle arbitrary accuracy.^{70–72}

In this review the family of high-dimensional neural network potentials (HDNNPs) originating from the first HDNNP proposed by Behler and Parrinello in 2007,^{50,73,74} recent extensions of this method, and related approaches will be discussed with a focus on the underlying methodology. Applications for specific systems will be mentioned in passing. The discussion will be guided by the introduction of a classification scheme for neural network potentials into four generations (see Figure 2), which is also applicable to many other types of ML potentials. First-generation NNPs were

mainly published in the early years. They have in common that they only depend on a few degrees of freedom, making them a useful tool for low-dimensional systems. The first high-dimensional ML potentials that became available are the HDNNPs proposed by Behler and Parrinello,⁵⁰ which are an example for the second generation. In these potentials the energy is constructed as a sum of environment-dependent atomic energy contributions. The environments are described by atom-centered symmetry functions,^{50,75} and the introduction of this type of descriptor enabled for the first time meeting the requirements of translational, rotational, and permutation invariance for many-atom systems of arbitrary size. Nowadays, a large variety of alternative descriptors is available. The third generation of HDNNPs includes long-range interactions—mainly electrostatics—beyond the local chemical environments but depending on local charges. HDNNPs of the fourth generation are also able to describe long-range charge transfer, which, for instance, can be achieved by global charge equilibration techniques.

Apart from this classification, the main steps of constructing HDNNPs will be discussed, which involve the selection of the reference structures, the training of the neural network parameters, and the validation of the potentials. After briefly mentioning a list of typical applications and addressing the accuracy that can be expected, the review concludes with some outlook on possible future developments and remaining challenges.

2. FIRST-GENERATION NEURAL NETWORK POTENTIALS

The first attempt to develop a ML potential energy surface was reported by Sumpter and Noid in 1992 for macromolecules employing a neural network trained on vibrational spectra derived from model force fields.⁷⁶ The birth of modern machine learning potentials, which are based on electronic structure calculations meeting the definition given in the introduction, is the seminal work published by Doren and co-workers in 1995.³⁰ This paper, which describes the first DFT-based ML PES for the example of H₂ adsorption at a model of the Si(100) surface, contains a detailed analysis of the advantages and challenges of using neural networks for the representation of potential-energy surfaces. Many solutions are presented in this work, which remain valid until today. This first ML potential made use of a feed-forward neural network (FFNN) as its central component, which is the common feature of essentially all first-generation NNPs developed by several groups in the following years. Most of these early NNPs have a very simple form and use only one FFNN for the description of the global potential energy of the system. Still, also more sophisticated NNPs have been proposed.^{77–80} It is interesting to note that this first generation of NNPs is equivalent to the first generation of ML potentials in general, as until the emergence of Gaussian approximation potentials in 2010⁵⁷ the field has been completely dominated by neural networks, while only in the past decade has an increasing variety of ML techniques found use in the field of PES representation.

The structure of a FFNN is shown in Figure 3 for a PES depending on two input coordinates G₁ and G₂ corresponding to the neurons—or nodes—of the input layer. The node in the output layer yields the potential energy E of the system as a function of these coordinate values. In between the input and the output layer there are one or more hidden layers, and the

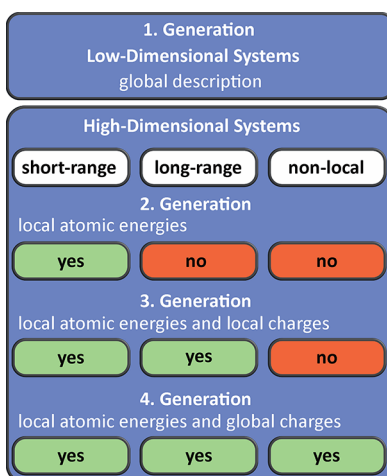


Figure 2. Overview of the four generations of neural network potentials discussed in this review. While first-generation NNPs are only applicable to low-dimensional systems, high-dimensional systems containing a large number of atoms can be described by potentials of the second and subsequent generations. Second-generation HDNNPs are based on environment-dependent atomic energies. Long-range electrostatic interactions are included in third-generation HDNNPs using local charges, while fourth-generation HDNNPs take the global charge distribution including nonlocal charge transfer into account.

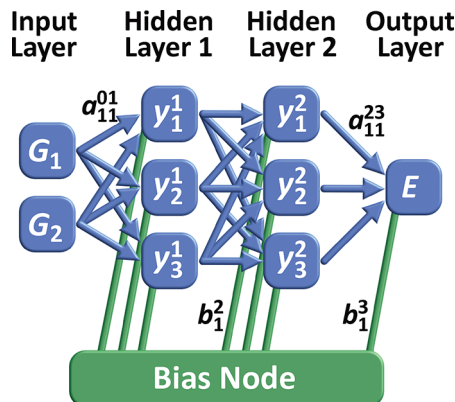


Figure 3. Structure of a small feed-forward neural network. For this two-dimensional system, the output energy E is a function of the two input coordinates G_1 and G_2 . The values y_i^k of the neurons i in layer k and E depend on the connecting weights a_{ij}^{kl} and the bias weights b_i^k . An explanation of the corresponding analytic functional form (eq 1) is given in the text.

nodes of these layers have no physical meaning but provide the functional flexibility of the neural network. The more hidden layers and neurons per layer are used, the higher is the fitting capability of the FFNN for complicated functions. As represented by the arrows in Figure 3, each neuron in each layer is connected to the neurons in the neighboring layers by weights, which are the fitting parameters of the FFNN. Here we use the notation that weight a_{ij}^{kl} is connecting neuron i in layer k with neuron j in layer $l = k + 1$. The layers are numbered such that the input layer has index 0, followed by the N_{hid} hidden layers, and the output layer having the index $N_{\text{hid}} + 1$. Further, there is a bias node connected to each node in the hidden layers and to the output node, which provides an input value of 1 that is scaled by the bias weight b_i^j targeting at node i in layer j . Like the connecting weights also the bias weights are optimized during the training of the NN. The purpose of the bias node is to act as an adjustable offset for each neuron in the FFNN, which is numerically advantageous with respect to the application of the nonlinear activation functions.

The analytic functional form of the FFNN is defined by its architecture, that is, the number of hidden layers and nodes, which can be different for each layer. For the small example FFNN shown in Figure 3 the analytic energy expression is given by

$$E = f_1^3 \left(b_1^3 + \sum_{l=1}^3 a_{l1}^{23} f_l^2 \left(b_l^2 + \sum_{k=1}^3 a_{kl}^{12} f_k^1 \left(b_k^1 + \sum_{j=1}^2 a_{jk}^{01} G_j \right) \right) \right) \quad (1)$$

In this nested function, first a linear combination of the two input coordinates is computed at each neuron k of the first hidden layer using the connecting weights a_{jk}^{01} as coefficients. The result is then shifted by the respective bias weight b_k^1 . Afterward, a nonlinear activation function f_k^1 is applied to each shifted sum, which makes the FFNN a nonlinear model allowing to represent arbitrary functions. Different types of differentiable activation functions can be used for constructing

PESs, as long as they have a nonlinear region and saturate for very large positive and negative arguments. Frequently used examples are the hyperbolic tangent, the sigmoid function, the softplus function, and Gaussians. The only exception is the output node since the typical nonlinear activation functions would restrict the range of possible output energies; therefore, as the activation function in the output neuron, typically the linear function $f(x) = x$ is used. There are other popular activation functions that are frequently used in neural networks in other contexts such as classification problems, but some of these functions, like the rectified linear unit (ReLU) activation function,⁸¹ which have a discontinuity in the derivative at the origin, can be very problematic for the representation of continuous functions such as PESs.

After applying the activation function, a number y_i^1 is obtained for each neuron in the first hidden layer. Starting from this layer, the values in the second layer are then calculated in the same way and so on until the output node $E = y_1^3$ is reached. This unidirectional flow of information is the reason for the name feed-forward NN. The output energy of the FFNN depends on the numerical values of the connecting and bias weight parameters, which are determined in a training process using a known reference data set as described in section 6.3.

FFNNs of this form offer many advantages for the construction of PESs: they are very flexible with a large number of fitting parameters, which allows the very accurate representation of the potential energy as a function of the atomic positions. No knowledge about the underlying physical principles is required and all types of bonding can be described on an equal footing. The simple functional form enables the calculation of analytic derivatives, which are required for the computation of analytic forces but also for the gradient-based optimization of the weight parameters. Energies and forces can be calculated many orders of magnitude faster compared to even efficient electronic structure methods such as DFT. Finally, for appropriately chosen types of input coordinates NNPs are reactive, because, in contrast to simple classical force fields, no specification of predefined chemical bonds or different atom types for a given chemical element is required.

Still, there are also important limitations, which prevented the early breakthrough of first-generation NNPs and applications to systems containing more than a few atoms. First, the size of the FFNN cannot be arbitrarily increased to adapt to the dimensionality of larger and larger systems, as the method becomes computationally more demanding and the training and sampling of large configuration spaces is a formidable challenge. Second, suitable input coordinates, which incorporate the translational, rotational, and permutational invariances of the PES, have not been available in the first decade. Finally, the use of a single FFNN does not allow us to apply the NNP to systems containing variable numbers of atoms, as the dimensionality of the input coordinate vector of a FFNN has to remain fixed and is thus restricted to the same dimensionality as used in the training process. Moreover, a simultaneous training to different system sizes is a difficult task, although solutions involving FFNNs of variable size have been proposed.^{79,80}

Despite these limitations, first-generation NNPs have been used with great success for the construction of a wide range of low-dimensional systems such as small molecules,^{49,82–86} reactive molecular systems,^{87–91} and the interaction of small molecules with metal surfaces,^{30,44,45,92–101} which have been

kept frozen to reduce the dimensionality of the system to a tractable size. A comprehensive list of applications of first-generation NNPs is given in some early reviews,^{39,40} and also a review in this issue is dedicated to more recent developments addressing the accurate representation of small molecules and molecular reactions.¹⁰²

Motivated by these limitations, steady progress has been made in the first years, and numerous suggestions have been made to extend the applicability of first-generation NNPs to more complex systems. Examples are the description of polarization in water¹⁰³ and electrolytes⁴⁶ in the form of additive terms that allow simulations of larger systems in the spirit of classical force fields; the use of variable-size NNs to deal with systems containing different numbers of atoms;^{79,80,104,105} many-body expansions using multiple NNs;⁷⁸ transformed coordinates for molecular systems employing a high-dimensional model representation;^{48,77} and the introduction of symmetry-adapted coordinates with exact permutation invariance and incorporation of the surface symmetry for molecules interacting with frozen surfaces.⁹⁵ The details of these developments, which led to significant insights and progress for specific systems, have been reviewed in detail elsewhere.⁴⁰

In summary, the first generation of NNPs is characterized by the use of feed-forward neural networks, and in most cases only a single FFNN has been used to describe the global PES of the system. Still, there are exceptions of more sophisticated combinations of several NNs. The most important common feature is the restriction of these early NNPs to low-dimensional systems of small molecules in the gas phase or small molecules interacting with frozen metal surfaces. Addressing larger systems in full dimensionality, as needed for applications in materials science or other condensed systems such as aqueous solutions, has been prevented by several technical limitations such as the growing complexity of NNs with the number of atoms, the need to use a fixed dimensionality of the vectors serving as inputs for the NNs, which did not allow the construction of NNPs for systems containing variable numbers of atoms, and the lack of generally applicable descriptors with the required properties of translational, rotational, and permutational, that is, atom-index, invariance. Consequently, in the first decade the use of ML potentials has remained a niche application with only a few pioneering groups working in the field.

3. SECOND-GENERATION NEURAL NETWORK POTENTIALS

3.1. General Structure and Energy Expression

The restriction of NNPs to low-dimensional systems has been a major obstacle preventing the application of ML potentials to complex systems. This limitation could finally be overcome by three steps, which are (1) the assumption that a large part of the atomic interactions can be described by interactions of the atoms with their local chemical environments, (2) a new type of descriptor with exact translational, rotational and permutation invariance, and (3) the use of active learning for the construction of the training set in high-dimensional configuration spaces.

The first key step has been abandoning the use of a single neural network for the global PES and exploiting the locality of a large part of the atomic interaction energies, which works surprisingly well for many systems. This locality approximation

was introduced into ML potentials by Behler and Parrinello in 2007,⁵⁰ and since then it also had become the basis of many other modern machine learning approaches developed in the following years. Accordingly, the potential energy can be written as a sum of atomic energy contributions E_j^i

$$E_{\text{short}} = \sum_{i=1}^{N_{\text{elem}}} \sum_{j=1}^{N_{\text{atom}}^i} E_j^i \quad (2)$$

where N_{elem} is the number of elements present in the system, and N_{atom}^i is the number of atoms of the respective element. The term “short-range energy” refers to all interactions between atoms closer to each other than a cutoff radius R_c , irrespective of the physical nature of the interactions. The cutoff radius represents a convergence parameter that in principle has to be tested for each system to include all energetically relevant interactions needed to reach the desired level of accuracy. Although truncating the atomic interactions beyond the cutoff is in principle a drastic approximation, for many systems it turns out that cutoffs between 6 and 10 Å are a reasonable choice for obtaining reliable potential-energy surfaces reproducing total energies with errors of only a few meV/atom. With such a cutoff radius, which is much larger than comparable cutoffs frequently used in empirical potentials,⁹ not only covalent interactions are well described, but also a substantial part of electrostatics and dispersion interactions up to the cutoff radius is included, since the HDNNP does not *a priori* distinguish these energy contributions. A high accuracy has also been found for metallic systems. This is because the energetic influence of atoms outside the cutoff sphere, which is shown schematically in Figure 4, is often small and on the order of only a few meV/V

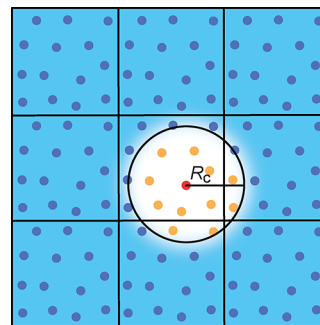


Figure 4. Schematic representation of the cutoff sphere of radius R_c around a central atom displayed in red in a system with periodic boundary conditions. All atoms inside the cutoff sphere, which enter the atomic energy contribution of the central atom, are shown in orange.

atom. However, it should be noted that the magnitude of the acceptable error depends on the physical and chemical questions to be answered. While the making and breaking of chemical bonds involves energy changes, which are several orders of magnitude larger than this error and thus can be very well described, subtle energy differences between different phases of a given system may require additional corrections to improve the accuracy.¹⁰⁶

Once the interacting atoms have been defined by the choice of the cutoff radius, the structural information has to be converted to a suitable input for the NNP. For this purpose, the second key step was the introduction of a new type of

descriptor called atom-centered symmetry functions (ACSF),⁷⁵ which for the first time enabled the construction of ML PESs exactly obeying the conditions of translational, rotational, and permutational invariance of the energy function for arbitrary systems. These descriptors, which provide local structural fingerprints of the atomic environments, will be discussed in detail in the following sections.

The combination of the locality approximation with the ACSF descriptors allows us to use a separate feed-forward atomic neural network for each atom in the system to express the atomic energy contributions. These atomic energies are then added to yield E_{short} as shown for the example of an arbitrary ternary system containing the elements a, b, and c in Figure 5. For each atom there is one line in this scheme

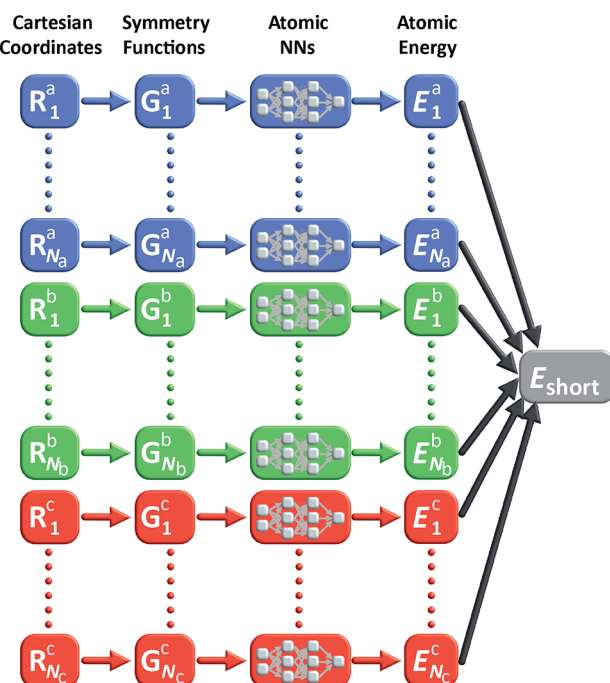


Figure 5. Structure of a second-generation high-dimensional neural network potential as proposed by Behler and Parrinello.⁵⁰ The three colors represent three chemical elements a, b, and c, and the numbers of atoms per element are N_a , N_b , and N_c , respectively. For each atom in the system there is one line. First, the Cartesian coordinate vector R_i^μ is converted to a vector of symmetry function values G_i^μ , which describes the local atomic environment of atom i of element μ . This vector depends on all Cartesian coordinates of all atoms inside the cutoff sphere. This symmetry function vector then serves as input for an atomic neural network yielding the atomic energy contribution E_i^μ . The sum of all atomic energy contributions is the short-range energy E_{short} of the system, which is equal to the total energy in second-generation HDNNPs.

starting with the Cartesian coordinate position vector R_i^μ of atom i and element μ . The Cartesian coordinates are then transformed to a vector of symmetry function values G_i^μ , which depends on the Cartesian coordinates of all neighboring atoms inside the respective atomic cutoff sphere. The atomic symmetry function vector then represents the input for an atomic network, which has the same architecture and weight parameters for all atoms of a given chemical element. This ensures that atoms of the same element are chemically equivalent and that their energy contribution is only a function of the atomic environment.

After training the weight parameters (see section 6.3), the second-generation HDNNP is then applicable to systems containing arbitrary numbers of atoms as for each atom in the system one atomic neural network is included in the scheme of Figure 5. If an atom is added to the system, another atomic NN of the respective element is included—or equivalently the atomic NN of the respective element is evaluated once for each atom of that element in the system—while an atomic NN is deleted if the associated atom is removed. Thus, the restriction of most first-generation NNPs to a system containing a fixed number of atoms is overcome. This not only allows the use of a combination of structures with different numbers of atoms for training the HDNNP, but also allows the application in simulations of much larger systems than were used in the determination of the weight parameters, which is an important advantage of second-generation HDNNPs.

This scheme fulfills the requirement of permutation invariance exactly for two reasons. First, adding the atomic energies is obviously independent of the order of the atoms. Second, and nontrivial, the ACSF input vectors of the atomic NNs must also be invariant with respect to the order of the neighboring atoms, which is discussed in more detail in section 3.3. Since all atomic NNs can be evaluated independently, this NN structure is well suited for efficient parallelization.

Finally, the third key step is the construction of the reference data set needed to train the HDNNPs. In recent years, active learning based on the automatic determination of structures missing in the training set has received a lot of attention. This step will be discussed in section 6.2.

Although in recent years many improvements have been suggested as detailed in the following sections, second-generation HDNNPs of this form nowadays are still among the most frequently used types of ML potentials with numerous successful applications for many different types of systems.

3.2. The Challenge of the Descriptor

Having discussed the total energy expression, we now turn to the second key step in the construction of HDNNPs, which is the choice of the descriptors used as input for the atomic NNs. This step has been central for the success of modern machine learning potentials. In fact, the applicability of first-generation ML potentials was severely limited to systems containing only a few atoms, because in the first decade suitable descriptors were available only for low-dimensional—in most cases molecular—systems.

Nowadays, a large number of descriptors is available, each with its own advantages and disadvantages, like the smooth overlap of atomic positions (SOAP),¹⁰⁷ the Coulomb matrix,⁶⁴ the bispectrum,⁵⁷ overlap matrix-based descriptors,¹⁰⁸ spherical harmonics-based descriptors,¹⁰⁹ orthogonal descriptors,¹¹⁰ the Faber-Christensen-Huang-Lilienfeld (FCHL) descriptors,^{111,112} bag of bonds,¹¹³ smoothed atomic densities,¹¹⁴ the many-body tensor representation (MBTR),¹¹⁵ polynomials in moment tensor potentials,⁵⁹ and many others. An incomplete list of typical descriptors used in this rapidly evolving field is given in Table 1. A discussion of all these descriptors, which have been shown to be very successful, is beyond the scope of this review and some comparisons can be found in the literature.^{107,116–121} We note that apart from their main purpose, i.e., the discrimination of different atomic configurations, the construction of ML potentials may benefit from direct or indirect physical information in the descriptors,

Table 1. List of Some Typical Descriptors Frequently Used in Machine Learning Potentials^a

descriptor	year	ref
atom-centered symmetry functions	2007	50,75
bispectrum	2010	57,60
Coulomb matrix	2012	64
SOAP	2013	107
permutation invariant polynomials	2013	69,90
Ewald sum matrix	2015	122
bag of bonds	2015	113
overlap matrix	2016	108
polynomials in MTPs	2016	59
spherical harmonics	2017	109
Chebyshev polynomials	2017	123
many-body tensor representation	2017	115
histogram of internal coordinates	2017	124
FCHL	2018	112,125
weighted symmetry functions	2018	126
smoothed atomic densities	2019	114
orthogonal descriptors	2019	110
long-distance equivariant repres.	2019	127

^aThe given year refers to the introduction of the descriptor or, in the case of descriptors which have been used in other contexts before, they refer to the first use in machine learning potentials.

for example, nuclear charges in the case of the Coulomb matrix.

Here, we will focus only on atom-centered symmetry functions (ACSFs), which are historically the first type of descriptors that has been developed to enable the construction of high-dimensional ML potentials. The reason is that even more than 10 years after their introduction⁵⁰ ACSFs still represent the dominant descriptor type for the construction of HDNNPs with a large number of applications, while other types of ML potentials often use different types of descriptors with great success. It should be noted that in principle many combinations of descriptors and ML algorithms are possible, and the combinations presently used in the literature are mainly a result of historical developments and not a consequence of the superiority or inferiority of certain descriptors for particular ML algorithms.

The main challenge in developing appropriate descriptors for high-dimensional systems has been the requirement to fulfill the mandatory invariances of the potential energy surface. These are the invariances of the potential energy of a system with respect to translation and rotation as well as to permutation—or more technically “the order”—of chemically equivalent atoms, that is, all atoms of the same chemical element. This general difficulty arises because ML algorithms “just process numbers”, and if the input numbers change, so do the output energies. This is not relevant as long as numerical changes in the input are connected to physically meaningful structural changes in the system, but the absolute values of many common coordinates—first of all Cartesian coordinates—often have no physical meaning. For instance, translating or rotating a rigid molecule in vacuum does not change the relative atomic positions and consequently the energy must remain invariant although the numerical values of the Cartesian coordinates change, rendering a set of Cartesian coordinates inappropriate as input for machine learning potentials. In passing we note here that recent attempts have started to include the description of the systems inside the ML

process itself, which may help to overcome this problem in the future in a general way.^{55,128–130}

A straightforward solution to the problem of translational and rotational invariance in descriptor-based methods would be the use of internal coordinates such as interatomic distances, not to be confused with “bonds”, angles, and dihedral angles, as employed successfully in classical forces fields for a long time. By using internal coordinates, conventional classical force fields fulfill the required invariances in an elegant way.¹³¹ However, this solution has to be taken with a grain of salt as internal coordinates fulfill the third requirement of permutational invariance only in the special but very common case of simple force fields. For instance, the two OH bonds of a water molecule are chemically equivalent, and in force fields the energy contributions of both bonding terms, which are just two-body terms, can simply be added such that the sum is invariant with respect to the order of the terms. For many-body potentials such as ML algorithms, which couple all coordinates in a single functional expression with a well-defined order and different prefactors, this is not the case. For instance, algorithms such as neural networks use vectors of input values, which do not allow for a permutation of the components without changing the predicted energy value.

In first-generation NNPs there have been only two solutions to ensure permutation invariance: Either the input coordinates are symmetrized, which has been proposed for molecular systems⁴⁶ as well as for small molecules interacting with surfaces,⁹⁵ or the symmetry is incorporated directly in the network structure itself.⁷⁹ While the use of symmetrized coordinates is an elegant solution ensuring exact permutation invariance, this approach is restricted to very small systems due to the rapidly growing complexity of the symmetrized terms for more than a few atoms.

It is important to note in this context that the problem of finding suitable coordinates with full permutation invariance has not only plagued early ML potentials but also other advanced potential energy surfaces fitted to high-level electronic structure data. The most important approach to be mentioned in this context is the method of permutation invariant polynomials (PIP) pioneered by Bowman, Braams, and co-workers^{68,132,133} who introduced this powerful method suitable to achieve spectroscopic accuracy for a wide range of small molecules. As interatomic potentials making use of PIPs also have a very general functional form, they represent a border case between mathematical fits and ML potentials. Because of the exact treatment of permutation invariance for small molecules, in recent years PIPs have also found use as input coordinates for first-generation neural network potentials.^{87–90,134,135}

Other important problems preventing the use of internal coordinates for ML potentials of larger systems are the redundancy of the information in complete sets of internal coordinates, which allows for different choices of minimal coordinate sets, and the unfavorable scaling of the number of coordinates with growing system size. While the first problem can be overcome, for example, by simply using a complete distance matrix, distance matrices soon become intractable for larger systems. Further, ML algorithms like neural networks require a constant dimensionality of the input vector, making the use of internal coordinates for variable numbers of atoms very difficult.

3.3. Atom-Centered Symmetry Functions

The solution for these problems has been the introduction of a new class of descriptors called atom-centered symmetry functions in 2007.^{50,75} Initially intended for the use in second-generation HDNNPs, ACSFs describe the positions of atoms in the environment of a given central atom up to a cutoff radius R_c . The use of a cutoff effectively reduces the dimensionality of the atomic environments to the positions of the close atoms enabling the use of the energy expression in eq 2. Further, the restriction to the local atomic environments reduces the computational effort in that for large systems only a subset of the atoms needs to be considered for the calculation of the energy contribution of each atom. If the cutoff is chosen too small, the impact of close atoms outside the cutoff spheres is treated as noise by the NN resulting in less accurate fits, which is a phenomenon that has been already observed when neglecting relevant coordinates in early low-dimensional first-generation NNPs.³⁰ We note that the use of cutoffs was common in conventional empirical potentials for a long time,⁹ and in fact also the bonded terms up to four-body interactions used in classical force fields restrict the range and dimensionality of the atomic interactions.

Many different functional forms can be used to define the cutoff function $f_c(R_{ij})$,^{75,136} where R_{ij} is the distance between the central atom i and a neighbor j , as long as certain criteria are met. The function must be differentiable and decay smoothly to zero in value, slope, and if possible, even higher derivatives at the cutoff radius. This is required to avoid discontinuities in the descriptor values and its derivatives, and consequently in the energy and its gradients, if atoms leave or enter the cutoff spheres in MD simulations. A frequently used cutoff function is the monotonously decaying part of the cosine function⁵⁰ (see Figure 6)

$$f_c(R_{ij}) = \begin{cases} 0.5 \left[\cos\left(\pi \frac{R_{ij}}{R_c}\right) + 1 \right] & \text{for } R_{ij} \leq R_c \\ 0 & \text{for } R_{ij} > R_c \end{cases} \quad (3)$$

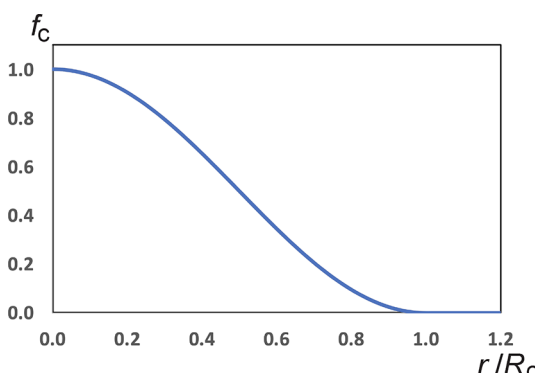


Figure 6. Cutoff function (eq 3) frequently used in atom-centered symmetry functions.⁵⁰

which is similar to the cutoff functions used in the Tersoff potential.¹³⁷ This function has continuous values and slope at the cutoff radius. The function⁷⁵

$$f_c(R_{ij}) = \begin{cases} \tanh^3\left(1 - \frac{R_{ij}}{R_c}\right) & \text{for } R_{ij} \leq R_c \\ 0 & \text{for } R_{ij} > R_c \end{cases} \quad (4)$$

in addition has continuous second derivatives at R_c . Another possible choice is the exponential function¹³⁶

$$f_c(R_{ij}) = \begin{cases} \exp\left(1 - \frac{1}{1 - \left(\frac{R_{ij}}{R_c}\right)^2}\right) & \text{for } R_{ij} \leq R_c \\ 0 & \text{for } R_{ij} > R_c \end{cases} \quad (5)$$

with continuous derivatives up to infinite order at the cutoff radius.

In all these cutoff functions it is also possible to replace the term $\frac{R_{ij}}{R_c}$ by $x = \frac{R_{ij} - R_{c_i}}{R_c - R_{c_i}}$ with $R_{c_i} < R_c$ being an inner cutoff such that

$$f_c(R_{ij}) = \begin{cases} 1 & \text{for } R_{ij} < R_{c_i} \\ f(x) & \text{for } R_{c_i} \leq R_{ij} \leq R_c \\ 0 & \text{for } R_{ij} > R_c \end{cases} \quad (6)$$

The advantage of including an inner cutoff is the possibility of focusing the numerical range of function values to the chemically meaningful range of interatomic distances R_{ij} .

Alternatively, the use of polynomials has been suggested, which are computationally advantageous compared to eqs 3–5.¹³⁶ These are

$$f_c^{\text{poly1}}(x) = x^2(2x - 3) + 1 \quad (7)$$

$$f_c^{\text{poly2}}(x) = x^3(x(15 - 6x) - 10) + 1 \quad (8)$$

$$f_c^{\text{poly3}}(x) = x^4(x(x(20x - 70) + 84) - 35 + 1 \quad (9)$$

$$f_c^{\text{poly4}}(x) = x^5(x(x(x(315 - 70x) - 540) + 420) - 126) + 1 \quad (10)$$

In the next step, the positions of the neighboring atoms inside the cutoff sphere must be described. For this purpose two types of symmetry functions called “radial” and “angular” ACSFs are used. They simultaneously depend on the positions of all neighboring atoms inside the cutoff sphere and thus formally represent many-body functions, although they include a large number of two- and three-body terms, respectively.

For each type a variety of different functional forms is available.^{75,138} These functions have to meet several requirements. First, they need to decay in value for distant neighbors close to the cutoff radius reflecting the decreasing physical interaction, which facilitates the representation by the HDNNP. Moreover, they need to be able to distinguish different structures. Finally, as the number of neighboring atoms inside the cutoff spheres can change in simulations, the number of symmetry functions describing an atomic environment must not depend on the instantaneous atomic coordinations, as this would be incompatible with the fixed input dimensionality of neural networks.

The most commonly used type of radial function consists of a sum of products of Gaussians and cutoff functions for all atoms j inside the cutoff sphere,

$$G_{i,\mu}^{\text{rad}} = \sum_{j \neq i}^{N_{\text{atom}} \in R_c} e^{-\eta(R_{ij}-R_s)^2} f_c(R_{ij}) \quad (11)$$

Using the Gaussian instead of the distance R_{ij} between central atom i and neighbor j together with the cutoff function ensures the required decay to zero in value and slope at the cutoff radius. The summation over the Gaussian functions of all neighboring atoms reduces the information to a single function value independent of the number of atoms inside R_c , which is required for the fixed input vector size of the atomic NNs. Hence, the resulting radial symmetry function value can be interpreted as a continuous coordination number. The parameter η determines the effective spatial extension of the radial function (see Figure 7), while the maximum extension is

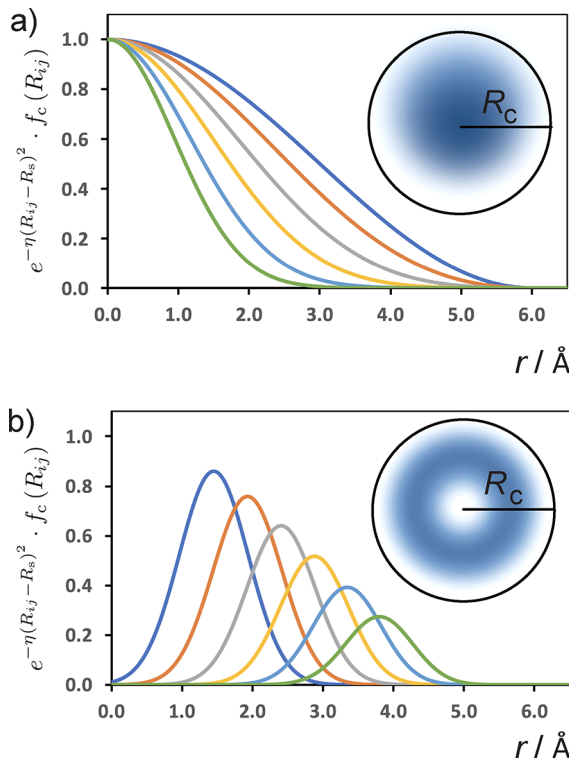


Figure 7. Radial symmetry functions.⁷⁵ The η parameters in panel a have been determined for a cutoff of 6 Å and a minimum interatomic distance of 1 Å to yield approximately equidistant turning points. The values from dark blue to green are $\eta = 0.0, 0.03, 0.08, 0.16, 0.3$, and 0.5 Å^{-2} with $R_s = 0 \text{ Å}$. In panel b, $\eta = 0$ has been used with $R_s = 1.5, 2.0, 2.5, 3.0, 3.5$, and 4.0 Å .

given by the cutoff radius. This is important, as it has been shown that decreasing the cutoff to too short-ranged Gaussians can result in artifacts in the potential and inaccurate forces close to the cutoff radius.⁷⁵ The optional shift parameter R_s can be used to shift the center of the Gaussians to a predefined distance from the central atom to form a diffuse sphere around the central atom such that only neighbors in a certain distance interval are considered. The radial function in eq 11 is plotted in Figure 7 for the unshifted (a) and the shifted (b) case for different values of η and R_s . Using such a set of functions with different parameter values ensures a good radial resolution and

is summarized in the second index μ in eq 11, which is the counting index of the radial function for the central atom i .

As the radial function in eq 11 cannot distinguish between different elements in the neighborhood, for each element combination in the system a separate set of radial functions is constructed such that the number of radial functions of a given central atom scales linearly with the number of elements in the system. Typically between four and eight radial functions are used for each element combination.

There are also alternative radial ACSFs, such as

$$G_{i,\mu}^{\text{rad}} = \sum_{j \neq i}^{N_{\text{atom}} \in R_c} \cos(\kappa R_{ij}) f_c(R_{ij}) \quad (12)$$

with the radial shape defined by parameter κ ; a more detailed discussion can be found in ref 75.

Using only radial functions, it is not possible to distinguish even very different environments such as a tetrahedral coordination and a square planar coordination, if the neighbors are all at the same distance from the central atom. This problem is solved by using in addition angular functions. The most commonly used angular ACSF has the form

$$G_{i,\mu}^{\text{ang}} = 2^{1-\zeta} \sum_{i,j,k} (1 + \lambda \cos \theta_{ijk})^\zeta e^{-\eta(R_{ij}^2 + R_{ik}^2 + R_{jk}^2)} f_c(R_{ij}) f_c(R_{ik}) f_c(R_{jk}) \quad (13)$$

where θ_{ijk} is the angle between the connections of the central atom i with neighbors j and k . In Figure 8 the individual angles

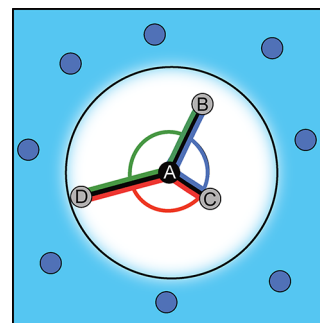


Figure 8. Angular environment of a central atom A. The three angles entering eq 13 are shown in red, blue, and green.

entering eq 13 are shown for a simplified environment consisting of only three atoms of the same element. For the optional Gaussian term, $\eta = 0$ is used in case of small symmetry function sets, but for complex environments several shells of angular functions can be constructed by using different values of η . A set of different ζ exponents is used to achieve angular resolution as shown in the plot of the separated angular terms $2^{1-\zeta}(1 + \lambda \cdot \cos \theta_{ijk})^\zeta$ in Figure 9. The prefactor $2^{1-\zeta}$ is a normalization factor balancing the ranges of values of all angular functions, which is not strictly needed as often the range of values of the symmetry functions is normalized before training. The parameter λ , which can have values of +1 and -1 is used to center the maxima of the cosine terms at $\theta_{ijk} = 0^\circ$ or $\theta_{ijk} = 180^\circ$, respectively (see Figure 9). The symmetry of the angular functions with respect to these angles is required due to the two possible ways of defining the angle, since the θ_{ijk} and $360^\circ - \theta_{ijk}$ must provide the same function value. Using all three pairwise cutoff functions in eq 13 for R_{ij} , R_{ik} , and R_{jk}

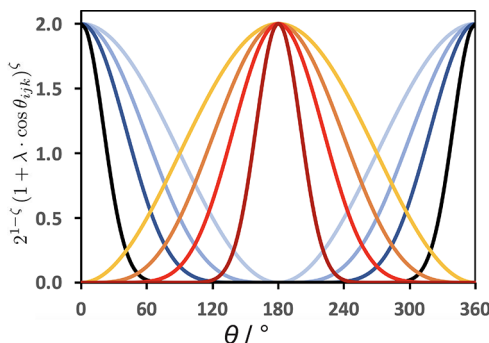


Figure 9. Angular terms $2^{1-\zeta}(1 + \lambda \cos \theta_{ijk})^\zeta$ used in the angular symmetry functions, eq 13. Terms with $\lambda = 1$ are shown in blue to black, terms with $\lambda = -1$ are shown in orange to brown. The employed exponents are $\zeta = 1, 2, 4$, and 16 (from light to dark tones).

ensures that only those terms enter the sum over all angles, in which all three distances are smaller than the cutoff radius. Thus, angular functions of this type contain a substantial number of terms lower than one, which typically results in a smaller range of function values compared to the radial functions. Thus, it is common practice to rescale the range of values for each individual symmetry function to the interval $[0,1]$. Alternatively, also the less restrictive angular function

$$G_{i,\mu}^{\text{ang}} = 2^{1-\zeta} \sum_{i,j,k} (1 + \lambda \cos \theta_{ijk})^\zeta e^{-\eta(R_{ij}^2 + R_{ik}^2)} f_c(R_{ij}) f_c(R_{ik}) \quad (14)$$

can be used, which includes a larger number of angle terms by omitting the restriction of $R_{jk} < R_c$ as shown in Figure 10.

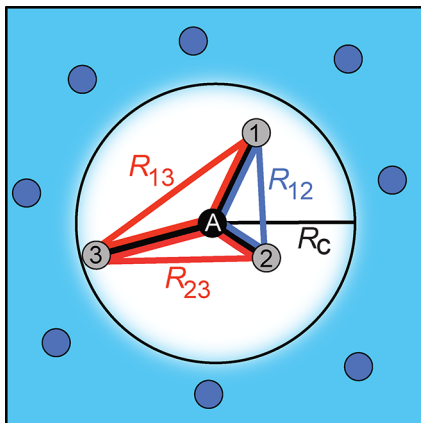


Figure 10. Comparison of the angular terms entering the angular symmetry functions for a local environment containing three atoms of the same element. In the angular function given by eq 14 the red and blue triples of atoms are considered as all gray atoms are inside the cutoff sphere, while the angular function defined by eq 13 only includes the blue triple, since R_{13} and R_{23} are larger than the cutoff radius R_c .

In the ANI-1 second-generation HDNNP,¹³⁹ which is an application of the Behler-Parrinello method to construct general-purpose ML potentials for organic molecular systems with a focus on transferability, a modified type of angular ACSF has been proposed,

$$G_{i,\mu}^{\text{ang}} = 2^{1-\zeta} \sum_{j \neq i} \sum_{k \neq i} (1 + \cos(\theta_{ijk} - \theta_s)^2)^\zeta e^{-\eta((R_j + R_{ik})/2 - R_s)} f_c(R_{ij}) f_c(R_{ik}) \quad (15)$$

which includes radial as well as angular shift parameters, θ_s and R_s , allowing to adapt the peaks of the angular functions to arbitrary values. Its parameters have to be selected carefully to maintain the angular symmetry with respect to 0° and 180° . Recent comparisons of the original ACSFs and the modified forms used in ANI-1 show that both types of functions are equally suited to describe and distinguish atomic environments.¹¹⁷

Finally, it should be mentioned that symmetry functions cannot only be constructed to describe atomic energy contributions as a function of the atomic environment according to eq 2, but also “pair symmetry” functions (PSF) have been suggested, which characterize the geometric environments of pairs of atoms in a similar way^{140,141} using the energy expression

$$E_{\text{short,pair}} = \frac{1}{2} \sum_{i=1}^{N_{\text{atom}}} \sum_{j \neq i}^{N_{\text{atom}}} E_{ij} \quad (16)$$

An example¹⁴⁰ for a radial PSF taking into account the environments of both atoms i and j in the pair, which is defined by all atoms k being at least in the cutoff sphere of atom i or j , is the simple function

$$G_{ij,\mu}^{\text{pair,rad}} = f_c(R_{ij}) \left[\sum_{k=1}^{N_{\text{atom}} \in R_c} f_c(R_{ik}) + \sum_{k=1}^{N_{\text{atom}} \in R_c} f_c(R_{jk}) \right] \quad (17)$$

Here, depending on its position, each atom k can thus contribute to one or to both cutoff terms $f_c(R_{ik})$ and $f_c(R_{jk})$ centered at atoms i and j , respectively. Extensions can be made in analogy to eq 11 by including a Gaussian term yielding

$$G_{ij,\mu}^{\text{pair,rad}} = f_c(R_{ij}) e^{-\eta R_{ij}^2} \left[\sum_{k=1}^{N_{\text{atom}} \in R_c} f_c(R_{ik}) e^{-\eta R_{ik}^2} + \sum_{k=1}^{N_{\text{atom}} \in R_c} f_c(R_{jk}) e^{-\eta R_{jk}^2} \right] \quad (18)$$

Also angular PSFs such as

$$G_{ij,\mu}^{\text{pair,ang}} = f_c(R_{ij}) e^{-\eta R_{ij}^2} 2^{1-\zeta} \sum_{\theta_{ijk}} [(1 + \lambda \cos \theta_{ijk})^\zeta e^{-\eta(R_{ik}^2 + R_{jk}^2)} f_c(R_{ik}) f_c(R_{jk})] \quad (19)$$

can be constructed.

Pair symmetry functions have been found to provide a comparable accuracy to ACFSs and an atom-based energy expression,¹⁴⁰ while the resulting HDNNPs are necessarily less efficient, if the same cutoff radius is used, since the number of pairs is typically much larger than the number of atoms in a given system.¹⁴⁰

3.4. Discussion of ACSFs

To date ACSFs represent the standard descriptors for the construction of HDNNPs. While they have been used in many successful applications, several challenges remain and some decisions have to be made, which affect the performance and accuracy of the obtained potentials.

First of all, the spatial shape of the ACSFs has to be defined by selecting the parameters in eqs 11 to 15. Several approaches exist to guide the selection of these parameters, and essentially two strategies can be distinguished, which either aim for an unbiased description of the spatial environment or for the best possible description of a given data set.

A first unbiased “default” starting set of ACSFs is typically obtained by selecting about six radial functions per element combination taking into account the minimum interatomic distance that is expected in the simulations for this pair of elements. The turning points of the product of the Gaussians and cutoff functions in eq 11 are then chosen to be equidistantly distributed between $R_{ij,\min}$ and $\eta = 0$, that is, the plain cutoff function, which has a turning point at $R_{ij} = \frac{1}{2}R_c$ (see Figure 7). For the angular functions all combinations of two neighboring elements need to be considered and for each of them, the values $\zeta = 1, 2, 4$, and 16 for both $\lambda = 1$ and $\lambda = 1$ are a good first choice (see Figure 9).

Alternatively, for a given data set, optimum symmetry functions sets can be generated systematically by selecting the best functions from a large pool of functions¹⁴² or by principal component analysis.¹⁴³ This can be done in a highly automatic way, but the drawback of this approach is the dependence on the underlying data set, which is often not static, but changes in particular in early stages of potential development, when new structures are regularly added (see section 6.2). Moreover, while the known structures may be efficiently distinguished by the symmetry functions generated in this way, new and possibly very different types of structures emerging in simulations may not be equally well described and may require a redefinition of the symmetry functions and consequently a new training of the HDNNP.

Thus, the best strategy depends on the particular situation. In early stages of potential construction, generic symmetry functions should be preferred, which provide an unbiased coverage of space, while for large available data sets, customized symmetry functions may be more efficient, which are often also determined empirically. It should be noted that it has also been proposed to optimize the parameters of the symmetry functions along with the potential in the fitting process¹⁴⁴ or to determine the best parameters using genetic algorithms,¹²⁶ and there is certainly much room for improvements in the more systematic construction of ACSFs.

For both strategies the range of function values for certain ACSFs being too small must be avoided. These functions would unnecessarily increase the size of the ACSF set, while they do not contribute to structural differentiation. The main problem, however, is that in this case very small and structurally irrelevant differences in the symmetry function values may be exploited by the NN in the training process to represent the potential energy. This unphysical behavior can result in numerical instabilities, and consequently such functions should be removed before the training is started.

One obvious limitation of the description of the atomic environments by symmetry functions and many related descriptors is the unfavorable scaling of the number of functions with the number of elements, as all possible permutations of the elements have to be included. In general, the number of symmetry functions is given by

$$N_{\text{sym}} = \frac{N_{\text{elem}}(N_{\text{elem}} + 1)}{2} + N_{\text{elem}} \quad (20)$$

where the first term refers to the angular functions and the second term to the radial functions. This number is then further extended depending on the specific number of angular and radial functions based on the choice of the symmetry function parameters. Nevertheless, depending on the composition of the system not all combinations may be required.

Another challenge is the high dimensionality of the atomic geometric environments. For instance a typical cutoff sphere with radius 6 Å of liquid water at ambient conditions contains about 90 atoms (270-dimensional atomic environments), while the number of atoms increases to 420 (1260-dimensional atomic environments) for $R_c = 10$ Å. Hence, already typical HDNNPs employing between 40 and 100 symmetry functions per atomic environment in a binary system effectively perform some form of dimensionality reduction.

With typical cutoff radii of about 6 Å studies of several ternary and quarternary systems have been reported.^{145–149} When a further increase in the number of elements is required, the complexity of the atomic environments may have to be reduced, for example, by decreasing the cutoff radius, which comes at the risk of less accurate energies and forces.⁷⁵ In the case of the ANI-1 force field, for a quarternary system containing the elements H, C, N, and O, 768 symmetry functions have been used with comparably small cutoff radii of 4.6 Å for the radial and 3.1 Å for the angular symmetry functions.¹³⁹ A recent reparameterization ANI-2 even reached seven elements (H, C, N, O, F, Cl, S) with slightly increased cutoff radii of 5.1 and 3.5 Å for the radial and angular functions, respectively.¹⁵⁰

To overcome the combinatorial growth in the number of symmetry functions, it has been suggested to include element-specific information directly into the ACSFs. One example are weighted atom-centered symmetry functions (wASCF),¹²⁶ which discard the use of separate functions for the individual element combinations and instead use element-dependent weighting functions in a single set of radial and angular functions resulting in

$$G_{i,\mu}^{\text{rad}} = \sum_{j \neq i}^{N_{\text{atom}} \in R_c} g(Z_j) e^{-\eta(R_{ij} - R_s)^2} f_c(R_{ij}) \quad (21)$$

and

$$G_{i,\mu}^{\text{ang}} = 2^{1-\zeta} \sum_{j \neq i}^{N_{\text{atom}} \in R_c} \sum_{k \neq j,k}^{N_{\text{atom}} \in R_c} h(Z_j, Z_k) (1 \pm \cos \theta_{ijk})^\zeta e^{-\eta(R_{ij}^2 + R_{jk}^2)} f_c(R_{ij}) f_c(R_{ik}) \quad (22)$$

where Z_j and Z_k are the nuclear charges, and it has been shown that even simple choices such as $g(Z_j) = Z_j$ and $h(Z_j, Z_k)$ yield satisfactory results. Alternative types of descriptors aiming for multicomponent systems have been suggested by Artrith et al.¹²³ and also by Rostami et al.¹⁵¹ Owing to the very small number of studies using these modified ACSFs it remains to be seen to what extent a reduction of the number of symmetry functions is possible. In view of the dimensionality estimate given above and the fact that already conventional ACSFs represent a dimensionality reduction, more work in this direction is certainly required, as accurate HDNNPs crucially depend on the quality of the descriptors.

The ability to distinguish different atomic environments is an important criterion for the choice of the descriptor. In contrast to other frequently used descriptors such as SOAP,¹⁰⁷ which allow a very systematic construction, the number of symmetry functions, which are not as systematic due to the choice of the parameters defining their spatial shapes, is typically rather small. This is the reason for the good computational performance of HDNNPs,¹¹⁶ while for a high accuracy of the potential the structural description must also be sufficiently accurate. A large number of successful applications⁷⁴ of HDNNPs clearly demonstrates that in practical applications ACSFs provide a reliable structural description, but studies addressing this aspect in detail are very rare. Recently, a careful analysis of different descriptors¹¹⁹ has shown that for small systems in combination with a small cutoff radius some atomic environments exist that cannot be distinguished by a combination of radial and angular ACSFs. This finding, which equally applies to a wide range of other descriptors consisting of two- and three-body terms, is very interesting and may lead to the development of improved descriptors. Still, these problems are of little relevance in practical applications, as the problems are not present in multicomponent systems and for larger cutoff radii, which are typically used in the construction of HDNNPs. Another recent study addressing the structural performance of descriptors has been carried out by Goedecker and co-workers.¹¹⁷ Using fingerprint distances, the quantitative differences between varying atomic environments have been studied for a series of descriptor types. The relation of these findings to the quality of the resulting potentials still remains to be determined, as no potential energy surfaces have been constructed for the investigated systems. Moreover, a direct relation of numerical differences to the accuracy of potentials is very difficult to establish, as ML algorithms are able to detect even small patterns in large data sets that can be used to construct reliable functional relations.

Finally it should be noted that of course the number of symmetry functions can also be reduced by omitting those functions, which represent interactions that are not present in a system. For instance, for the adsorption of a single atom, for example, hydrogen, on a clean metal surface, no $G^{\text{rad}}(\text{H}, \text{H})$ and no angular functions including two or three hydrogen atoms need to be present.

3.5. Forces and Stress

The energy expression in eq 2 enables the calculation of analytic derivatives, which are required to obtain the atomic forces needed for applications such as molecular dynamics simulations or geometry optimizations. The force component $F_{\mu\alpha}$ acting on atom μ in direction $\alpha = \{x, y, z\}$, that is, the negative derivative of E_{short} with respect to coordinate $R_{\mu\alpha}$ is given by

$$\begin{aligned} F_{\mu\alpha}^{\text{short}} &= -\frac{\partial E_{\text{short}}}{\partial R_{\mu\alpha}} = -\sum_{i=1}^{N_{\text{elem}}} \sum_{j=1}^{N_{\text{atom}}^i} \frac{\partial E_j^i}{\partial R_{\mu\alpha}} \\ &= -\sum_{i=1}^{N_{\text{elem}}} \sum_{j=1}^{N_{\text{atom}}^i} \sum_{k=1}^{N_{\text{sym}}^i} \frac{\partial E_j^i}{\partial G_{jk}^i} \frac{\partial G_{jk}^i}{\partial R_{\mu\alpha}} \end{aligned} \quad (23)$$

As can be seen in this equation, the chain rule has to be applied to take into account the transformation from the Cartesian coordinates to the atom-centered symmetry functions yielding a sum over products of two partial derivatives. N_{sym}^i is the

number of symmetry functions used to describe the local chemical environments of atoms of element i . The first partial derivatives of the atomic energy with respect to the symmetry functions are given by the architecture of the atomic NNs, while the partial derivatives of the symmetry functions with respect to the Cartesian coordinates are defined by the functional forms of the ACSFs (see section 3.3). In a similar way also other gradient-related properties such as the stress tensor⁷⁵ and the Hessian are accessible in analytic form.

The relation between the potential energy E_{short} and $F_{\mu\alpha}$ in eq 23 is exact ensuring consistent energies and forces, and has some interesting implications for the environment-dependence of the forces⁷⁴ that is illustrated in Figure 11. While the atomic

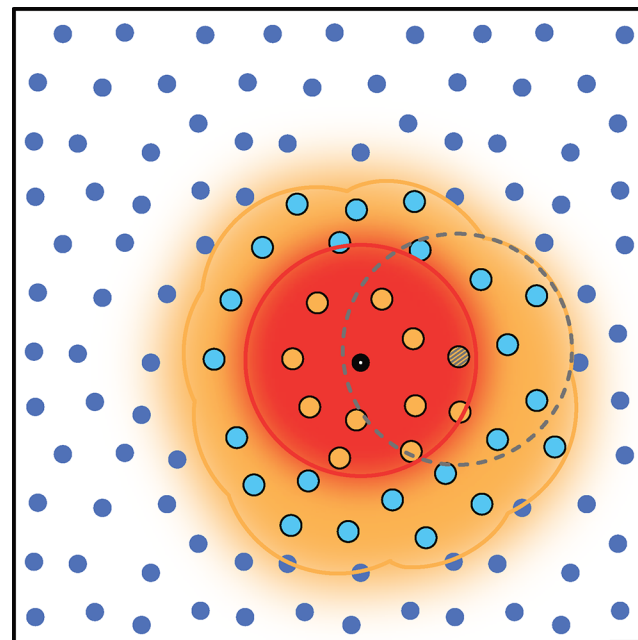


Figure 11. Illustration of the environment-dependence of the forces. The force components of the central atom shown in black depend on the atomic energies of all orange atoms inside the cutoff sphere of radius R_c shown in red. Since these atomic energies depend on the positions of all atoms inside their own atomic environments (an example is shown as black dashed circle) in total the positions of all atoms inside the orange region, that is, all orange and light blue atoms, determine the force components of the central atom.

energies by definition only depend on the positions of the neighboring atoms up to the cutoff radius, the forces depend on the atomic energies E_j^i of all atoms inside R_c . Since in turn these atomic energies depend on their individual full local environments, the forces can effectively depend on the positions of atoms up to twice the cutoff radius around the atom of interest. It should be noted that the atomic forces in the HDNNP are not obtained as independent additional output neurons, but as analytic derivatives of the energy they depend on the same weight parameters as the atomic energy contributions. As will be discussed in section 6.3, this dependence can be employed to use the force components in addition to the energies to train HDNNPs.

The stress tensor $\underline{\sigma}$ is of interest e.g. for MD simulations in the *NPT* ensemble and for structural relaxations of solids including the lattice parameters. It contains a kinetic contribution and a static contribution,

$$\underline{\underline{\sigma}} = \underline{\underline{\sigma}}^{\text{kin}} + \underline{\underline{\sigma}}^{\text{static}} \quad (24)$$

The kinetic stress contribution $\underline{\underline{\sigma}}^{\text{kin}}$ is a dynamical property that can be calculated from the atomic velocities \mathbf{v}_i and the atomic masses m_i in MD simulations. Its components are given by

$$\sigma_{\alpha\beta}^{\text{kin}} = \frac{1}{V} \sum_{k=1}^{N_{\text{atom}}} m_k v_{k\alpha} v_{k\beta} \quad (25)$$

with α and β being $\{x,y,z\}$, and $v_{k\alpha}$ and $v_{k\beta}$ being components of the velocity vector. V is the volume of the simulation cell.

The static stress $\underline{\underline{\sigma}}^{\text{static}}$ depends on the atomic positions and can be calculated from the HDNNP forces. Defining the Cartesian coordinate difference as $R_{ij,\alpha} = R_{i\alpha} - R_{j\alpha}$ the contributions of the radial and the angular symmetry functions (see section 3.3) for atom i can be determined separately according to

$$\sigma_{i,\alpha\beta}^{\text{static,rad}} = \sum_{j=1}^{N_{\text{atom}}} R_{ij,\alpha} F_{j\beta} = - \sum_{k=1}^{N_{\text{atom}}} \sum_{\mu=1}^{N_{\text{sym}}^k} \frac{\partial E_k}{\partial G_{k\mu}} \sum_{j=1}^{N_{\text{atom}}} R_{ij,\alpha} \frac{\partial G_{k\mu}}{\partial R_{j\beta}} \quad (26)$$

with $F_{j\beta}$ being the force component of atom j in direction β . The angular stress contribution of atom i is given by

$$\begin{aligned} \sigma_{i,\alpha\beta}^{\text{static,ang}} &= \sum_{j=1}^{N_{\text{atom}}} R_{ij,\alpha} F_{j\beta} + \sum_{k=1}^{N_{\text{atom}}} R_{ik,\alpha} F_{k\beta} \\ &= - \sum_{k=1}^{N_{\text{atom}}} \sum_{\mu=1}^{N_{\text{sym}}^k} \frac{\partial E_k}{\partial G_{k\mu}} \left(\sum_{j=1}^{N_{\text{atom}}} R_{ij,\alpha} \frac{\partial G_{k\mu}}{\partial R_{j\beta}} + \sum_{m=1}^{N_{\text{atom}}} R_{im,\alpha} \frac{\partial G_{k\mu}}{\partial R_{m\beta}} \right) \end{aligned} \quad (27)$$

For simplicity, joint indices k and m have been used for the element and atom number. Like for the forces in eq 23, also for the evaluation of the elements of the stress tensor in eqs 26 and 27 the intermediate transformation of the Cartesian coordinates to ACSFs has been taken into account in the force components. The complete static stress tensor elements are then obtained by summing over all atomic contributions

$$\sigma_{\alpha\beta}^{\text{static}} = \sum_{i=1}^{N_{\text{atom}}} (\sigma_{i,\alpha\beta}^{\text{static,rad}} + \sigma_{i,\alpha\beta}^{\text{static,ang}}) \quad (28)$$

More details on the calculation of the stress can be found in ref 75.

4. THIRD-GENERATION NEURAL NETWORK POTENTIALS

4.1. Structure and Energy Expression

An obvious approximation in second-generation HDNNPs is the restriction to atomic interactions inside the cutoff sphere. The resulting short-ranged potentials are well-suited to describe local bonding even for complex atomic environments, but nevertheless it can be expected that for many systems long-range interactions, primarily electrostatics but to some extent also dispersion interactions, will be important.

Long-range electrostatic interactions have been a central component of atomistic potentials since the advent of classical force fields. In most cases, simple force fields rely on fixed partial atomic charges depending on the classification into atom types,^{2,4,152,153} but also polarizable force fields are common.^{154,155}

It is straightforward to include long-range electrostatics in a similar way in ML potentials making use of element-specific fixed charges, and this has been proposed, for example, for an early GAP potential of GaN⁵⁷ and in an electrostatic spectral neighbor analysis potential (eSNAP) for α -Li₃N.⁶¹ While this approach, which can be considered as an intermediate step between second and third-generation ML potentials, offers a solution for specific systems, the resulting potentials have a limited applicability and cannot easily be generalized to systems with atoms in chemically different environments requiring flexibility in the atomic charges, such as a metal covered by a layer of its oxide.

Already in the early times of ML potential development, the limitations of fixed charges in conventional force fields motivated the first attempts to express partial atomic charges and higher multipole moments by neural networks and Kriging by Popelier and co-workers^{156–158} with the final aim to construct improved and more transferable force fields.¹⁵⁹

Including long-range electrostatic interactions in ML potentials is promising not only to take into account interactions beyond the cutoff radius without truncation, but also to include physically meaningful energy terms in the form of Coulomb's law, which does not represent an approximation and is thus compatible with the definition of ML potentials given in the introduction. A better description of the long-range part of the PES might also enable the reduction of the cutoff radius to smaller values, which would facilitate sampling a reduced configuration space and allow to focus the use of the flexible short-range atomic energy contributions to describe the covalent interactions, for which no simple analytic functional relations are available. These considerations have led to the development of third-generation HDNNPs, which are defined by the introduction of environment-dependent atomic charges, which are expressed by ML and used to compute long-range electrostatic interactions explicitly.

The first third-generation HDNNP including long-range electrostatic interactions was published in 2012, and applications to zinc oxide¹⁶⁰ and the water dimer¹⁶¹ have been reported. Here, the environment-dependent charges are expressed by a second set of atomic neural networks as illustrated in Figure 12. Like the environment-dependent atomic energies, also the atomic charges depend on vectors of ACSFs describing the atomic environments, and they are obtained as output of the atomic charge NNs. These charges can then be used with standard methods such as Coulomb's law for nonperiodic systems or an Ewald sum¹⁶² for periodic systems to calculate the long-range electrostatic energy E_{elec} without truncation. The total potential energy of the system is then given by

$$E_{\text{total}} = \sum_{i=1}^{N_{\text{elem}}} \sum_{j=1}^{N_{\text{atom}}^i} E_j^i + E_{\text{elec}} \quad (29)$$

The training procedure of third-generation HDNNPs is based on the following steps to avoid double counting the electrostatic energy contributions in the electrostatic and the short-range part:

1. The atomic charge NNs are trained using reference atomic charges obtained from electronic structure calculations.
2. The short-range energies are extracted from the reference total potential energies by removing the

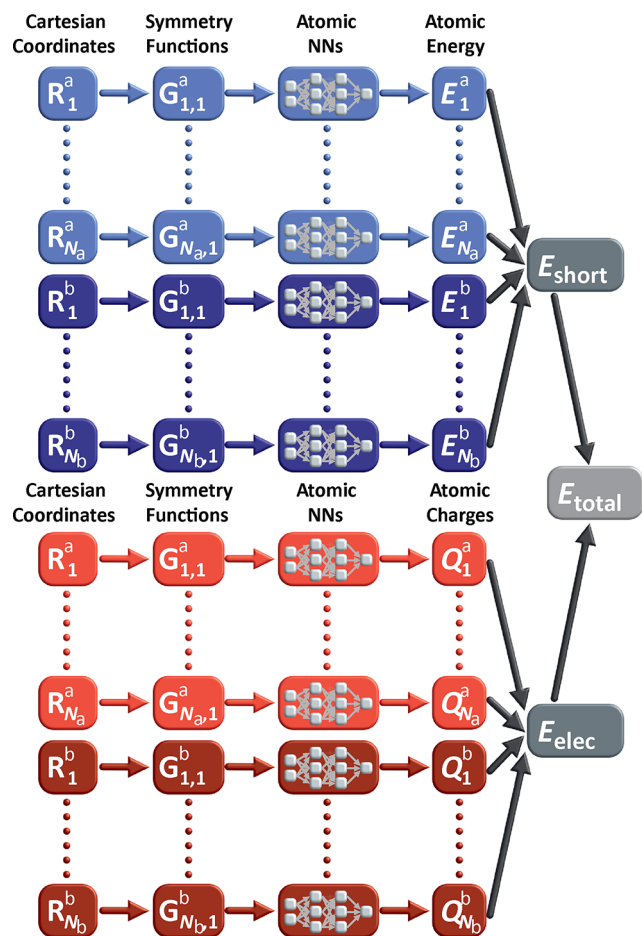


Figure 12. Third-generation high-dimensional neural network potential for the example of a binary system containing elements *a* and *b*.¹⁶⁰ In addition to the short-range atomic energy contributions in the upper part, which correspond to Figure 5, a second set of atomic neural networks shown in red is used to construct environment-dependent atomic charges that can be used to calculate the long-range electrostatic energy without truncation, i.e., using an Ewald sum. The total energy of the system is then given by the sum of the short-range and the electrostatic energies.

electrostatic energies computed from the charges given by the charge NNs.

3. Using the constructed functional relation between the atomic environments and the partial charges also the electrostatic forces can be computed and removed from the reference forces to yield the short-range part of the forces.
4. The extracted short-range energy and force contributions are used for training the short-range atomic NNs in the same way as in second-generation NNPs.
5. In applications both the short-range and the electrostatic energies and forces are then computed separately and combined to yield the complete total energy surface. By construction, double counting the electrostatic interactions is avoided, as the short-range and charge NNs are trained to provide the correct total target energies and forces.

In this procedure, the short-range energies and the charges are not independent, which is unavoidable if the aim is to reach a very high accuracy based on consistent short and long-range energies.

An obvious drawback of third-generation HDNNPs is the need to use reference partial charges obtained in electronic structure calculations. A variety of different charge partitioning methods is readily available in most electronic structure codes, such as Mulliken charges,¹⁶³ Hirshfeld charges,¹⁶⁴ or Bader charges,¹⁶⁵ but, although all of them are mathematically well-defined, atomic partial charges are not physical observables and there is no unique best choice with respect to these partitioning methods. It has been demonstrated in detailed benchmark studies that different partitioning schemes can provide very different results.¹⁶⁶ Fortunately, most charge partitioning methods still provide very similar partial charges for large interatomic distances, that is, the region beyond the cutoff radius of the symmetry functions, and any arbitrariness that may be present for shorter distances will be compensated by the short-range part by construction. Therefore, the method is surprisingly robust with respect to the choice of the partitioning method. In principle, also alternative approaches without the use of reference charges are possible by training the NN parameters under the only constraint to yield the correct overall energies and forces, but such a procedure is more complicated and thus less attractive due to the coupled optimization of the weight parameters of the short-range and charge neural networks.

4.2. Electrostatic Forces

A characteristic feature of third-generation HDNNPs is the need for a sequential training of charges and short-range contributions in the above scheme. While the electrostatic energy could be determined directly from the charges obtained in the reference electronic calculations, a sequential training cannot be avoided, if forces shall be used in the training process of the short-range part. The reason is that the electrostatic forces are not directly available as separate quantities in electronic structure calculations. Further, in the case of environment-dependent charges the electrostatic forces contain the partial derivatives of the charges, which can only be determined once the analytic relation between charges and atomic environments is known. Hence, for nonperiodic systems and the case of environment-dependent charges in third-generation HDNNPs the forces must be determined in a consistent way from the NN charges and Coulomb's law according to

$$\begin{aligned} F_{\mu\alpha}^{\text{elec}} &= -\frac{\partial E_{\text{elec}}}{\partial R_{\mu\alpha}} \\ &= -\frac{\partial}{\partial R_{\mu\alpha}} \frac{1}{2} \sum_{i=1}^{N_{\text{atom}}} \sum_{j \neq i}^{N_{\text{atom}}} \frac{Q_i Q_j}{R_{ij}} \\ &= -\sum_{i=1}^{N_{\text{atom}}} \sum_{j \neq i}^{N_{\text{atom}}} \frac{1}{2 R_{ij}^2} \left[\frac{\partial Q_i}{\partial R_{\mu\alpha}} Q_j R_{ij} + Q_i \frac{\partial Q_j}{\partial R_{\mu\alpha}} R_{ij} - Q_i Q_j \frac{\partial R_{ij}}{\partial R_{\mu\alpha}} \right] \end{aligned} \quad (30)$$

with $R_{ij} = |\mathbf{R}_i - \mathbf{R}_j|$, and Q_i and Q_j being the NN partial atomic charges. The first two terms can be combined by first splitting the three sums and renaming the indices in the second sum to yield

$$\begin{aligned} F_{\mu\alpha}^{\text{elec}} &= -\sum_{i=1}^{N_{\text{atom}}} \sum_{j \neq i}^{N_{\text{atom}}} \left(\frac{Q_i}{R_{ij}} \frac{\partial Q_j}{\partial R_{\mu\alpha}} \right) + \sum_{i=1}^{N_{\text{atom}}} \sum_{j \neq i}^{N_{\text{atom}}} \left(\frac{Q_i Q_j}{2 R_{ij}^2} \frac{\partial R_{ij}}{\partial R_{\mu\alpha}} \right) \\ &= \sum_{i=1}^{N_{\text{atom}}} \sum_{j \neq i}^{N_{\text{atom}}} \frac{Q_i}{R_{ij}} \left[\left(\frac{-\partial Q_j}{\partial R_{\mu\alpha}} \right) + \frac{1}{2} \frac{Q_j}{R_{ij}} \frac{\partial R_{ij}}{\partial R_{\mu\alpha}} \right] \end{aligned} \quad (31)$$

Considering further the chain rule due to the transformation from Cartesian coordinates to symmetry functions by using

$$\frac{\partial Q_i}{\partial R_{\mu\alpha}} = \sum_{k=1}^{N_{\text{sym}}^{\mu}} \frac{\partial Q_i}{\partial G_{ik}^{\mu}} \frac{\partial G_{ik}^{\mu}}{\partial R_{\mu\alpha}} \quad (32)$$

we finally obtain

$$F_{\mu\alpha}^{\text{elec}} = \sum_{i=1}^{N_{\text{atom}}} \sum_{j \neq i}^{N_{\text{atom}}} \frac{Q_i}{R_{ij}} \left[\frac{1}{2} \frac{Q_j}{R_{ij}} \frac{\partial R_{ij}}{\partial R_{\mu\alpha}} - \sum_{k=1}^{N_{\text{sym}}^{\mu}} \frac{\partial Q_j}{\partial G_{jk}^{\mu}} \frac{\partial G_{jk}^{\mu}}{\partial R_{\mu\alpha}} \right] \quad (33)$$

The short-range part of the forces can then be extracted from the reference electronic structure calculations as

$$F_{\mu\alpha}^{\text{short}} = F_{\mu\alpha}^{\text{ref}} - F_{\mu\alpha}^{\text{elec}} \quad (34)$$

and used for training the short-range NNs to reproduce the short-range forces. Similar equations can also be derived for the case for periodic systems making use of an Ewald summation.^{162,167}

When extracting the short-range forces from the reference forces the order of magnitude of the electrostatic energy and force contributions has to be taken into account. Since the Coulomb energy exhibits a singularity for short interatomic distances, the absolute values of the electrostatic energies and forces become very large for close atomic encounters, in fact much larger than typical binding energies. Thus, removing the electrostatic energies and forces before training the remaining short-range part may not simplify the training process by smoothening the PES, but instead singularities of opposite sign can be introduced in the short-range part complicating the fitting procedure instead. Similar problems have been encountered and solved in empirical correction schemes to include dispersion interactions in DFT calculations¹⁶⁸ due to the steep energy increase in the repulsive part. To overcome this problem, for third-generation HDNNPs the following screening function has been suggested¹⁶¹

$$f_{\text{scr}} = \begin{cases} \frac{1}{2} \left[1 - \cos \left(\frac{\pi R_{ij}}{R_{\text{scr}}} \right) \right] & \text{for } R_{ij} \leq R_{\text{scr}} \\ 1 & \text{for } R_{ij} > R_{\text{scr}} \end{cases} \quad (35)$$

that is, for short interatomic distances below a screening radius R_{scr} the electrostatic energy is screened to zero. Although this screening numerically changes the electrostatic energies and forces, this preprocessing of the electrostatic contributions does not introduce any errors in the resulting HDNNP total energy, as the missing electrostatic energy at short distances is fully compensated by the short-range part inside the cutoff spheres. Alternative damping schemes have been suggested for example in the PhysNet approach.⁵⁵

A final comment addresses the requirement of overall charge neutrality—or charge conservation in case of ionic systems—that is particularly important for periodic systems. Since the charges are trained as a function of the environment, it is a priori not clear if the sum of these charges, which exhibit small fitting errors, will correctly produce the total charge of the system. A simple but effective solution to enforce the correct total charge is rescaling the NN charges.^{55,160} According to experience the required adjustments are about 1 order of magnitude smaller than the fitting errors and thus only marginally relevant for the accuracy of the HDNNP. An

essentially equivalent procedure of evenly spreading a neutralizing charge over the system has also been proposed.¹⁴⁴

A variety of alternative approaches to construct environment-dependent charges has been proposed in the literature using NNs and other ML techniques. Examples are a hierarchically interacting particle neural network (HIPNN) for producing charges to be used in the ANI-1 potential,¹⁶⁹ NNs simultaneously yielding atomic energies and charges in PhysNet,⁵⁵ environment-dependent electrostatic multipole coefficients for small organic molecules from kernel-ridge regression,^{170,171} random forest regression for conformation independent charges for force fields,¹⁷² the combination of symmetry functions with random forest,¹⁷³ and many others.¹⁷⁴ Depending on the particular method, the environment-dependence of the charges can extend over varying distances. For instance in message passing neural networks, as employed in HIPNN,¹⁶⁹ PhysNet,⁵⁵ and extensions of AIMNet,¹⁷⁵ the range can be controlled by the number of information passing steps.

Apart from training environment-dependent charges to reference partial charges obtained in electronic structure calculations, it has also been proposed to determine charges to reproduce molecular dipole moments,^{144,166,176} which facilitates applications in the computation of infrared spectra. Moreover, recently, an interesting new descriptor called long-distance equivariant representation (LODE) has been proposed, which allows the efficient calculation of the long-range electrostatic energy in local machine learning frameworks with an accuracy similar to the use of machine learned environment-dependent charges.¹²⁷

In spite of these advances, third-generation HDNNPs are not frequently used, with the exception of potentials aiming at a high transferability for a wide range of organic molecules.^{139,144} The main reason is that for many systems, in particular condensed systems, long-range electrostatic energy contributions beyond the cutoff, which cannot be described by the short-range atomic energies in second-generation HDNNPs, are effectively screened and thus very small. The possible reduction of the energy error by a few meV/atom has to be put into relation to training a second set of atomic NNs, which also doubles the computational costs in the evaluation of the potential in addition to the relatively demanding Ewald summation, which can become the speed-determining step in MD simulations of large periodic systems.

As a final note, it has also been recently proposed to use ML to directly learn the electron density^{177,178} instead of atomic partial charges or multipoles, which in the future might enable a closer connection between ML potentials and electronic structure methods.

5. FOURTH-GENERATION NEURAL NETWORK POTENTIALS

5.1. The Challenge of Nonlocality

The main improvement of third-generation HDNNPs has been the inclusion of long-range interactions, in most cases electrostatics, but also dispersion interactions, which can act over large distances, have been considered, for example, in the form of the Grimme D3 dispersion correction¹⁶⁸ in TensorMol¹⁴⁴ and also in other types of ML potentials such as PhysNet.⁵⁵

The charges underlying the electrostatic interactions in third-generation HDNNPs have in common that they depend

on the local chemical environments, and this dependence is expressed using ML. While this is a clear step forward compared to many classical force fields and conventional empirical potentials using element or atom-type specific fixed charges, the use of environment-dependent charges is not sufficient if long-range charge transfer is present. In this case, the charge of an atom may strongly depend on structural—or electronic—changes very far away in the system outside its local chemical environment. Further, also different ionization states of a given system can change the charge distribution globally, and methods relying on local structural information only are unable to distinguish these states.

Long-range charge transfer is omnipresent in chemistry, molecular biology, and materials science for many types of compounds and reactions, from molecules to complex condensed systems. Figure 13 illustrates long-range charge

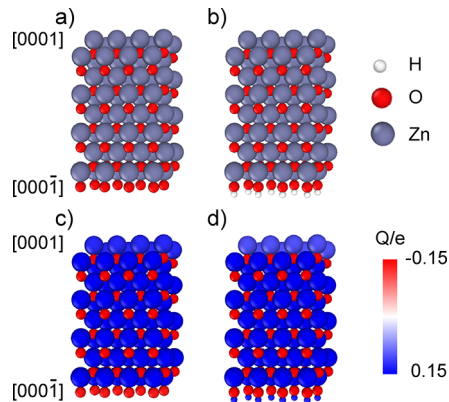


Figure 13. Long-range charge transfer in a polar zinc oxide slab. In the side view of the slab (a) the $[0001]$ surface is zinc-terminated (gray atoms) and the $[000\bar{1}]$ surface is oxygen-terminated (red atoms); (b) an additional layer of hydrogen atoms is attached to the oxygen atoms (white); (c, d) atomic partial charges for both systems. In both cases the local chemical environments of the zinc atoms in the top layer are identical while the charges are different, which cannot be captured correctly by third-generation HDNNPs. The figure was generated with Ovito.¹⁹¹ The DFT Hirshfeld charges¹⁶⁴ have been computed with the FHI-aims program¹⁹² using the PBE functional.¹⁹³

transfer for the example of a periodic polar zinc oxide surface. Here, the local environments of the zinc atoms in the topmost layer do not include the bottom side of the slab, and consequently the local Zn geometries are identical for the oxygen-terminated (Figure 13a) as well as for the hydrogen-terminated (Figure 13b) $\text{ZnO}[000\bar{1}]$ surface, while the overall dipole moment, the global electronic structure, and the charge distribution are different. Thus, in both cases the top layer zinc atoms are assigned the same atomic energy contributions and charges in third-generation HDNNPs, which is qualitatively incorrect.

Figure 14 shows 4-(4-phenyl-1,3-butadien-1-yl)benzoic acid as a molecular example in the neutral and in the negatively charged deprotonated form. It can be clearly seen that the change in the global charge results in modifications of the atomic partial charges even far away from the carboxyl group. Hence, also in this case second and third-generation HDNNPs, and also the vast majority of other types of machine learning potentials reported in the literature, will provide qualitatively incorrect results, as the missing proton and the change in global charge are invisible to most of the atomic NNs.

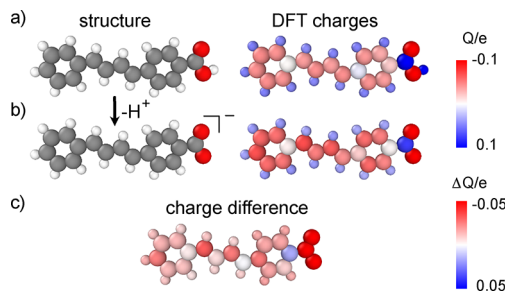


Figure 14. Long-range changes in the atomic partial charges obtained with DFT for 4-(4-phenyl-1,3-butadien-1-yl)benzoic acid (a) and its deprotonated form (b). (c) Change of the partial charges if the proton of the carboxylic group is removed. The figure was generated with Ovito.¹⁹¹ The DFT Hirshfeld charges¹⁶⁴ have been computed with the FHI-aims program¹⁹² using the PBE functional.¹⁹³

Interactions with parts of the system outside local chemical environments have been observed for many other systems, from elemental carbon^{179,180} to the adsorption of metal clusters on doped substrates,¹⁸¹ demonstrating the need for methods accurately including nonlocal effects. Simply extending the cutoff radius of the local environments does not represent a general solution of this problem, as larger problematic systems can always be found, and an increased cutoff gives rise to other complications such as the description and sampling of the larger atomic environments.

It is important to note that there is a difference between long-range interactions and nonlocal interactions. Long-range interactions can be included using environment-dependent charges in third-generation HDNNPs if the charges only show a local dependence, and in fact even the most basic force fields include long-range interactions based on fixed charges. Nonlocal interactions, on the other hand, depend on a global charge (re)distribution and thus cannot be described by third-generation HDNNPs. Potentials, which can deal with long-range charge transfer, that is, nonlocal charge dependencies, define the fourth-generation of HDNNPs. These long-range or even global changes in the electronic structure may result from distant functional groups, reactions such as protonation and deprotonation, doping in solids, or changes in the overall charge of the system.

A possible solution for the challenge of long-range charge transfer was proposed a long time ago in advanced force fields in the form of charges determined by the electronegativity equalization^{182,183} and charge equilibration^{184–187} methods. The reactive force field ReaxFF is a prominent example using this technique.⁶ Also approximate electronic structure methods such as the density-functional tight binding (DFTB) approach make use of self-consistently determined charges.¹⁵ However, charge equilibration methods have been rarely used in the context of ML potentials to date, and methods belonging to the group of fourth-generation HDNNPs are just emerging. Several promising examples of such methods allowing for a global redistribution of charges will be discussed in the following sections.

Also alternative methods have been used to extend the interaction range in ML potentials. An important example are message passing neural networks (MPNN), which are used for instance in AIMNet,^{175,188} electron-passing neural networks,¹⁸⁹ and others.^{55,190} In these methods information is passed through the system iteratively from atom to atom, and the resulting effective range is determined by the number of

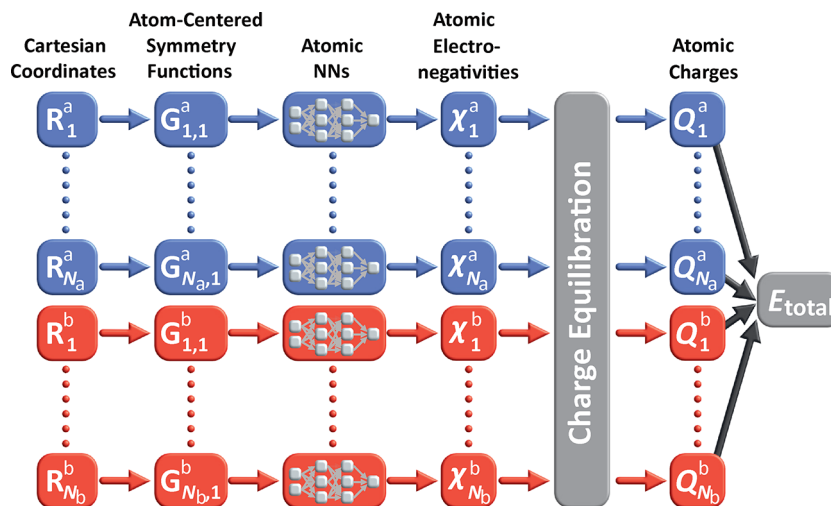


Figure 15. Structure of the charge equilibration neural network technique (CENT)^{54,194} for a binary system with N_a atoms of element a and N_b atoms of element b. First, the Cartesian coordinates are transformed to atom-centered symmetry function vectors describing the atomic environments. They serve as input for atomic neural networks yielding environment-dependent electronegativities χ , which are then used in a charge equilibration scheme to determine the atomic charges Q_i^μ . The total energy is computed from these charges using eq 38.

included information passing steps. Depending on the distance of information passing, these methods form a continuum between second-generation HDNNPs, if they cover the interactions with a few local neighbor shells, and fourth-generation HDNNPs, which include the full system globally, in the limit of an infinite number of information passing steps. Consequently, an unambiguous classification of message passing methods according to the generations used in this review is not possible. Since both families, MPNNs and also fourth-generation HDNNPs, are just emerging, a detailed comparison of the scope and limitations of both methods will remain a task for future work.

5.2. The CENT Approach

A first important step toward the inclusion of nonlocal charge-transfer in ML potentials has been the charge equilibration neural network technique (CENT) proposed by Goedecker and co-workers in 2015.^{54,194,195} This method allows the charge density to redistribute over the entire system to minimize the electrostatic energy. The starting point is the use of a second order Taylor expansion in terms of the atomic charges Q_i as an approximate energy expression

$$E_{\text{total}}(\{Q_i\}) = \sum_{i=1}^{N_{\text{atom}}} \left(E_i^0 + \chi_i Q_i + \frac{1}{2} J_i Q_i^2 \right) + \frac{1}{2} \iint \frac{\rho(\mathbf{R})\rho(\mathbf{R}')}{|\mathbf{R} - \mathbf{R}'|} d\mathbf{R} d\mathbf{R}' \quad (36)$$

The E_i^0 are the energies of the free neutral atoms, χ_i are the atomic electronegativities, and the J_i are element-specific hardness terms obtained by fitting. The charge density $\rho = \sum_i \rho_i$ is given by spherical Gaussian charges

$$\rho_i(\mathbf{R}) = \frac{Q_i}{\alpha_i^3 \pi^{3/2}} \exp\left(-\frac{|\mathbf{R} - \mathbf{R}_i|^2}{\alpha_i^2}\right) \quad (37)$$

of width defined by α_i . With these Gaussian charge distributions the energy can be rewritten as

$$E_{\text{total}}(\{Q_i\}) = \sum_{i=1}^{N_{\text{atom}}} \left(E_i^0 + \chi_i Q_i + \frac{Q_i^2}{2} \left(J_i + \frac{2\gamma_{ii}}{\sqrt{\pi}} \right) \right) + \sum_{i=1}^{N_{\text{atom}}} \sum_{j>i}^{N_{\text{atom}}} Q_i Q_j \frac{\text{erf}(\gamma_{ij} R_{ij})}{R_{ij}} \quad (38)$$

The γ_{ij} are given by

$$\gamma_{ij} = (\alpha_i^2 + \alpha_j^2)^{-1/2} \quad (39)$$

The charge distribution in the system is then determined in a charge-equilibration process assuming the electronegativities χ_i to be environment-dependent. They are constructed as local properties employing atomic neural networks as shown in Figure 15. Like in previous HDNNP generations, the input vectors of these atomic NNs are ACSFs. The weight parameters of the element-specific atomic neural networks are optimized to yield charges minimizing the energy in eq 38, that is, the charges are only indirectly determined via the electronegativities and they are no longer local properties.

Since the CENT energy expression in eq 38 has a quadratic dependence on the charges, its minimization using first derivatives results in a set of linear equations. An additional condition to be fulfilled is the conservation of the total charge Q_{tot} , which in summary gives rise to the set of $N_{\text{atom}} + 1$ equations

$$\left(\begin{array}{c|cc} \mathbf{A} & 1 \\ \hline 1 & \vdots & 1 \\ \dots & & 0 \end{array} \right) \left(\begin{array}{c} Q_1 \\ \vdots \\ Q_{N_{\text{atom}}} \\ \hline \lambda \end{array} \right) = \left(\begin{array}{c} -\chi_1 \\ \vdots \\ -\chi_{N_{\text{atom}}} \\ \hline Q_{\text{tot}} \end{array} \right) \quad (40)$$

where the matrix elements A_{ij} are given by

$$A_{ij} = \begin{cases} J_i + \frac{2\gamma_{ii}}{\sqrt{\pi}} & \text{if } i = j \\ \frac{\text{erf}(\gamma_{ij} R_{ij})}{R_{ij}} & \text{otherwise} \end{cases} \quad (41)$$

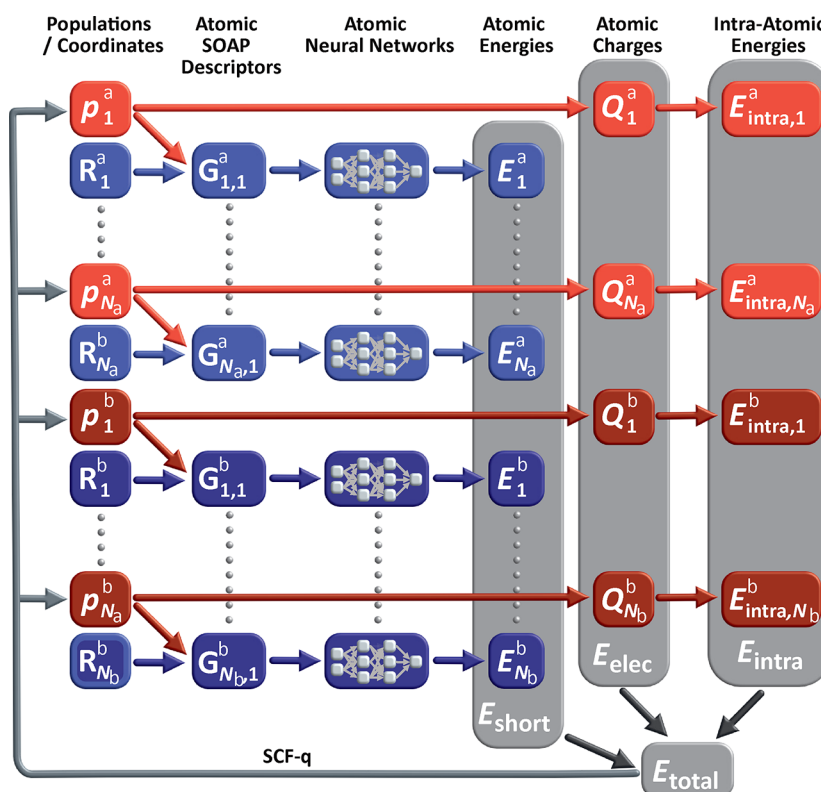


Figure 16. Schematic structure of a Becke population neural network (BpopNN).¹⁹⁷ The energy (eq 42) depends on the atomic positions, nuclear charges, and atomic populations, which are transformed to SOAP descriptors serving as input vectors for atomic neural networks. The populations minimizing the total energy of the system are determined self-consistently.

A unique solution to these equations can always be found, and there is no need for Q_{tot} to be zero such that the method is also applicable to charged systems.

In first applications it has been found that the CENT energy expression of eq 38 provides remarkably high-quality results in particular for systems with predominantly ionic bonding.^{54,194–196} Still, the overall accuracy of the energy for these systems is about 1 order of magnitude lower compared to second and third-generation HDNNPs if these methods are suitable for the systems. The main achievement of the CENT method is the ability to include long-range charge transfer in a qualitatively correct way for the first time in the context of a ML potential. Further it represents the first type of ML potential that has been applicable simultaneously to systems of different global charges.

5.3. Becke Population Neural Networks

Another important step toward the inclusion of long-range charge transfer has been taken by Xie, Persson, and Small.¹⁹⁷ They introduced a neural network-based method called Becke population neural network (BpopNN) (see Figure 16) applicable to systems with different global charges. Using Becke atomic populations p_i ¹⁹⁸ derived from the electron density, the energy $E[\mathbf{p}]$ is expressed as a function of an atom-based population vector $\mathbf{p} = \{p_i\}$, and this energy function is minimized in a self-consistent process termed “SCF-q” by varying the populations under the constraint of maintaining a given total charge of the system. Training data for different population vectors, which represent an additional degree of freedom to be mapped, are obtained in a controlled way using constrained DFT.^{199–201}

The BpopNN total energy is written as a sum of atomic energy contributions E_i defined by a large cutoff of 13.2 Å and expressed by element-specific neural networks as

$$E_{\text{total}} = \sum_{i=1}^{N_{\text{atom}}} E_i + E_{\text{intra}} + E_{\text{elec}} \quad (42)$$

with an additional atomic charge-dependent intra-atomic energy

$$E_{\text{intra}} = \sum_{i=1}^{N_{\text{atom}}} E_{\text{intra},i}(Q_i) \quad (43)$$

that has an element-dependent functional form and is used as an atomic energy baseline applicable to states with different global charges. In addition pairwise long-range electrostatic interactions represented by

$$E_{\text{elec}} = \sum_{i=1}^{N_{\text{atom}}} \sum_{j>i}^{N_{\text{atom}}} \tanh(\kappa R_{ij}) \frac{Q_i Q_j}{R_{ij}} \quad (44)$$

are included. Here, κ is an element-specific parameter that is optimized together with the parameters of the atomic neural networks.

The employed descriptor, a modified version of the SOAP¹⁰⁷ descriptor, contains nuclear charges, populations, and atomic positions of the respective central atom and in addition also depends of this information of the neighboring atoms inside the cutoff sphere. First applications of the BpopNN method have been published for Li_nH_n clusters.¹⁹⁷

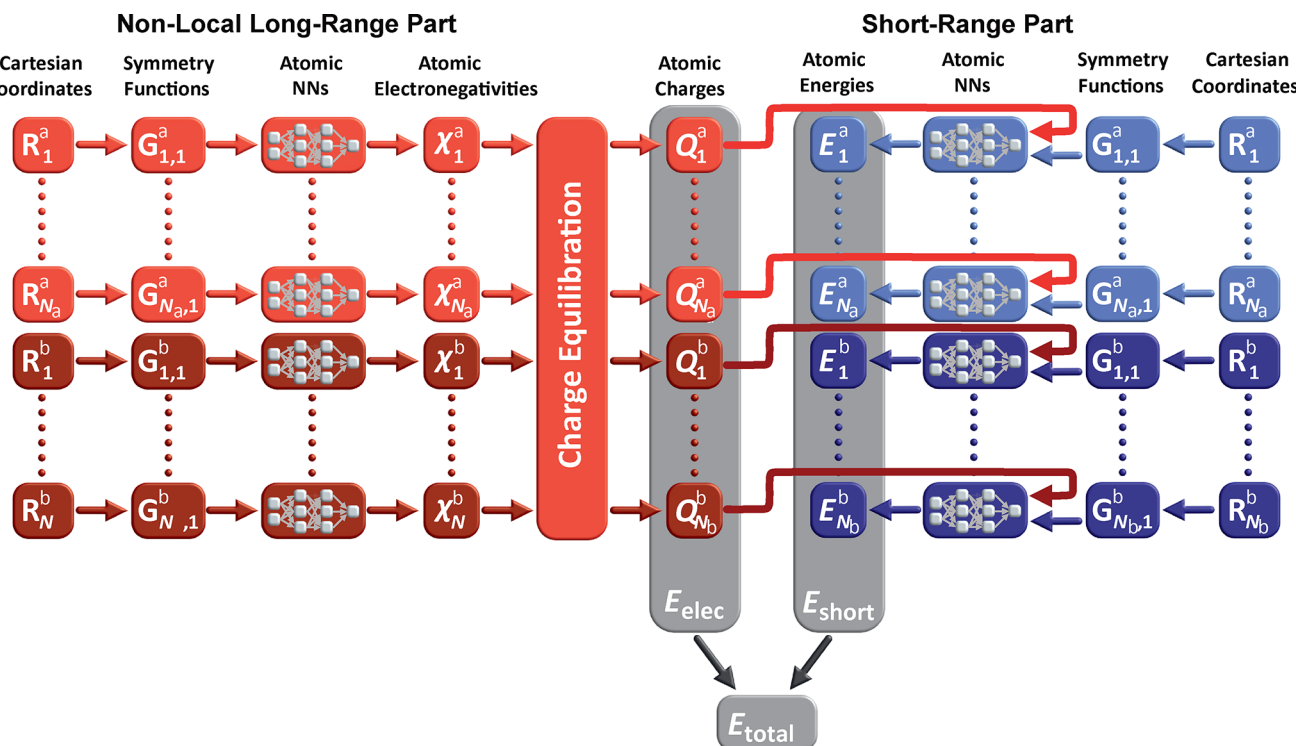


Figure 17. Structure of a 4G-HDNNP.¹⁸¹ The energy consists of an electrostatic and a short-range contribution. Like in the CENT approach⁵⁴ the atomic charges depend on the global system and are obtained from a charge equilibration process relying on environment-dependent atomic electronegativities. In contrast to CENT, the electronegativities are trained to reproduce reference charges obtained in electronic structure calculations. The short-range energy is constructed in a similar way to second-generation HDNNPs, and the main difference is that the input vectors of the short-range atomic neural networks in addition contain the atomic charges as global descriptors for changes in the local electronic structure.

5.4. 4G-HDNNPs

Recently, the advantages of second-generation HDNNPs and of the CENT approach were combined in the development of a fourth-generation high-dimensional neural network potential (4G-HDNNP),¹⁸¹ which includes long-range charge transfer as well as an accurate description of local bonding. Like in third-generation HDNNPs, the total energy of 4G-HDNNPs is the sum of a short-range part and a long-ranged electrostatic energy,

$$E_{\text{total}} = E_{\text{short}} + E_{\text{elec}} \quad (45)$$

Both contributions are, however, calculated in a different way as illustrated in Figure 17.

First, the electrostatic energy is determined employing charges derived from a charge equilibration process. Like in CENT, the charge equilibration relies on environment-dependent electronegativities that are expressed by individual atomic neural networks, which are constrained to be the same for a given element. Different from the procedure in CENT, in the training process of these networks it is not the goal to minimize the electrostatic energy. Instead, the electronegativities are constructed to reproduce a reference data set of Hirshfeld charges¹⁶⁴ obtained from DFT calculations. As these charges are not trained directly but indirectly via the electronegativities, they depend on the full system. These charges are then used to compute the long-range electrostatic energy E_{elec} . Compared to CENT, which uses atomic charges primarily as auxiliary quantities to construct the total energies using eq 38, the charges in 4G-HDNNPs have a qualitative physical meaning within the well-known limitations of the

underlying charge partitioning scheme. The resulting electrostatic energy would be most affected by this uncertainty in the absolute values of the charges for short interatomic distances, which is avoided by using a screening function inside the cutoff spheres. Remaining errors are corrected by the short-range part by construction like in third-generation HDNNPs.

To avoid double counting the energy terms, the electrostatic energies and forces are removed from the respective reference data and the remaining contributions are represented by the short-range networks as a sum of atomic energies,

$$E_{\text{short}} = E_{\text{ref}} - E_{\text{elec}} = \sum_{i=1}^{N_{\text{atom}}} E_i(\mathbf{G}_i, Q_i) \quad (46)$$

In contrast to second-generation HDNNPs the “short range” atomic energies depend not only on the local atomic environments up to a cutoff radius, which are described by ACSFs, but in addition also on the partial charge of the respective atom as obtained from the charge equilibration, which is used as an additional input neuron. This partial charge contains information about the global electronic structure and ensures that both the electrostatic energy as well as the short-range energy can consistently adapt to redistributions in the global charge density. For the training of the short-range atomic neural networks energies, as well as forces, are used, which requires taking into account the derivatives of the atomic charges with respect to the positions of all atoms in the system.

Compared to second and third-generation HDNNPs and also to the CENT approach, 4G-HDNNPs have a much broader applicability, as they are suitable for systems with and

without nonlocal charge transfer, are able to describe covalent bonds with high accuracy, and in contrast to CENT are not restricted to materials with predominantly ionic interactions. Like CENT and BpopNNs, also 4G-HDNNPs can be constructed to simultaneously describe different global charge states of a system, for example, a set of ionized clusters, or (de)protonation reactions.

In first applications, 4G-HDNNPs have provided very promising results for organic molecules, ionic and metal clusters, and metal clusters adsorbed at periodic oxide surfaces.¹⁸¹ It remains to be seen to which extent 4G-HDNNPs are able to describe mainly nonelectrostatic long-range interactions resulting, for example, from Fermi-level shifts in semiconductors caused by defects. There are first hints that 4G-HDNNPs are sensitive to distant doping, as has been shown for the doping-dependent adsorption geometry of small metal clusters at surfaces,¹⁸¹ but a further analysis is needed to disentangle electrostatic effects from nonlocal information provided to the short-range neural networks.

6. CONSTRUCTION OF HIGH-DIMENSIONAL NEURAL NETWORK POTENTIALS

6.1. General Strategy

The development of HDNNPs is a multistep process consisting of the construction of the underlying reference data set, which is obtained in electronic structure calculations, the determination of the weight parameters of the atomic neural networks, and the final validation of the potential. All steps are equally important and not separable from each other, because they are intimately connected in a self-consistent workflow.

6.2. Construction of the Reference Data Set

The selection of the structures in the reference data set is an important step in the construction of any ML potential, as the underlying functional form is not based on physical principles. Instead, the physical shape of the PES has to be learned from the information provided in the reference data. Although in principle most low-dimensional systems would allow the development of first-generation NNPs based on a systematic grid of configurations, even early NNPs typically relied on nonuniform distributions of data points,³⁰ which enabled focusing on the chemically most relevant configurations.

For HDNNPs, the use of grids is no option due to the exponential growth in the number of points as a function of the degrees of freedom. Although the number of neighboring atoms in the atomic environments is limited by the cutoff radius, which drastically simplifies the problem, even within the cutoff spheres the number of possible structures exceeds by far the available computational resources needed for a systematic mapping of the configuration space. Consequently, the calculations need to be restricted to those structures that are most important. Once this relevant configuration space within the cutoff spheres has been mapped and included in a potential, HDNNPs can be applied to simulations of very large systems, which represent a combination of the known energy contributions of all the individual atomic environments that can be learned from smaller systems.

Initial data sets can be obtained in a variety of ways. If the main structural features, like crystal structures or molecular entities, are known, the construction of a first data set can be based on this information, ideally also including distorted structures and thermal fluctuations. For molecular systems,

also normal mode sampling can be used.^{139,202} Often, ab initio molecular dynamics simulations are employed to sample parts of the configuration space as starting point. However, these approaches are usually insufficient for an exhaustive sampling of the full relevant configuration space including repulsive structures²⁰³ and transition states, which have been suggested¹⁴⁴ to be included, for example, by metadynamics.²⁰⁴ The search for missing but physically relevant configurations can in general be guided by many simulation techniques such as molecular dynamics, which has been demonstrated already for other types of potentials such as the modified Shepard interpolation for the example of gas-surface dynamics.¹⁹

The key for generating the reference data sets for constructing high-dimensional ML potentials is their high flexibility, which is an important difference to conventional potentials. To illustrate this advantage, we first turn to classical force fields. In force fields and other physics-based conventional empirical potentials it is possible to generate a large number of structures, for example, by molecular dynamics, which can then be computed by electronic structure methods. If the deviation between the force field prediction and the electronic structure result is too large, the data point can be used to improve the potential. However, the possible improvement is limited by the often very inflexible functional form, and a disadvantage of this approach is the need for demanding electronic structure calculations that are even needed just for the assessment of the quality of the potential. Consequently, many unnecessary electronic structure calculations have to be performed for configurations, which are already reasonably well described by the potential, as there is no other way for testing the potential.

In this respect ML potentials such as HDNNPs offer a substantial advantage due to their high flexibility resulting from the very large number of parameters in a hierarchical functional form. Due to their nonphysical, that is, unbiased, functional form and their highly flexible structure, there are many different local minima that can be obtained in the training process. All these local minima will adequately reproduce the known training set, but predictions for structures that are far from the training data will often strongly differ among the available HDNNPs. Consequently, the difference in predictions for structures not included in the training process can be used to identify those structures that are not yet well described. For this identification just the cheap evaluation of several different HDNNPs is required while no expensive electronic structure calculation needs to be performed. This concept called “active learning” or “query by committee” has been well-known in the computer science community²⁰⁵ for many years and has been applied in the development of ML potentials in 2012²⁰⁶ for the construction of a second-generation HDNNP for copper. Nowadays, active learning is a standard procedure in the generation of reference data sets^{207–211} for many different types of ML potentials, and a detailed description of the procedure in case of HDNNPs can be found, for example, in refs 138 and 210. Active learning has also been demonstrated independently to be a very useful tool for other types of machine learning potentials such as moment tensor potentials.²¹²

The general procedure of active learning for the construction of a reference data set is shown schematically in Figure 18. The goal is the representation of the unknown energy curve shown in black. In panel a only a few data points highlighted as yellow diamonds are available, which cover only a part of the

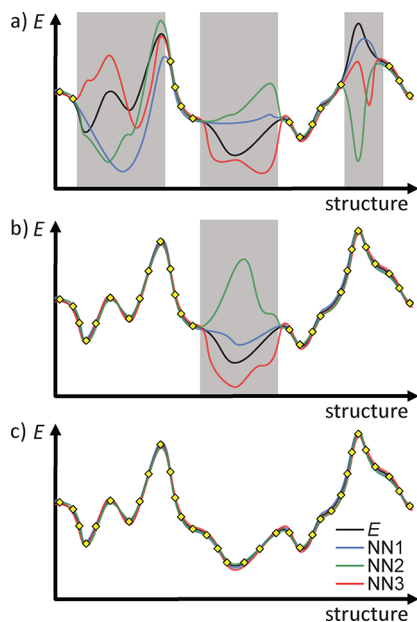


Figure 18. Active learning: Panels a, b, and c each contain three different neural network potentials (blue, green, and red curves) approximating the unknown black potential energy curve E . Only the yellow points are known for the training process. In the regions close to the known data points all three neural network potentials agree very well, while in between these points they can differ strongly. This difference can be used to identify new structures that should be added to the training set from panels a–c until the poorly sampled regions shown as gray areas are completely filled by data points and disappear.

configuration space. Now several HDNNPs shown in red, green and blue are trained, which well reproduce the regions close to these training data. In the large gaps indicated as gray regions in between the training points, all potentials predict very different energies and forces. These differences can be used to select additional reference structures for electronic structure calculations, which have been added in panel b to reduce the regions that are not well sampled. This process is repeated iteratively until the full relevant configuration space is well covered in panel c. In practice, the relevant configuration space is defined by the structures that are accessible in simulations of the desired type, and a large number of trial configurations should be generated with preliminary potentials under the simulation conditions for the system of interest. As soon as the set of HDNNPs predicts the same PES within a predefined error threshold of typically a few meV/atom, the potential is ready for applications.

Often the data sets used to construct HDNNPs are very large and contain tens of thousands of electronic structure calculations. Consequently, efficient electronic structure methods such as DFT are most frequently used for condensed systems. Several strategies have been developed in recent years to reduce this effort. Apart from the active learning approach described above, which allows running electronic structure calculations selectively for those structures that are important but missing, methods have been developed to select only those configurations that are structurally distinct.¹⁴² Further, it is common practice to combine different types of systems such as molecules, clusters, bulk, and surface calculations in a single training set. In these cases it is very important to use a very high level of convergence in the electronic structure calculations, in particular with respect to k-point grids in

periodic calculations, to keep numerical noise to a minimum. Even the use of different electronic structure codes for the same method and physical model typically leads to numerically inconsistent data that cannot be combined easily for training. Further, it has been demonstrated that HDNNPs for large systems can be constructed from smaller molecular fragments,^{55,147,213,214} which is a direct consequence of the locality of the atomic energy contributions in eq 2. These fragment-based approaches are expected to work best for local methods such as second and third-generation HDNNPs, but similar strategies might also be applicable to fourth-generation potentials.

To exploit the maximum amount of information from electronic structure calculations, apart from the total energy also forces are now routinely used for the determination of the neural network parameters,^{206,215–217} and even the stress tensor has been suggested for training HDNNPs.²¹⁸ Forces offer substantial advantages in particular for larger systems, as total energies can suffer from error compensation among the individual atomic energy contributions,¹⁴⁷ while forces are physically well-defined observables. For other types of ML potential, even the exclusive use of forces has been suggested.^{55,66}

6.3. Training

For a given data set, the values of the weight parameters have to be determined. This is usually done iteratively by repeatedly cycling through the data, in most cases consisting of energies as well as forces,^{66,206,215–217} employing a gradient-based optimization algorithm. A full presentation of the data set is called epoch. The required gradients are the derivatives of the energy and force errors, that is, the differences between the neural network predictions and the reference values from electronic structure calculations to be minimized, with respect to the neural network weights. Since the electronic structure data does not depend on the NN weights, merely the gradients of the NN energies and forces with respect to the NN weights are needed. These gradients can be calculated very efficiently using backpropagation,²¹⁹ a recursive scheme computing the terms of the derivatives step by step starting from the output layer and progressing through the network until the input layer is reached. These gradients can then be used in a variety of gradient-based optimization algorithms. Often the term backpropagation is used in the meaning of a steepest-descent optimization, but the gradients are applicable to all types of gradient-based learning algorithms such as conjugate gradients methods²²⁰ and the Levenberg–Marquardt algorithm.^{221,222} In the most basic case, the error function Γ to be minimized takes the simple form¹⁴⁴

$$\begin{aligned} \Gamma = & \frac{1}{N_{\text{energies}}} \sum_{A=1}^{N_{\text{energies}}} \left(\frac{E_{A,\text{ref}} - E_{A,\text{NN}}}{N_{\text{atom}}} \right)^2 \\ & + \gamma \frac{1}{N_{\text{forces}}} \sum_{A=1}^{N_{\text{forces}}} \left(\frac{F_{A,\text{ref}} - F_{A,\text{NN}}}{N_{\text{atom}}} \right)^2 \end{aligned} \quad (47)$$

The energies used for training HDNNPs are total energies, or binding energies that are obtained by removing the free atom energies. Hence, a preparatory partitioning of the reference energies into individual atomic energies is not required. Instead the total energy is automatically distributed into individual atomic energies by the HDNNP in the training process. These atomic energies are no physical observables but just represent

mathematical auxiliary quantities to construct the total energy. It has been shown for example for metal–organic frameworks that different HDNNPs of the same quality can have very different internal distributions of the energy.¹⁴⁷ The prefactor γ is used to balance the impact of the force components, which outnumber the energies by far, and the potential energies in the training process.

Modern HDNNPs are rarely trained by minimizing simple loss functions such as eq 47. Instead, sophisticated algorithms such as the Kalman filter^{223,224} are often used. In fact, the adaptive, global, extended Kalman filter²²⁴ was proposed very early for training NNPs.³⁰ An important feature of the Kalman filter is the frequent weight update after the presentation of each single piece of information, that is, energy or force component, while other state-of-the-art optimization algorithms rely only on one weight update per epoch, that is, after processing the full data set, using an averaged gradient. The latter algorithms are consequently more suitable for parallelization, while the explicit use of each piece of information with subsequent weight update makes the Kalman filter particularly efficient in terms of iterations needed to reach a local minimum. As a consequence these iterations are computationally more demanding, but overall the Kalman filter is often still more efficient. The efficiency can be further increased by defining a threshold for the error and only those data points exceeding this threshold are used in the update process. A detailed discussion of the Kalman filter can be found elsewhere²²⁴ and is beyond the scope of this review. Also parallel training using a multistream Kalman filter has been proposed.^{225,226} Many other algorithms are available, and the training of neural networks is a very active field of research with promising new developments such as the adaptive moment solver (ADAM),²²⁷ and dropout.²²⁸

The optimization of the HDNNP starts from a set of initial weights, which can be chosen randomly, and also a variety of initialization schemes like the one proposed by Nguyen and Widrow²²⁹ or the adapted weight initialization method²³⁰ are available. The initial error of the HDNNP can further be reduced by employing a preconditioning scheme¹³⁸ to adjust the average and standard deviation of the NN energies to those of the reference data before starting the weight optimization. Alternatively, it has also been suggested to optimize neural network weights using other methods such as genetic algorithms²³¹ or simulated annealing.²³²

Apart from the initial weights, also the architecture of the atomic NNs must be chosen. For most systems it has been found that between 50 and 100 ACSFs and only two to three hidden layers, each containing between 15 and 45 neurons, are sufficient to construct very accurate potentials, with very little changes in the errors if a few neurons are added or removed. Still, also very large NNs have been used, for example, in the case of the ANI-1 potential aiming for a broad transferability across a wide range of organic molecules, which made use of 768 input neurons in a large 768–128–128–64–1 architecture.¹³⁹

The error of ML potentials is typically measured by the root mean squared error (RMSE),

$$\text{RMSE} = \sqrt{\frac{1}{N} \sum_{i=1}^N (E_{i,\text{ref}} - E_{i,\text{NN}})^2} \quad (48)$$

and sometimes also alternatively by the mean absolute deviation (MAD), and it is common practice to specify the

energy errors normalized per atom. This has been found useful to report size-consistent errors, which are essential if systems of different sizes are used in the same training set. Otherwise, larger systems like supercells would artificially increase the error. Still, in general the RMSE of the energy must be treated with some caution as a measure for accuracy as error compensation may be present for the atomic energies, and the specific values of the atomic energies have a high degree of uncertainty if they are trained with the total energy as target property only. Thus, for large systems, monitoring as well the RMSEs of the forces in the training process is important.

The training of the atomic neural networks is intimately connected to the validation process, which will be discussed in the following section. Because of the large number of weight parameters N_w in HDNNPs, which for an atomic NN with N_{hid} hidden layers is given by

$$N_w = \sum_{k=1}^{N_{\text{hid}}+1} (N_{k-1} N_k + N_k) \quad (49)$$

where N_k is the number of neurons in the respective layer, often several thousand parameters need to be optimized. Thus, the determination of the weight values is a very high-dimensional optimization problem and there is no hope to find the global minimum. Still, sufficiently accurate local minima suitable for reliable simulations are typically found, which then need to be carefully validated before application. Further details on the training process of HDNNPs and a discussion of some technical aspects can be found in ref 138.

6.4. Validation

The challenge of assessing the accuracy of an interatomic potential is as old as atomistic simulations. Conventional empirical potentials rely on physically meaningful functional forms employing more or less drastic approximations, which might give rise to inaccuracies or even failures resulting from the limitations of the functional form and/or the parameter values. Still, they offer the advantage that a physical understanding of their limitations is possible in many cases. For machine learning potentials the situation is different as it is a priori clear that the functional form is nonphysical in the sense that the analytic form is not based on physical interaction models. The advantage of this ansatz is that there are no intrinsic limitations of the functional form which could restrict the accuracy of the potential. In combination with the high flexibility arising from a large number of rather simple functional units and the associated parameters a very close agreement with the references data can be achieved typically reaching about 1 meV/atom for energies and about 0.1 eV/Å for the forces.

Like all ML potentials, HDNNPs learn the atomic interactions only from the information included in the training set. Failures and inaccuracies can thus result primarily from three sources: the available data, the number of parameters in the model, that is, the architectures of the atomic NNs defining the flexibility, and in limitations of the optimization process, for example, trapping in local minima. Therefore, validating ML potentials is a crucial step before production simulations can be carried out.

The validation of HDNNPs is a multistep process. First, a preliminary HDNNP is constructed based on an initial data set, which may consist, for example, of ab initio MD trajectories or even random structures. This data set is not expected to cover the full relevant configuration space and may

include only a few hundred structures. The first analysis to be done is to determine the range of coordinate, that is, descriptor, values that is already covered by the data set. This is important as neural networks exhibit a poor performance when used for extrapolation outside the training set as shown schematically for a one-dimensional system described by one descriptor function G_1 in Figure 19. In this

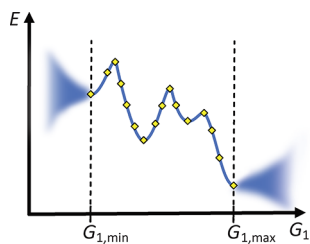


Figure 19. Illustration of extrapolation for a one-dimensional potential energy surface. While ML potentials provide reliable energy predictions in regions with a high density of reference data (yellow symbols), they have very limited extrapolation ability and the uncertainty is high outside this region.

example, the energies outside the interval $[G_{1,\min}, G_{1,\max}]$ have a very high uncertainty and predicted energies and forces can be dramatically wrong. Fortunately, it is very easy to automatically detect these extrapolation cases even in high-dimensional systems by comparing the ACSF values for each atomic environment of interest with the respective intervals covered by the training set. If a case of extrapolation is found for one or more symmetry functions, an electronic structure calculation can be carried out for this structure, which can then be included in the training set to extend the applicability of the HDNNP.

In the next step, the early stopping method (Figure 20) is used to check if the reference data set is densely sampled or if in some region the available structures are too sparse. For this purpose, the reference data set is randomly split into a training set, which is used to optimize the weight parameters of the

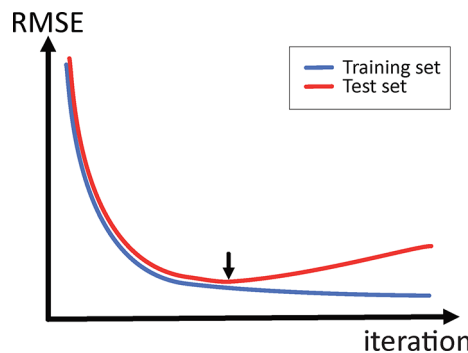


Figure 20. Illustration of “early stopping”. The available reference data set is randomly split into a training set used to determine the weight parameters of the neural network and an independent test that is not used in the training process. While the root mean squared error (RMSE) of the training set typically decreases as the HDNNP learns to represent the training data, the RMSE of the test set first decreases as the HDNNP learns the overall topology of the potential energy surface. Then the test set error often starts to increase slightly again when overfitting sets in. The black arrow indicates the iteration with the best generalization properties of the potential for structures not included in the training set.

HDNNP, and an independent test set not used in the fitting process. The RMSE values of both data sets are then monitored during the fit. Initially, both RMSE values decrease as the HDNNP learns the overall topology of the PES. After a few iterations, the test set RMSE may then exhibit a local minimum followed by a slight increase while the RMSE of the training set further decreases. This is the onset of overfitting, which is a very accurate representation of the training data while intermediate data points show very large errors. HDNNPs with significant overfitting, for example, an RMSE of the test that is notably larger than the RMSE of the training set, should not be used in simulations. In general, the tendency for overfitting increases with the flexibility of the HDNNP, that is, with a growing number of weight parameters resulting from large numbers of neurons in the atomic neural networks. Reliable potentials will show very similar small errors for both the training and the test set. If the RMSE values of both sets remain large, the flexibility of the atomic NNs is too small and more neurons and possibly hidden layers should be used, but this can also be an indication of numerical inconsistencies in the data set. Although the test set is not used for training the NNs, the final potential is not fully independent of the test set as its RMSE is used for the selection of the fit. Thus, it is also common practice to use a third validation set for assessing the overall performance once a decision based on the test set has been made.

The early stopping method is a standard procedure for training neural networks. Nevertheless, it is not a sufficient test to ensure that the reference data set covers all relevant configurations. The reason is that in the early stopping method only those points can be distributed into a training and a test set that are in principle available in the reference set. If, however, certain types of configurations are completely missing, an unreliable description of these structures will remain undetected. The problem is illustrated for a system described by two symmetry functions G_1 and G_2 in Figure 21.

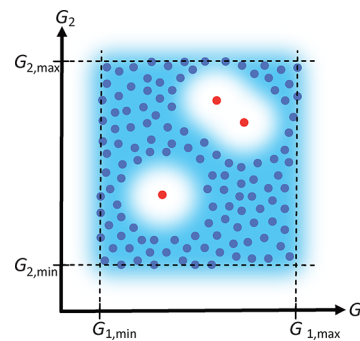


Figure 21. Illustration of “holes” in the reference data set for a two-dimensional system described by the symmetry functions G_1 and G_2 . While the blue region is well represented by the data set shown as blue dots, the red points are far from the training structures and thus cannot be expected to be accurately predicted by the HDNNP.

The blue reference data points cover the light blue region very well, while the red points are far from these data points. If we are interested in the prediction of the energies and forces of the red points, neither the extrapolation check nor the early stopping method will detect a possible problem with the reliability of these points. In principle the situation is the same as in the gray regions in Figure 18, which have a very high uncertainty due to the absence of training points. Still, the

presence of these “holes” in the data set can be detected using active learning. Starting from several HDNNPs trained to the same data set, a large number of candidate configurations is screened for deviations between the predictions for the energies or forces of the available HDNNPs. If for a structure a large uncertainty is found, an electronic structure calculation should be performed and the structure should be included in the training set to refine the HDNNPs.

This example clearly shows that the validation, training, and construction of the data set are intimately related and cannot be dealt with individually. Instead, the whole process involving all three steps has to be repeated iteratively as shown in Figure 22 until a converged data set and potential has been obtained.

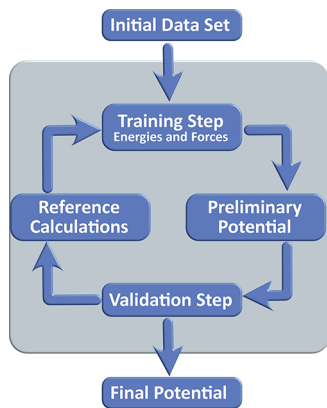


Figure 22. Iterative construction of a high-dimensional neural network potential. Starting from an initial data set, a first preliminary HDNNP is obtained. This HDNNP is validated in a multistep process (Figure 23). If the quality of the potential is insufficient, problematic structures are identified and added to the training set until the final potential is obtained.

We note that this search for holes in the data set is the most general validation step, which is in principle also able to detect extrapolating structures and less well sampled regions like the early stopping method. Therefore, it represents the most stringent test for the construction and validation of HDNNPs.

The overall validation process is summarized in the flowchart in Figure 23. Once a potential has passed all the

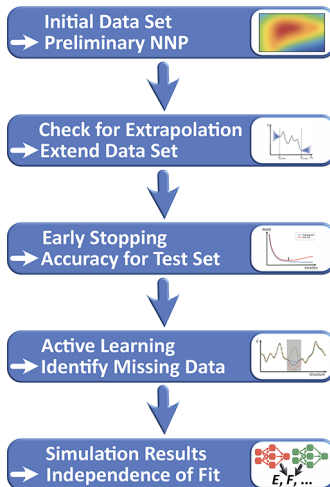


Figure 23. Flowchart of the multistep validation process of high-dimensional neural network potentials.

steps consisting of extrapolation checks, early stopping, and the active learning search for holes, the simulations should be finally carried out with several HDNNPs of the same quality, differing, for example, in the architectures of the atomic neural networks or the initial seeds used to generate the random starting weights for the training, to ensure that the results are independent of the particular fit and physically meaningful.

Several comments should be made at this point regarding the validation of the potential. First, the overall validation process relies on the availability of a high-quality and consistent reference data set. If the data is too noisy, for example, if only a moderate convergence level has been chosen in the electronic structure calculations, or if even wrong data points are included, a rather high error for the energies and forces will be obtained. For the identification of wrong electronic structure calculations there is a rather simple but efficient test (Figure 24). In this test the errors of all data

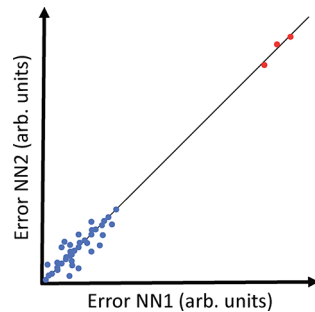


Figure 24. Illustration of the consistency check of the reference data set. For this test the energy or force errors of all data points obtained with one HDNNP are plotted as a function of the respective errors of a second HDNNP. The blue points show the typical behavior in that the overall errors are small and each of the potentials provides a better representation of some of the points. The red points correspond to critical structures, as they cannot be represented by any of the HDNNPs. This may be an indication of contradictory data in the training set.

points of one HDNNP are plotted versus the respective errors of another HDNNP. For “normal” fitting errors, the respective points will be found close to the axes with overall low errors, as it is very likely that most points will be accurately represented at least by one of the potentials. Therefore, the vast majority of points will be found in the bottom left region corresponding to a good representation in both HDNNPs. If, however, points are located in the upper right corner, this indicates that these points cannot be represented accurately by any of the HDNNPs. In such a situation the reason is usually contradictory information in the data set, which may result, for example, from convergence problems in the electronic structure calculations or large numerical noise due to a poor k-point sampling. Such points should then be investigated and removed from the data set.

Another comment addresses the use of learning curves²³³ as shown schematically in Figure 25. Learning curves are frequently used to check the convergence of potentials with respect to the number of data points available in the training process. In this respect they provide similar information to the early stopping method. Initially, a first HDNNP is constructed using only a small fraction of the available data. As a few data points are straightforward to learn, the resulting training set RMSE is very small. On the other hand, the small training set

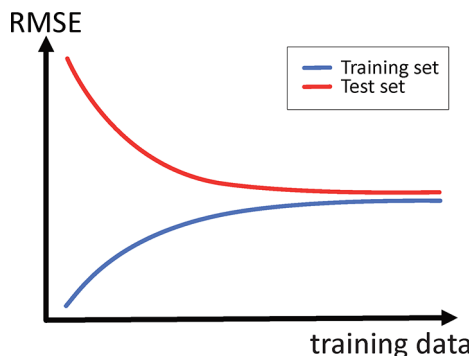


Figure 25. Learning curve monitoring the root mean squared error (RMSE) of the training and the test set as the training data set size is increased. The training error slightly increases with data set size as the representation of the more and more complete set of features of the potential energy surfaces becomes more challenging. At the same time the RMSE of the test set decreases and finally converges indicating that the configuration space covered by the training data is sampled in a dense and representative way.

does not cover the full configuration space and the RMSE of the test set is very large due to overfitting. If now step by step more data are used, the fitting problem becomes more challenging for the HDNNP and the training set error increases, while the test set error decreases. Finally both errors converge indicating that a sufficient number of data points has been used. This approach is very instructive, but unfortunately it suffers from the same limitations as the early stopping method in that inaccuracies in regions of the configuration space, for which no data are available, remain undetected. Therefore, learning curves have to be treated with care unless a full coverage of the configuration space is guaranteed.

7. DISCUSSION

7.1. Applicability and Applications

Of all generations of neural network potentials discussed above, to date second-generation HDNNPs—like equivalent alternative second-generation ML potential types, for example, GAPs^{57,58}—have been used most frequently in applications throughout the literature. Further, to some extent also first-generation NNPs are still in use, if the description of low-dimensional systems is sufficient for the scientific question. This is the case, for instance, in the field of reaction dynamics of small molecules in the gas phase,^{87,88,234} which can be described in full dimensionality also by NNPs of the first generation. Although also second-generation HDNNPs are equally applicable to these systems, the advantage of using first-generation NNPs employing a single neural network for expressing the energy globally is the higher computational efficiency with about equal accuracy, as second-generation HDNNPs involve the evaluation of one neural network per atom. The explicit treatment of long-range electrostatic and dispersion interactions is usually not required for small systems, as global descriptions in first-generation NNPs allow taking these interactions fully into account irrespective of the atomic distance. Nevertheless, most systems of interest contain a large number of atoms, and are thus beyond the scope of first-generation NNPs that are applicable to systems with up to about 10 atoms only.

Compared to electronic structure calculations HDNNPs of the second generation allow an extension of atomistic

simulations in two ways. First, the size of the system can be drastically increased compared to the number of atoms in the structures of the training set. While the system size in the training data is restricted by the number of atoms that can be dealt with in the reference electronic structure calculations, that is, up to a few hundred atoms in case of DFT, once the HDNNP has been trained much larger systems can be studied by increasing the number of atomic neural networks in Figure 5 accordingly. For this extension of the system size it must be taken into account that the atomic configurations emerging in the atomic environments of the extended system must also be present in the smaller structures of the training set to avoid unreliable extrapolations. If, on the other hand, in large-scale simulations problematic environments are found, they can be extracted and included to the training set using systems of reduced size for the electronic structure calculations.^{235,236} As there is one neural network per atom that can be evaluated independently, the method is well suited for parallelization,¹³⁶ and as a rule of thumb current CPU architectures allow computing the energies and forces of about 500 atoms per second and CPU core.

Apart from the increase of the system size, the second possible extension of atomistic simulations enabled by HDNNPs concerns the number of configurations that can be computed. Molecular dynamics simulations can be run on much longer time scales, like tens or hundreds of nanoseconds for systems containing thousands of atoms, while in ab initio MD only a few 100 ps of systems of moderate size are accessible. Also other simulation techniques such as Monte Carlo simulations benefit from the larger number of configurations that can be processed^{145,235,237}

While the extension of the time and length scales of atomistic simulations with respect to electronic structure methods is a clear advantage of HDNNPs, this extension would also be possible using conventional empirical potentials and force fields, which often can be constructed with less effort in terms of the number of reference calculations and are even cheaper to use. This raises the question for which systems HDNNPs offer additional significant advantages, making them a better choice than conventional types of potentials. One important advantage of HDNNPs—and ML potentials in general—is that no knowledge about the physical functional form of the atomic interactions is required to reach a very high accuracy. This enables the construction of potentials for systems which are difficult to describe, such as interfaces with unconventional atomic environments, amorphous systems,²³⁸ and organic–inorganic hybrid systems,¹⁴⁷ and also systems with very different types of bonding present in different parts, such as covalent bonds in molecules and metallic bonding in a surface, can be studied. Further, HDNNPs are reactive and enable the description of the making and breaking of bonds, which is obviously necessary for studying chemical processes, but is also very important for major atomic rearrangements in structural phase transitions.²³⁹ This reactivity is not only included in certain regions of the system, like in QM/MM methods,²⁴⁰ but instead the whole system is treated on an equal footing, which is important if reactions can take place throughout the system, such as the dissociation and recombination of water molecules in solution or at interfaces.²⁴¹

HDNNPs, in particular of second generation, have been applied for almost 15 years to a manifold of systems and a wide range of problems in chemistry, physics, and materials science.

It is thus impossible to provide a complete list of the numerous systems that have been studied using HDNNPs, but typical examples and the corresponding references are given in Table 2.

Table 2. Example Applications of High-Dimensional Neural Network Potentials

system	ref
Elemental Bulk Systems	
silicon	50,116,218,239,242,278
carbon	243,279
sodium	280,281
copper	116,140,206,218
molybdenum	116
nickel	116
lithium	116
germanium	116,218
gold	218,282
Multielement Bulk Systems	
MOFs	147
LiMn ₂ O ₄	148,283
simple oxides	160,196,245,246
GeTe	247,248,284
SiGe	218
alloys	123,250,253–255,285,286
Mn _x Ge _y	244
perovskites	251
vdW heterostr.	252
LiPON	287
WS ₂ (CENT)	288
CaF ₂ (CENT)	194,195
NaCl (CENT)	54
Water and Aqueous Systems	
water clusters	161,211,270,289–294
bulk water	106,210,271,272,295,296
NaOH solutions	273,274,297–299
water at copper	275,300
water at ZnO	241,276,277,301
water at alloys	145
water at hBN	149
Surfaces	
supported clusters	146,236,259,260
gas-surface dynamics	261–263,302
alloy surfaces	237
adsorption	256,258,303,304
metal surfaces	206,305
Molecular Systems and Clusters	
metal clusters	206,235,267–269,306,307
alloy clusters	235,266,304,308
organic molecules	139,140,176,213,264,126,144,211,265,309
gas phase reactions	87,135,234

The very first applications of HDNNPs addressed elemental bulk materials like silicon, a prominent benchmark system for the development and assessment of interatomic potentials, for which pressure-induced phase transitions have been studied.²³⁹

It could be shown that HDNNPs are able to describe the structural and energetic properties of a wide range of crystalline phases involving very different atomic environments with DFT accuracy.²⁴² Further applications to elemental solids addressed the graphite-to-diamond transition in carbon²⁴³ and the melting properties of sodium.²⁸¹ Apart from their general

relevance, elemental solids have to date remained important benchmark systems.^{116,218} Moreover, numerous binary solids such as ZnO,¹⁶⁰ Mn_xGe_y,²⁴⁴ zirconia,²⁴⁵ and TiO₂²⁴⁶ have been studied. A particularly exhaustive characterization of the phase change material GeTe has also been reported,^{238,247–249} which demonstrated the applicability of HDNNPs to amorphous phases and order-disorder transitions. For the binary MgCa system it has been shown that phase diagrams of alloys can be explored systematically.²⁵⁰ Further bulk solids that have been studied include more complex systems such as metal-organic frameworks (MOFs)¹⁴⁷ as an example for an organic-inorganic hybrid system, perovskites,²⁵¹ van-der Waals heterostructures,²⁵² and lithium intercalation compounds,¹⁴⁸ as well as lithium-alloys,^{253,254} which are very important for modern battery technology, and even multicomponent alloys.^{123,255}

Apart from bulk solids, also surfaces have received a lot of attention.²⁰⁶ HDNNPs have been used to study adsorbate structures²⁵⁶ including efficient saddle-point searches²⁵⁷ and adsorbate-induced facetting of surfaces,²⁵⁸ the morphology of supported nanoparticles and clusters,^{146,236,259,260} and molecule-surface scattering processes.^{261–263} In the latter field, the use of HDNNPs has finally enabled overcoming the limitation to frozen surfaces in atomistic simulations, thus allowing the inclusion of the role of surface temperature and mobility in gas-surface dynamics, a long-standing problem in the surface science community.

In addition, HDNNPs have also been successfully constructed for a series of nonperiodic systems such as organic molecules,^{176,264,265} and gas phase reactions of multichannel systems,^{135,234} and even highly transferable general-purpose potentials for organic molecules, such as ANI-1,¹³⁹ ANI-2,¹⁵⁰ and the tensormol model chemistry^{144,266} have been introduced. Numerous studies have also been reported for free metal^{206,235,267–269} as well as alloy²³⁵ nanoclusters.

Water, the most important solvent, has received a lot of attention as well, in the form of small clusters,^{211,270} but most importantly for the bulk. Liquid water is certainly among the most frequently studied systems, and in spite of all efforts, numerous interesting properties have remained a challenge for computer simulations, either because the simulations would be too demanding for ab initio MD, or because of the limited accuracy of classical water potentials. HDNNPs have allowed study of the role of dispersion interactions and the hydrogen bond network on the melting temperature and the density anomaly,^{106,271} the relative stability of hexagonal and cubic ice,¹⁰⁶ and the role of nuclear quantum effects.²⁷² The possibility of investigating the dissociation and recombination of water molecules using HDNNPs has also been essential in simulations of aqueous NaOH solutions.^{273,274} Further, interfacial water at the metal²⁷⁵ and oxide surfaces²⁷⁶ has received a lot of attention. For water at zinc oxide surfaces it could be shown that the computation of vibrational signatures allows identification of the interfacial water species and their hydrogen-bond patterns.²⁷⁷ Moreover, nanoparticles in contact with water¹⁴⁵ and water confined between hBN sheets¹⁴⁹ have been investigated.

Most of these applications refer to second-generation HDNNPs, while third-generation HDNNPs have been rarely used,^{160,161} as the inclusion of environment-dependent charges introduces substantial computational overhead with only little overall improvement of the potentials for many systems. HDNNPs of the fourth generation, which provide a more

accurate description of long-range interactions and include nonlocal effects, are just emerging. Examples are the CENT approach, which has been applied to systems with predominantly ionic bonding,^{54,194,195} BpopNN for Li_nH_n,¹⁹⁷ and 4G-HDNNPs, which have been reported for a series of benchmark cases.¹⁸¹

7.2. Outlook

The development of HDNNPs—like the development of ML potentials in general—is a very active and rapidly growing field, and many challenges remain to be solved. Apart from the further development of fourth-generation HDNNPs, the construction of the data sets, the inclusion of additional physics into the energy expressions, the development of new descriptor types, the treatment of multielement systems, and the prediction of additional physical properties are just a few examples.

Probably the most demanding step in the development of HDNNPs is the construction of the large reference data sets by electronic structure calculations. These calculations have to be carried out at a high level of convergence as noisy data can be problematic for two reasons: first, contradictory data will be present if similar atomic environments are associated with different energies and forces, which prevents a smooth convergence of the weight parameters in the optimization. Second, in the case of noisy data, some deviations between the HDNNP and the reference data are tolerable as the PES should not reproduce numerical noise, but as a consequence the formal fitting errors will remain relatively high and thus are of little use as a measure for the accuracy of the potential.

Instead of reducing the quality of the reference calculations, which is also problematic as ML potentials can only provide results as reliable as the underlying electronic structure method, the effort in the construction should be reduced by a more efficient choice of the reference configurations³¹⁰ resulting in a smaller number of data points and smaller systems. Work along both directions is in progress, for instance by selecting only the most representative structures from a pool of structures,¹⁴² which is not without challenges as a metric for the comparison of structures is required.^{108,311} An advantage of HDNNPs is that by construction they allow the combination of the reference structures with different numbers of atoms—with and without periodic boundary conditions—in a single training set in a consistent way, which enables construction of the reference data set in the most efficient way. Further, atomic environments, which are not well described, can be included in the training set using smaller molecular fragments designed to describe only the required environments,^{147,213,312} avoiding the computation of redundant information in other parts of the systems. The size of these fragments depends on the system and has to be carefully converged.

Recently, it has been proposed to focus the capabilities of ML potential on many-body terms, which are the most challenging to describe, by expressing a part of the PES as a sum of two- and three-body terms.^{179,313} This is a very promising step, in particular if combined with an explicit electrostatic treatment as in HDNNPs of third and fourth-generation. Another route of improving electrostatics is to go beyond point charge models and to include higher order multipoles¹⁵⁷ with the expression of the electron density through ML models as the extreme case.¹⁷⁷ The inclusion of higher-order multipoles might also yield further improved

fourth-generation potentials. Another possible improvement, which is currently receiving much attention, is the consideration of dispersion interactions,^{127,314} which in most cases are not as problematic as electrostatics, but may accumulate for some systems to form an important contribution that must not be neglected.¹⁷⁰ Formally, although less long-ranged, such dispersion-corrected HDNNPs would be classified as third-generation. A straightforward solution to include dispersion interactions without significant truncation would be a direct combination with dispersion correction schemes originally developed for DFT, such as the D3 method proposed by Grimme.¹⁶⁸ As HDNNPs can reach a very close numerical agreement with reference DFT data, D3 corrections can simply be added in the same way such that an inclusion in the training process, which would be an alternative approach,²⁷¹ is not needed.

A series of suggestions has been made to facilitate the construction of HDNNPs for systems containing more than a few elements. A possible starting point is the reduction of the number of descriptors by merging information about the nuclear charges^{123,126} or ion charges¹⁵¹ directly into the functional form. Alternatively, also reduced cutoffs have been used.¹³⁹ A different route has been taken by Onat et al. in implanted neural networks²⁵³ and in stratified neural networks.²⁸⁵ In this ansatz, first the HDNNPs of the involved elements are constructed, which are then combined with additional NNs describing their interactions. Another method is SingleNN, a modified HDNNP with weights shared across the elements.²⁵⁵

A field, which to date has remained to a large extent unexplored is the analysis of the properties and the interpretability of ML potentials. For empirical potentials it has been shown that a large number of spurious minima can be present compared to DFT.³¹⁵ Because of their high flexibility ML potentials could also be expected to show the same problem, but this has not been reported so far. Concerning the interpretation of ML potentials, for other types of potentials it has been attempted to physically interpret the individual atomic energies used in eq 2,^{316,317} but first results for HDNNPs have shown that the numerical values of the atomic energies, which are just mathematical auxiliary quantities, can strongly differ even for potentials of the same quality.¹⁴⁷

Recent progress has also been made in the field of descriptors and the prediction of further physical properties, like the expression of atomic spins and oxidation states by HDNNPs²⁸³ and the description of tensorial properties,³¹⁸ and this field is currently rapidly growing.³¹⁹ Next to descriptor-based approaches also message passing approaches based on deep tensor NNs processing Cartesian coordinates and nuclear charges such as SchNet,^{52,53,130} HIP-NN,³²⁰ AIMNet,¹⁸⁸ and PhysNet⁵⁵ learn the features and represent an important new direction of development. Such MPNNs are difficult to classify according to the hierarchy of generations used in this review, as the effective interaction range depends on the number of passing steps and covers the full range between second and fourth-generation potentials. Possible extensions toward fifth-generation HDNNPs remain speculative at this point, but such potentials may involve a closer integration of ML into electronic structure methods. Although different in spirit from atomistic machine learning potentials, it has already been demonstrated that, for example, exchange correlation functionals may be improved based on ML.^{321,322}

Finally, a lot of progress has also been made by the large variety of available software. Next to the RuNNer code,^{74,138,323} which was the first code implementing HDNNPs and has been used for their development, a wide range of alternative implementations is now available^{139,226,246,299,324–328} providing an easy entry to the field. Modern software libraries such as tensorflow³²⁹ have substantially facilitated the development of several of these codes.

8. SUMMARY

In this review, the current status of high-dimensional neural network potentials has been summarized. A classification scheme consisting of four generations has been introduced for this purpose, which can also be applied in a similar way to many other types of machine learning potentials. First-generation NNPs are applicable to low-dimensional systems, such as small molecules in vacuum or small molecules interacting with frozen surfaces. They make use of a global description of the potential energy, often employing a single feed-forward neural network only. The second generation of NNPs allows addressing high-dimensional systems with an arbitrary number of atoms in full dimensionality by expressing the total energy as a sum of environment-dependent atomic energies, which are computed by individual atomic neural networks. The first and to date most frequently used type of second-generation HDNNP is the approach proposed by Behler and Parrinello.⁵⁰ The input of the atomic neural networks is formed by a set of atom-centered symmetry functions describing the local chemical environments of the atoms up to a cutoff radius. Long-range interactions, most prominently electrostatics, are included without truncation in third-generation HDNNPs, which add a second set of atomic neural networks providing environment-dependent charges. Atomic neural networks corresponding to second-generation HDNNPs are then used to construct the remaining short-range part of the energy. Third-generation HDNNPs are applicable, if the charges depend on the local chemical environments only. In the case of long-range charge transfer or multiple charge states fourth-generation HDNNPs must be used, which allow for a global redistribution of the charge throughout the entire system. HDNNPs of the fourth generation are currently just emerging, but several very promising approaches have already been proposed to close this remaining gap in the applicability of current state-of-the-art ML potentials. Nowadays, in particular, HDNNPs of the second generation have found use in atomistic simulations, as for many systems they offer a very high accuracy close to the underlying electronic structure calculations, while their efficiency allows the calculation of millions of configurations with tens of thousands of atoms.

AUTHOR INFORMATION

Corresponding Author

Jörg Behler – Universität Göttingen, Institut für Physikalische Chemie, Theoretische Chemie, 37077 Göttingen, Germany;
 orcid.org/0000-0002-1220-1542; Email: joerg.behler@uni-goettingen.de

Complete contact information is available at:

<https://pubs.acs.org/10.1021/acs.chemrev.0c00868>

Notes

The author declares no competing financial interest.

Biography

Jörg Behler graduated in chemistry at the Universität Dortmund in 2000. He then joined the theory department of the Fritz-Haber-Institute of the Max-Planck-Society in Berlin, where he received his Ph.D. in physics in 2004. After a postdoctoral stay at the same place he moved to the ETH Zurich in 2006. In 2007 he established an independent research group at the Ruhr-Universität Bochum funded by several grants including a Liebig fellowship, as well as the DFG Emmy Noether and Heisenberg programs. In 2014 he obtained his habilitation in theoretical chemistry. In 2017 he became a full professor for theoretical chemistry at the Georg-August-Universität Göttingen. His main research interest is the development of machine learning potentials with applications to complex systems in chemistry and materials science.

ACKNOWLEDGMENTS

The author is grateful for financial support by the Deutsche Forschungsgemeinschaft (Be3264/12-1, Project No. 405479457). Discussions on Figure 16 with David Small are gratefully acknowledged.

ABBREVIATIONS

4G-HDNNP	fourth-generation HDNNP
ACSF	atom-centered symmetry function
AIMNet	atoms in molecules network
BpopNN	Becke population neural network
CENT	charge equilibration neural network technique
DFT	density functional theory
DFTB	density functional tight binding
eSNAP	electrostatic spectral neighbor analysis potential
FCHL	Faber-Christensen-Huang-Lilienfeld descriptor
FFNN	feed-forward neural network
GAP	Gaussian approximation potential
GDML	gradient domain machine learning
HDNNP	high-dimensional neural network potential
HIPNN	hierarchically interacting particle neural network
KRR	kernel ridge regression
LiPON	lithium phosphorus oxynitride
MD	molecular dynamics
ML	machine learning
MOF	metal–organic framework
MPNN	message passing neural networks
MTP	moment tensor potential
NN	neural network
NNP	neural network potential
PES	potential energy surface
PIP	permutation invariant polynomials
PSF	pair symmetry function
ReLU	rectified linear unit
RDF	radial distribution function
RMSE	root mean squared error
SNAP	spectral neighbor analysis potential
SOAP	smooth overlap of atomic positions
SVM	support vector machines

REFERENCES

- (1) Marx, D.; Hutter, J. *Ab initio Molecular Dynamics: Basic Theory and Advanced Methods*; Cambridge University Press, 2009.
- (2) Cornell, W. D.; Cieplak, P.; Bayly, C. I.; Gould, I. R., Jr; Merz, K. M.; Ferguson, D. M.; Spellmeyer, D. C.; Fox, T.; Caldwell, J. W.; Kollman, P. A. A Second Generation Force Field for the Simulation of

- Proteins, Nucleic Acids, and Organic Molecules. *J. Am. Chem. Soc.* **1995**, *117*, 5179–5197.
- (3) MacKerell, A. D., Jr; et al. All-Atom Empirical Potential for Molecular Modeling and Dynamics Studies of Proteins. *J. Phys. Chem. B* **1998**, *102*, 3586–3616.
- (4) Allinger, N. L.; Yuh, Y. H.; Lii, J.-H. Molecular Mechanics. The MM3 Force Field for Hydrocarbons. *J. Am. Chem. Soc.* **1989**, *111*, 8551–8566.
- (5) Jorgensen, W. L.; Chandrasekhar, J.; Madura, J. D.; Impey, R. W.; Klein, M. L. Comparison of Simple Potential Functions for Simulating Liquid Water. *J. Chem. Phys.* **1983**, *79*, 926–935.
- (6) van Duin, A. C. T.; Dasgupta, S.; Lorant, F.; Goddard, W. A. III ReaxFF: A Reactive Force Field for Hydrocarbons. *J. Phys. Chem. A* **2001**, *105*, 9396–9409.
- (7) Daw, M. S.; Foiles, S. M.; Baskes, M. I. The Embedded-Atom Method: A Review of Theory and Applications. *Mater. Sci. Rep.* **1993**, *9*, 251–310.
- (8) Stillinger, F. H.; Weber, T. A. Computer Simulation of Local Order in Condensed Phases of Silicon. *Phys. Rev. B: Condens. Matter Mater. Phys.* **1985**, *31*, 5262–5271.
- (9) Tersoff, J. New Empirical Model for the Structural Properties of Silicon. *Phys. Rev. Lett.* **1986**, *56*, 632–635.
- (10) Drautz, R.; Zhou, X. W.; Murdick, D. A.; Gillespie, B.; Wadley, H. N. G.; Pettifor, D. G. Analytic Bond-Order Potentials for Modelling the Growth of Semiconductor Thin Films. *Prog. Mater. Sci.* **2007**, *52*, 196–229.
- (11) Lenosky, T. J.; Sadigh, B.; Alonso, E.; Bulatov, V. V.; de la Rubia, T. D.; Kim, J.; Voter, A. F.; Kress, J. D. Highly Optimized Empirical Potential Models of Silicon. *Mod. Sim. Mater. Sci. Eng.* **2000**, *8*, 825–841.
- (12) Hammerschmidt, T.; Drautz, R.; Pettifor, D. G. Atomistic Modelling of Materials with Bond-Order Potentials. *Int. J. Mater. Res.* **2009**, *100*, 1479–1487.
- (13) Cohen, R. E.; Mehl, M. J.; Papaconstantopoulos, D. A. Tight-Binding Total-Energy Method for Transition and Noble Metals. *Phys. Rev. B: Condens. Matter Mater. Phys.* **1994**, *50*, 14694–14697.
- (14) Goringe, C. M.; Bowler, D. R.; Hernandez, E. Tight-Binding Modelling of Materials. *Rep. Prog. Phys.* **1997**, *60*, 1447–1512.
- (15) Elstner, M.; Cui, Q.; Munih, P.; Kaxiras, E.; Frauenheim, T.; Karplus, M. Modeling Zinc in Biomolecules with the Self Consistent Charge-Density Functional Tight Binding (SCC-DFTB) Method: Applications to Structural and Energetic Analysis. *J. Comput. Chem.* **2003**, *24*, 565–581.
- (16) Goedecker, S. Linear Scaling Electronic Structure Methods. *Rev. Mod. Phys.* **1999**, *71*, 1085–1123.
- (17) Colombo, L. Tight-Binding Molecular Dynamics Simulations. *Comput. Mater. Sci.* **1998**, *12*, 278–287.
- (18) Friedman, J. H. Multivariate Adaptive Regression Spline. *Ann. Statist.* **1991**, *19*, 1–67.
- (19) Ischtwan, J.; Collins, M. A. Molecular Potential Energy Surfaces by Interpolation. *J. Chem. Phys.* **1994**, *100*, 8080–8088.
- (20) Crespos, C.; Collins, M. A.; Pijper, E.; Kroes, G. J. Multi-Dimensional Potential Energy Surface Determination by Modified Shepard Interpolation for a Molecule-Surface Reaction: $H_2+Pt(111)$. *Chem. Phys. Lett.* **2003**, *376*, 566–575.
- (21) Makarov, D. E.; Metiu, H. Fitting Potential Energy Surfaces: A Search in the Function Space by Directed Genetic Programming. *J. Chem. Phys.* **1998**, *108*, 590–598.
- (22) Mitchell, T. M. *Machine Learning*; McGraw-Hill, 1997.
- (23) Rasmussen, C. E.; Williams, C. K. I. *Gaussian Processes for Machine Learning*; MIT Press, 2006.
- (24) Bishop, C. M. *Neural Networks for Pattern Recognition*; Oxford University Press, 1995.
- (25) Gasteiger, J.; Zupan, J. Neural Networks in Chemistry. *Angew. Chem., Int. Ed. Engl.* **1993**, *32*, 503–527.
- (26) Mater, A. C.; Coote, M. L. Deep Learning in Chemistry. *J. Chem. Inf. Model.* **2019**, *59*, 2545–2559.
- (27) Carleo, G.; Cirac, I.; Cranmer, K.; Daudet, L.; Schuld, M.; Tishby, N.; Vogt-Maranto, L.; Zdeborova, L. Machine Learning and the Physical Sciences. *Rev. Mod. Phys.* **2019**, *91*, 045002.
- (28) Segler, M. H. S.; Preuss, M.; Waller, M. P. Planning Chemical Syntheses with Deep Neural Networks and Symbolic AI. *Nature* **2018**, *555*, 604–610.
- (29) Kitchin, J. R. Machine Learning in Catalysis. *Nature Catalysis* **2018**, *1*, 230–232.
- (30) Blank, T. B.; Brown, S. D.; Calhoun, A. W.; Doren, D. J. Neural Network Models of Potential Energy Surfaces. *J. Chem. Phys.* **1995**, *103*, 4129–4137.
- (31) Behler, J. Perspective: Machine Learning Potentials for Atomistic Simulations. *J. Chem. Phys.* **2016**, *145*, 170901.
- (32) Dral, P. O. Quantum Chemistry in the Age of Machine Learning. *J. Phys. Chem. Lett.* **2020**, *11*, 2336–2347.
- (33) Noé, F.; Tkatchenko, A.; Müller, K.-R.; Clementi, C. Machine Learning for Molecular Simulation. *Annu. Rev. Phys. Chem.* **2020**, *71*, 361–390.
- (34) Deringer, V. L.; Caro, M. A.; Csányi, G. Machine Learning Interatomic Potentials as Emerging Tools for Materials Science. *Adv. Mater.* **2019**, *31*, 1902765.
- (35) Wood, M. A.; Cusentino, M. A.; Wirth, B. D.; Thompson, A. P. Data-Driven Material Models for Atomistic Simulation. *Phys. Rev. B: Condens. Matter Mater. Phys.* **2019**, *99*, 184305.
- (36) Botu, V.; Batra, R.; Chapman, J.; Ramprasad, R. Machine Learning Force Fields: Construction, Validation, and Outlook. *J. Phys. Chem. C* **2017**, *121*, 511–522.
- (37) Mueller, T.; Kusne, A. G.; Ramprasad, R. Machine Learning in Materials Science: Recent Progress and Emerging Applications. *Rev. Comp. Chem.* **2016**, *29*, 186–273.
- (38) Handley, C. M.; Behler, J. Next Generation Interatomic Potentials for Condensed Systems. *Eur. Phys. J. B* **2014**, *87*, 152.
- (39) Handley, C. M.; Popelier, P. L. A. Potential Energy Surfaces Fitted by Artificial Neural Networks. *J. Phys. Chem. A* **2010**, *114*, 3371–3383.
- (40) Behler, J. Neural Network Potential-Energy Surfaces in Chemistry: a Tool for Large-Scale Simulations. *Phys. Chem. Chem. Phys.* **2011**, *13*, 17930–17955.
- (41) Manzhos, S.; Dawes, R.; Carrington, T., Jr Neural Network-Based Approaches for Building High Dimensional and Quantum Dynamics-Friendly Potential Energy Surfaces. *Int. J. Quantum Chem.* **2015**, *115*, 1012–1020.
- (42) Artrith, N. Machine Learning for the Modeling of Interfaces in Energy Storage and Conversion Materials. *J. Phys. Energy* **2019**, *1*, 032002.
- (43) Li, H.; Zhang, Z.; Liu, Z. Application of Artificial Neural Networks for Catalysis: A Review. *Catalysts* **2017**, *7*, 306.
- (44) Lorenz, S.; Groß, A.; Scheffler, M. Representing High-Dimensional Potential-Energy Surfaces for Reactions at Surfaces by Neural Networks. *Chem. Phys. Lett.* **2004**, *395*, 210–215.
- (45) Lorenz, S.; Scheffler, M.; Groß, A. Descriptions of Surface Chemical Reactions Using a Neural Network Representation of the Potential Energy Surface. *Phys. Rev. B: Condens. Matter Mater. Phys.* **2006**, *73*, 115431.
- (46) Gassner, H.; Probst, M.; Lauenstein, A.; Hermansson, K. Representation of Intermolecular Potential Functions by Neural Networks. *J. Phys. Chem. A* **1998**, *102*, 4596–4605.
- (47) Manzhos, S.; Carrington, T., Jr Using Neural Networks to Represent Potential Surfaces as Sums of Products. *J. Chem. Phys.* **2006**, *125*, 194105.
- (48) Manzhos, S.; Carrington, T., Jr Using Neural Networks, Optimized Coordinates, and High-Dimensional Model Representations to Obtain a Vinyl Bromide Potential Surface. *J. Chem. Phys.* **2008**, *129*, 224104.
- (49) Raff, L. M.; Malshe, M.; Hagan, M.; Doughan, D. I.; Rockley, M. G.; Komanduri, R. Ab initio Potential-Energy Surfaces for Complex, Multichannel Systems Using Modified Novelty Sampling and Feedforward Neural Networks. *J. Chem. Phys.* **2005**, *122*, 084104.

- (50) Behler, J.; Parrinello, M. Generalized Neural-Network Representation of High-Dimensional Potential-Energy Surfaces. *Phys. Rev. Lett.* **2007**, *98*, 146401.
- (51) Zhang, L.; Han, J.; Wang, H.; Car, R.; E, W. Deep Potential Molecular Dynamics: A Scalable Model with the Accuracy of Quantum Mechanics. *Phys. Rev. Lett.* **2018**, *120*, 143001.
- (52) Schütt, K.; Kindermans, P.-J.; Felix, H. E. S.; Chmiela, S.; Tkatchenko, A.; Müller, K.-R. SchNet: A Continuous-Filter Convolutional Neural Network for Modeling Quantum Interactions. *Advances in Neural Information Processing Systems 30 (NIPS 2017) 2017*, 991–1001.
- (53) Schütt, K. T.; Sauceda, H. E.; Kindermans, P.-J.; Tkatchenko, A.; Müller, K.-R. SchNet - A Deep Learning Architecture for Molecules and Materials. *J. Chem. Phys.* **2018**, *148*, 241722.
- (54) Ghasemi, S. A.; Hofstetter, A.; Saha, S.; Goedecker, S. Interatomic Potentials for Ionic Systems with Density Functional Accuracy Based on Charge Densities Obtained by a Neural Network. *Phys. Rev. B: Condens. Matter Mater. Phys.* **2015**, *92*, 045131.
- (55) Unke, O. T.; Meuwly, M. PhysNet: A Neural Network for Predicting Energies, Forces, Dipole Moments, and Partial Charges. *J. Chem. Theory Comput.* **2019**, *15*, 3678–3693.
- (56) Pun, G. P. P.; Batra, R.; Ramprasad, R.; Mishin, Y. Physically Informed Artificial Neural Networks for Atomistic Modeling of Materials. *Nature Comm.* **2019**, *10*, 2339.
- (57) Bartók, A. P.; Payne, M. C.; Kondor, R.; Csányi, G. Gaussian Approximation Potentials: The Accuracy of Quantum Mechanics, without the Electrons. *Phys. Rev. Lett.* **2010**, *104*, 136403.
- (58) Bartók, A. P.; Csányi, G. Gaussian Approximation Potentials: A Brief Tutorial Introduction. *Int. J. Quantum Chem.* **2015**, *115*, 1051–1057.
- (59) Shapeev, A. V. Moment Tensor Potentials: a Class of Systematically Improvable Interatomic Potentials. *Multiscale Model. Simul.* **2016**, *14*, 1153–1173.
- (60) Thompson, A. P.; Swiler, L. P.; Trott, C. R.; Foiles, S. M.; Tucker, G. J. Spectral Neighbor Analysis Method for Automated Generation of Quantum-Accurate Interatomic Potentials. *J. Comput. Phys.* **2015**, *285*, 316–330.
- (61) Deng, Z.; Chen, C.; Li, X.-G.; Ong, S. P. An Electrostatic Spectral Neighbor Analysis Potential for Lithium Nitride. *npj Computational Materials* **2019**, *5*, 75.
- (62) Drautz, R. Atomic Cluster Expansion for Accurate and Transferable Interatomic Potentials. *Phys. Rev. B: Condens. Matter Mater. Phys.* **2019**, *99*, 014104.
- (63) Chen, C.; Ye, W.; Zuo, Y.; Zheng, C.; Ong, S. P. Graph Networks as a Universal Machine Learning Framework for Molecules and Crystals. *Chem. Mater.* **2019**, *31*, 3564–3572.
- (64) Rupp, M.; Tkatchenko, A.; Müller, K.-R.; von Lilienfeld, O. A. Fast and Accurate Modeling of Molecular Atomization Energies with Machine Learning. *Phys. Rev. Lett.* **2012**, *108*, 058301.
- (65) Sauceda, H. E.; Chmiela, S.; Poltavsky, I.; Müller, K.-R.; Tkatchenko, A. Molecular Force Fields with Gradient-Domain Machine Learning: Construction and Application to Dynamics of Small Molecules with Coupled Cluster Forces. *J. Chem. Phys.* **2019**, *150*, 114102.
- (66) Chmiela, S.; Sauceda, H. E.; Poltavsky, I.; Müller, K.-R.; Tkatchenko, A. sGML: Constructing Accurate and Data Efficient Molecular Force Fields Using Machine Learning. *Comput. Phys. Commun.* **2019**, *240*, 38–45.
- (67) Vitek, A.; Stachon, M.; Krömer, P.; Snasel, V. Towards the Modeling of Atomic and Molecular Clusters Energy by Support Vector Regression. *IEEE 5th International Conference on Intelligent Networking and Collaborative Systems 2013*, 121–126.
- (68) Braams, B. J.; Bowman, J. M. Permutationally Invariant Potential Energy Surfaces in High Dimensionality. *Int. Rev. Phys. Chem.* **2009**, *28*, 577–606.
- (69) Brown, A.; Braams, B. J.; Christoffel, K.; Jin, Z.; Bowman, J. M. Classical and Quasiclassical Spectral Analysis of Using an ab initio Potential Energy Surface. *J. Chem. Phys.* **2003**, *119*, 8790–8793.
- (70) Cybenko, G. Approximation by Superpositions of a Sigmoidal Function. *Math. Control Sign. Systems* **1989**, *2*, 303–314.
- (71) Hornik, K.; Stinchcombe, M.; White, H. Multilayer Feedforward Networks are Universal Approximators. *Neural Networks* **1989**, *2*, 359–366.
- (72) Hornik, K. Approximation Capabilities of Multilayer Feedforward Networks. *Neural Networks* **1991**, *4*, 251–257.
- (73) Behler, J. Representing Potential Energy Surfaces by High-Dimensional Neural Network Potentials. *J. Phys.: Condens. Matter* **2014**, *26*, 183001.
- (74) Behler, J. First Principles Neural Network Potentials for Reactive Simulations of Large Molecular and Condensed Systems. *Angew. Chem., Int. Ed.* **2017**, *S6*, 12828–12840.
- (75) Behler, J. Atom-Centered Symmetry Functions for Constructing High-Dimensional Neural Network Potentials. *J. Chem. Phys.* **2011**, *134*, 074106.
- (76) Sumpter, B. G.; Noid, D. W. Potential Energy Surfaces for Macromolecules. A Neural Network Technique. *Chem. Phys. Lett.* **1992**, *192*, 455–462.
- (77) Manzhos, S.; Carrington, T., Jr Using Redundant Coordinates to Represent Potential Energy Surfaces with Lower-Dimensional Functions. *J. Chem. Phys.* **2007**, *127*, 014103.
- (78) Malshe, M.; Narulkar, R.; Raff, L. M.; Hagan, M.; Bukkapatnam, S.; Agrawal, P. M.; Komanduri, R. Development of Generalized Potential-Energy Surfaces Using Many-Body Expansions, Neural Networks, and Moiety Energy Approximations. *J. Chem. Phys.* **2009**, *130*, 184102.
- (79) Hobday, S.; Smith, R.; BelBruno, J. Applications of Neural Networks to Fitting Interatomic Potential Functions. *Modell. Simul. Mater. Sci. Eng.* **1999**, *7*, 397–412.
- (80) Hobday, S.; Smith, R.; BelBruno, J. Application of Genetic Algorithms and Neural Networks to Interatomic Potentials. *Nucl. Instrum. Methods Phys. Res., Sect. B* **1999**, *153*, 247–263.
- (81) Zeiler, M. D.; Ranzato, M.; Monga, R.; Mao, M.; Yang, K.; Le, Q. V.; Nguyen, P.; Senior, A.; Vanhoucke, V.; Dean, J.; Hinton, G. E. On Rectified Linear Units for Speech Processing. *2013 IEEE International Conference on Acoustics, Speech and Signal Processing*. **2013**, 3517–3521.
- (82) Brown, D. F. R.; Gibbs, M. N.; Clary, D. C. Combining ab initio Computations, Neural Networks, and Diffusion Monte Carlo: An Efficient Method to Treat Weakly Bound Molecules. *J. Chem. Phys.* **1996**, *105*, 7597–7604.
- (83) Manzhos, S.; Wang, X.; Dawes, R.; Carrington, T., Jr A Nested Molecule-Independent Neural Network Approach for High-Quality Potential Fits. *J. Phys. Chem. A* **2006**, *110*, 5295–5304.
- (84) Lee, H. M.; Raff, L. M. Cis → Trans, Trans → Cis Isomerizations and N-O Bond Dissociation of Nitrous Acid (HONO) on an ab initio Potential Surface Obtained by Novelty Sampling and Feed-Forward Neural Network Fitting. *J. Chem. Phys.* **2008**, *128*, 194310.
- (85) Prudente, F. V.; Soares Neto, J. J. The Fitting of Potential Energy Surfaces Using Neural Networks. Application to the Study of the Photodissociation processes. *Chem. Phys. Lett.* **1998**, *287*, 585–589.
- (86) Rocha Filho, T. M.; Oliveira, Z. T., Jr; Malbouisson, L. A. C.; Gargano, R.; Soares Neto, J. J. The Use of Neural Networks for Fitting Potential Energy Surfaces: A Comparative Case Study for the Molecule. *Int. J. Quantum Chem.* **2003**, *95*, 281–288.
- (87) Lu, D.; Behler, J.; Li, J. Accurate Global Potential Energy Surfaces for the H + CH₃OH Reaction by Neural Network Fitting with Permutation Invariance. *J. Phys. Chem. A* **2020**, *124*, 5737–5745.
- (88) Jiang, B.; Li, J.; Guo, H. Potential Energy Surfaces from high Fidelity Fitting of ab initio Points: the Permutation Invariant Polynomial - Neural Network Approach. *Int. Rev. Phys. Chem.* **2016**, *35*, 479–506.
- (89) Li, J.; Jiang, B.; Guo, H. Permutation Invariant Polynomial Neural Network Approach to Fitting Potential Energy Surfaces. II. Four-Atom Systems. *J. Chem. Phys.* **2013**, *139*, 204103.

- (90) Jiang, B.; Guo, H. Permutation Invariant Polynomial Neural Network Approach to Fitting Potential Energy Surfaces. *J. Chem. Phys.* **2013**, *139*, 054112.
- (91) Le, H. M.; Raff, L. M. Molecular Dynamics Investigation of the Bimolecular Reaction $\text{BeH} + \text{H}_2 \rightarrow \text{BeH}_2 + \text{H}$ on an ab Initio Potential-Energy Surface Obtained Using Neural Network Methods with Both Potential and Gradient Accuracy Determination. *J. Phys. Chem. A* **2010**, *114*, 45–53.
- (92) Behler, J.; Delley, B.; Lorenz, S.; Reuter, K.; Scheffler, M. Dissociation of O_2 at Al(111): The Role of Spin Selection Rules. *Phys. Rev. Lett.* **2005**, *94*, 36104.
- (93) Ludwig, J.; Vlachos, D. G. Ab initio Molecular Dynamics of Hydrogen Dissociation on Metal Surfaces Using Neural Networks and Novelty Sampling. *J. Chem. Phys.* **2007**, *127*, 154716.
- (94) Behler, J.; Reuter, K.; Scheffler, M. Nonadiabatic Effects in the Dissociation of Oxygen Molecules at the Al(111) Surface. *Phys. Rev. B: Condens. Matter Mater. Phys.* **2008**, *77*, 115421.
- (95) Behler, J.; Lorenz, S.; Reuter, K. Representing Molecule-Surface Interactions with Symmetry-Adapted Neural Networks. *J. Chem. Phys.* **2007**, *127*, 014705.
- (96) Carbogno, C.; Behler, J.; Groß, A.; Reuter, K. Fingerprints for Spin-Selection Rules in the Interaction Dynamics of O_2 at Al(111). *Phys. Rev. Lett.* **2008**, *101*, 096104.
- (97) Latino, D. A. R. S.; Fartaria, R. P. S.; Freitas, F. F. M.; de Sousa, J. A.; Fernandes, F. M. S. S. Mapping Potential Energy Surfaces by Neural Networks: The Ethanol/Au(111) Interface. *J. Electroanal. Chem.* **2008**, *624*, 109–120.
- (98) Carbogno, C.; Behler, J.; Reuter, K.; Groß, A. Signatures of Nonadiabatic O_2 Dissociation at Al(111): First-Principles Fewest-Switches Study. *Phys. Rev. B: Condens. Matter Mater. Phys.* **2010**, *81*, 035410.
- (99) Manzhos, S.; Yamashita, K. A Model for the Dissociative Adsorption of N_2O on Cu(100) Using a Continuous Potential Energy Surface. *Surf. Sci.* **2010**, *604*, 554–560.
- (100) Goikoetxea, I.; Beltrán, J.; Meyer, J.; Juaristi, J. I.; Alducin, M.; Reuter, K. Non-Adiabatic Effects During the Dissociative Adsorption of O_2 at Ag(111)? A first-Principles Divide and Conquer Study. *New J. Phys.* **2012**, *14*, 013050.
- (101) Zhou, X.; Nattino, F.; Zhang, Y.; Chen, J.; Kroes, G.-J.; Guo, H.; Jiang, B. Dissociative Chemisorption of Methane on Ni(111) Using a Chemically Accurate Fifteen Dimensional Potential Energy Surface. *Phys. Chem. Chem. Phys.* **2017**, *19*, 30540–30550.
- (102) Manzhos, S.; Carrington, T. Neural Network Potential Energy Surfaces for Small Molecules and Reactions. *Chem. Rev.* **2020**, *1*.
- (103) Cho, K.-W.; No, K. T.; Scheraga, H. A. A Polarizable Force Field for Water Using an Artificial Neural Network. *J. Mol. Struct.* **2002**, *641*, 77–91.
- (104) Bhola, A.; Kenny, S. D.; Smith, R. A New Approach to Potential Fitting Using Neural Networks. *Nucl. Instrum. Methods Phys. Res., Sect. B* **2007**, *255*, 1–7.
- (105) Sanville, E.; Bhola, A.; Smith, R.; Kenny, S. D. Silicon Potentials Investigated Using Density Functional Theory Fitted Neural Networks. *J. Phys.: Condens. Matter* **2008**, *20*, 285219.
- (106) Cheng, B.; Engel, E. A.; Behler, J.; Dellago, C.; Ceriotti, M. Ab initio Thermodynamics of Liquid and Solid Water. *Proc. Natl. Acad. Sci. U. S. A.* **2019**, *116*, 1110–1115.
- (107) Bartók, A. P.; Kondor, R.; Csányi, G. On Representing Chemical Environments. *Phys. Rev. B: Condens. Matter Mater. Phys.* **2013**, *87*, 184115.
- (108) Zhu, L.; Amsler, M.; Fuhrer, T.; Schaefer, B.; Faraji, S.; Rostami, S.; Ghasemi, S. A.; Sadeghi, A.; Grauzintye, M.; Wolverton, C.; Goedecker, S. A Fingerprint Based Metric for Measuring Similarities of Crystalline Structures. *J. Chem. Phys.* **2016**, *144*, 034203.
- (109) Jindal, S.; Chiriki, S.; Bulusu, S. S. Spherical Harmonics Based Descriptor for Neural Network Potentials: Structure and Dynamics of Au_{147} Nanocluster. *J. Chem. Phys.* **2017**, *146*, 204301.
- (110) Kocer, E.; Mason, J. K.; Erturk, H. A Novel Approach to Describe Chemical Environments in High-Dimensional Neural Network Potentials. *J. Chem. Phys.* **2019**, *150*, 154102.
- (111) Christensen, A. S.; Faber, F. A.; von Lilienfeld, O. A. Operators in Quantum Machine Learning: Response Properties in Chemical Space. *J. Chem. Phys.* **2019**, *150*, 064105.
- (112) Christensen, A. S.; Bratholm, L. A.; Faber, F. A.; von Lilienfeld, O. A. FCHL Revisited: Faster and More Accurate Quantum Machine Learning. *J. Chem. Phys.* **2020**, *152*, 044107.
- (113) Hansen, K.; Biegler, F.; Ramakrishnan, R.; Pronobis, W.; von Lilienfeld, O. A.; Müller, K.-R.; Tkatchenko, A. Machine Learning Predictions of Molecular Properties: Accurate Many-Body Potentials and Nonlocality in Chemical Space. *J. Phys. Chem. Lett.* **2015**, *6*, 2326–2331.
- (114) Willatt, M. J.; Musil, F.; Ceriotti, M. Atom-Density Representations for Machine Learning. *J. Chem. Phys.* **2019**, *150*, 154110.
- (115) Huo, H.; Rupp, M. Unified Representation of Molecules and Crystals for Machine Learning. [arXiv:1704.06439v2](https://arxiv.org/abs/1704.06439v2), 2017.
- (116) Zuo, Y.; Chen, C.; Li, X.; Deng, Z.; Chen, Y.; Behler, J.; Csányi, G.; Shapeev, A. V.; Thompson, A. P.; Wood, M. A.; Ong, S. P. A Performance and Cost Assessment of Machine Learning Interatomic Potentials. *J. Phys. Chem. A* **2020**, *124*, 731–745.
- (117) Parsaeifard, B.; De, D. S.; Christensen, A. S.; Faber, F. A.; Kocer, E.; De, S.; Behler, J.; von Lilienfeld, O. A.; Goedecker, S. An Assessment of the Structural Resolution of Various Fingerprints Commonly Used in Machine Learning. *Mach. Learn. Sci. Technol.* **2020** submitted. DOI: [10.1088/2632-2153/abb212](https://doi.org/10.1088/2632-2153/abb212)
- (118) Himanen, L.; Jägera, M. O. J.; Morooka, E. V.; Canova, F. F. S.; Ranawat, Y.; Gao, D. Z.; Rinke, P.; Foster, A. S. Dscribe: Library of Descriptors for Machine Learning in Materials Science. *Comput. Phys. Commun.* **2020**, *247*, 106949.
- (119) Pozdnyakov, S. N.; Willatt, M. J.; Bartók, A. P.; Ortner, C.; Csányi, G.; Ceriotti, M. Incompleteness of Atomic Structure Representations. *Phys. Rev. Lett.* **2020**, *125*, 166001.
- (120) Nguyen, T. T.; Székely, E.; Imbalzano, G.; Behler, J.; Csányi, G.; Ceriotti, M.; Götz, A. W.; Paesani, F. Comparison of Permutationally Invariant Polynomials, Neural Networks, and Gaussian Approximation Potentials in Representing Water Interactions Through Many-Body Expansions. *J. Chem. Phys.* **2018**, *124*, 241725.
- (121) Langer, M. F.; Goessmann, A.; Rupp, M. Representations of Molecules and Materials for Interpolation of Quantum-Mechanical Simulations via Machine Learning. [arXiv:2003.12081v1](https://arxiv.org/abs/2003.12081v1), 2020.
- (122) Faber, F.; Lindmaa, A.; von Lilienfeld, O. A.; Armiento, R. Crystal Structure Representations for Machine Learning Models of Formation Energies. *Int. J. Quantum Chem.* **2015**, *115*, 1094–1101.
- (123) Artrith, N.; Urban, A.; Ceder, G. Efficient and Accurate Machine-Learning Interpolation of Atomic Energies in Compositions with many Species. *Phys. Rev. B: Condens. Matter Mater. Phys.* **2017**, *96*, 014112.
- (124) Faber, F. A.; Hutchison, L.; Huang, B.; Gilmer, J.; Schoenholz, S. S.; Dahl, G. E.; Vinyals, O.; Kearnes, S.; Riley, P. F.; von Lilienfeld, O. A. Machine Learning Prediction Errors Better than DFT Accuracy. [arXiv:1702.05532v2](https://arxiv.org/abs/1702.05532v2) 2017.
- (125) Faber, F. A.; Christensen, A. S.; Huang, B.; von Lilienfeld, O. A. Alchemical and Structural Distribution Based Representation for Universal Quantum Machine Learning. *J. Chem. Phys.* **2018**, *148*, 241717.
- (126) Gastegger, M.; Schwiedrzik, L.; Bittermann, M.; Berzenyi, F.; Marquetand, P. WACSF - Weighted Atom-Centred Symmetry Functions as Descriptors in Machine Learning Potentials. *J. Chem. Phys.* **2018**, *148*, 241709.
- (127) Grisafi, A.; Ceriotti, M. Incorporating Long-Range Physics in Atomic-Scale Machine Learning. *J. Chem. Phys.* **2019**, *151*, 204105.
- (128) Herr, J. E.; Koh, K.; Yao, K.; Parkhill, J. Compressing Physics with an Autoencoder: Creating an Atomic Species Representation to Improve Machine Learning Models in the Chemical Sciences. *J. Chem. Phys.* **2019**, *151*, 084103.

- (129) Schütt, K. T.; Tkatchenko, A.; Müller, K.-R. In *Machine Learning Meets Quantum Physics*; Schütt, K. T., Chmiela, S., von Lilienfeld, O. A., Tkatchenko, A., Tsuda, K., Müller, K.-R., Eds.; Springer International Publishing: Cham, 2020; pp 215–230.
- (130) Schütt, K. T.; Arbabzadah, F.; Chmiela, S.; Müller, K. R.; Tkatchenko, A. Quantum-Chemical Insights from Deep Tensor Neural Networks. *Nature Commun.* **2017**, *8*, 13890.
- (131) Tai No, K.; Ha Chang, B.; Yeon Kim, S.; Shik Jhon, M.; Scheraga, H. A. Description of the Potential Energy Surface of the Water Dimer with an Artificial Neural Network. *Chem. Phys. Lett.* **1997**, *271*, 152–156.
- (132) Huang, X.; Braams, B. J.; Bowman, J. M. Ab initio Potential Energy and Dipole Moment Surfaces for. *J. Chem. Phys.* **2005**, *122*, 044308.
- (133) Huang, X.; Braams, B. J.; Bowman, J. M. Ab Initio Potential Energy and Dipole Moment Surfaces of (H_2O)₂. *J. Phys. Chem. A* **2006**, *110*, 445–451.
- (134) Kolb, B.; Zhao, B.; Li, J.; Jiang, B.; Guo, H. Permutation Invariant Potential Energy Surfaces for Polyatomic Reactions Using Atomistic Neural Networks. *J. Chem. Phys.* **2016**, *144*, 224103.
- (135) Li, J.; Song, K.; Behler, J. A Critical Comparison of Neural Network Potentials for Molecular Reaction Dynamics with Exact Permutation Symmetry. *Phys. Chem. Chem. Phys.* **2019**, *21*, 9672–9682.
- (136) Singraber, A.; Behler, J.; Dellago, C. Library-Based LAMMPS Implementation of High-Dimensional Neural Network Potentials. *J. Chem. Theory Comput.* **2019**, *15*, 1827–1840.
- (137) Tersoff, J. Modeling Solid State Chemistry: Interatomic Potentials for Multicomponent Systems. *Phys. Rev. B: Condens. Matter Mater. Phys.* **1989**, *39*, 5566.
- (138) Behler, J. Constructing High-Dimensional Neural Network Potentials: A Tutorial Review. *Int. J. Quantum Chem.* **2015**, *115*, 1032–1050.
- (139) Smith, J. S.; Isayev, O.; Roitberg, A. E. ANI-1: An Extensible Neural Network Potential with DFT Accuracy at Force Field Computational Cost. *Chem. Sci.* **2017**, *8*, 3192–3203.
- (140) Jose, K. V. J.; Artrith, N.; Behler, J. Construction of High-Dimensional Neural Network Potentials Using Environment-Dependent Atom Pairs. *J. Chem. Phys.* **2012**, *136*, 194111.
- (141) Glick, Z. L.; Metcalf, D. P.; Koutsoukas, A.; Spronk, S. A.; Cheney, D. L.; Sherrill, C. D. AP-Net: An Atomic-Pairwise Neural Network for Smooth and Transferable Interaction Potentials. *ChemRxiv* **2020**, 1.
- (142) Imbalzano, G.; Anelli, A.; Giofre, D.; Klees, S.; Behler, J.; Ceriotti, M. Automatic Selection of Atomic Fingerprints and Reference Configurations for Machine-Learning Potentials. *J. Chem. Phys.* **2018**, *148*, 241730.
- (143) Casier, B.; Carniato, S.; Miteva, T.; Capron, N.; Sisourat, N. Using Principal Component Analysis for Neural Network High-Dimensional Potential Energy Surface. *J. Chem. Phys.* **2020**, *152*, 234103.
- (144) Yao, K.; Herr, J. E.; Toth, D. W.; Mckintyre, R.; Parkhill, J. The TensorMol-0.1 Model Chemistry: A Neural Network Augmented with Long-Range Physics. *Chem. Sci.* **2018**, *9*, 2261–2269.
- (145) Artrith, N.; Kolpak, A. M. Understanding the Composition and Activity of Electrocatalytic Nanoalloys in Aqueous Solvents: A Combination of DFT and Accurate Neural Network Potentials. *Nano Lett.* **2014**, *14*, 2670–2676.
- (146) Artrith, N.; Hiller, B.; Behler, J. Neural Network Potentials for Metals and Oxides - First Applications to Copper Clusters at Zinc Oxide. *Phys. Status Solidi B* **2013**, *250*, 1191–1203.
- (147) Eckhoff, M.; Behler, J. From Molecular Fragments to the Bulk: Development of a Neural Network Potential for MOF-5. *J. Chem. Theory Comput.* **2019**, *15*, 3793–3809.
- (148) Eckhoff, M.; Schönewald, F.; Risch, M.; Volkert, C. A.; Blöchl, P. E.; Behler, J. Closing the Gap Between Theory and Experiment for Lithium Manganese Oxide Spinel Using a High-Dimensional Neural Network Potential. *Phys. Rev. B: Condens. Matter Mater. Phys.* **2020**, *102*, 174102.
- (149) Ghorbanfekr, H.; Behler, J.; Peeters, F. M. Insights Into Water Permeation Through hBN Nanocapillaries by ab initio Machine Learning Molecular Dynamics Simulations. *J. Phys. Chem. Lett.* **2020**, *11*, 7363.
- (150) Devereux, C.; Smith, J.; Davis, K.; Barros, K.; Zubatyuk, R.; Isayev, O.; Roitberg, A. Extending the Applicability of the ANI Deep Learning Molecular Potential to Sulfur and Halogens. *ChemRxiv* **2020**, 1.
- (151) Rostami, S.; Amsler, M.; Ghasemi, S. A. Optimized Symmetry Functions for Machine-Learning Interatomic Potentials of Multi-component Systems. *J. Chem. Phys.* **2018**, *149*, 124106.
- (152) Mayo, S. L.; Olafson, B. D.; Goddard, W. A. III DREIDING: A Generic Force Field for Molecular Simulations. *J. Phys. Chem.* **1990**, *94*, 8897–8909.
- (153) Rappe, A. K.; Casewit, C. J.; Colwell, K. S.; Goddard, W. A., III; Skiff, W. M. UFF, a Full Periodic Table Force Field for Molecular Mechanics and Molecular Dynamics Simulations. *J. Am. Chem. Soc.* **1992**, *114*, 10024–10035.
- (154) Leontyev, I. V.; Stuchebrukhov, A. A. Polarizable Mean-Field Model of Water for Biological Simulations with AMBER and CHARMM Force Fields. *J. Chem. Theory Comput.* **2012**, *8*, 3207–3216.
- (155) Lamoureux, G.; Harder, E.; Vorobyov, I. V.; Roux, B.; MacKerell, A. D. A Polarizable Model of Water for Molecular Dynamics Simulations of Biomolecules. *Chem. Phys. Lett.* **2006**, *418*, 245.
- (156) Darley, M. G.; Handley, C. M.; Popelier, P. L. A. Beyond Point Charges: Dynamic Polarization from Neural Net Predicted Multipole Moments. *J. Chem. Theory Comput.* **2008**, *4*, 1435–1448.
- (157) Handley, C. M.; Popelier, P. L. A. Dynamically Polarizable Water Potential Based on Multipole Moments Trained by Machine Learning. *J. Chem. Theory Comput.* **2009**, *5*, 1474–1489.
- (158) Handley, C. M.; Hawe, G. I.; Kell, D. B.; Popelier, P. L. A. Optimal Construction of a Fast and Accurate Polarisable Water Potential Based on Multipole Moments Trained by Machine Learning. *Phys. Chem. Chem. Phys.* **2009**, *11*, 6365–6376.
- (159) Popelier, P. L. A. QCTFF: On the Construction of a Novel Protein Force Field. *Int. J. Quantum Chem.* **2015**, *115*, 1005–1011.
- (160) Artrith, N.; Morawietz, T.; Behler, J. High-Dimensional Neural-Network Potentials for Multicomponent Systems: Applications to Zinc Oxide. *Phys. Rev. B: Condens. Matter Mater. Phys.* **2011**, *83*, 153101.
- (161) Morawietz, T.; Sharma, V.; Behler, J. A Neural Network Potential-Energy Surface for the Water Dimer Based on Environment-Dependent Atomic Energies and Charges. *J. Chem. Phys.* **2012**, *136*, 064103.
- (162) Ewald, P. P. Die Berechnung Optischer und Elektrostatischer Gitterpotentiale. *Ann. Phys.* **1921**, *64*, 253–287.
- (163) Mulliken, R. S. Electronic Population Analysis on LCAO-MO Molecular Wave Functions. I. *J. Chem. Phys.* **1955**, *23*, 1833.
- (164) Hirshfeld, F. L. Bonded-Atom Fragments for Describing Molecular Charge Densities. *Theor. Chim. Acta* **1977**, *44*, 129–138.
- (165) Bader, R. Atoms in Molecules. *Acc. Chem. Res.* **1985**, *18*, 9.
- (166) Sifain, A. E.; Lubbers, N.; Nebgen, B. T.; Smith, J. S.; Lokhov, A. Y.; Isayev, O.; Roitberg, A. E.; Barros, K.; Tretiak, S. Discovering a Transferable Charge Assignment Model Using Machine Learning. *J. Phys. Chem. Lett.* **2018**, *9*, 4495–4501.
- (167) Toukmaji, A. A. B.; Board, J. Ewald Summation Techniques in Perspective: a Survey. *Comput. Phys. Commun.* **1996**, *95*, 73–92.
- (168) Grimme, S.; Antony, J.; Ehrlich, S.; Krieg, H. A Consistent and Accurate ab initio Parametrization of Density Functional Dispersion Correction (DFT-D) for the 94 Elements H–Pu. *J. Chem. Phys.* **2010**, *132*, 154104.
- (169) Nebgen, B.; Lubbers, N.; Smith, J. S.; Sifain, A. E.; Lokhov, A.; Isayev, O.; Roitberg, A. E.; Barros, K.; Tretiak, S. Transferable Dynamic Molecular Charge Assignment Using Deep Neural Networks. *J. Chem. Theory Comput.* **2018**, *14*, 4687–4698.
- (170) Bereau, T.; DiStasio, R. A., Jr.; Tkatchenko, A.; von Lilienfeld, O. A. Non-Covalent Interactions Across Organic and Biological

- Subsets of Chemical Space: Physics-Based Potentials Parametrized from Machine Learning. *J. Chem. Phys.* **2018**, *148*, 241706.
- (171) Bereau, T.; Andrienko, D.; von Lilienfeld, O. A. Transferable Atomic Multipole Machine Learning Models for Small Organic Molecules. *J. Chem. Theory Comput.* **2015**, *11*, 3225–3233.
- (172) Bleiziffer, P.; Schaller, K.; Riniker, S. Machine Learning of Partial Charges Derived from High-Quality Quantum-Mechanical Calculations. *J. Chem. Inf. Model.* **2018**, *58*, 579–590.
- (173) Rai, B. K.; Bakken, G. A. Fast and Accurate Generation of ab initio Quality Atomic Charges Using Nonparametric Statistical Regression. *J. Comput. Chem.* **2013**, *34*, 1661–1671.
- (174) Korolev, V. V.; Mitrofanov, A.; Marchenko, E. I.; Eremin, N. N.; Tkachenko, V.; Kalmykov, S. N. Transferable and Extensible Machine Learning-Derived Atomic Charges for Modeling Hybrid Nanoporous Materials. *Chem. Mater.* **2020**, *32*, 7822–7831.
- (175) Zubatyuk, R.; Smith, J. S.; Nebgen, B. T.; Tretiak, S.; Isayev, O. Teaching a Neural Network to Attach and Detach Electrons from Molecules. *ChemRxiv* **2020**, *1*.
- (176) Gastegger, M.; Behler, J.; Marquetand, P. Machine Learning Molecular Dynamics for the Simulation of Infrared Spectra. *Chem. Sci.* **2017**, *8*, 6924–6935.
- (177) Grisafi, A.; Fabrizio, A.; Meyer, B.; Wilkins, D. M.; Corminboeuf, C.; Ceriotti, M. Transferable Machine-Learning Model of the Electron Density. *ACS Cent. Sci.* **2019**, *5*, 57–64.
- (178) Chandrasekaran, A.; Kamal, D.; Batra, R.; Kim, C.; Chen, L.; Ramprasad, R. Solving the Electronic Structure Problem with Machine Learning. *njp Comp. Mater.* **2019**, *5*, 22.
- (179) Deringer, V. L.; Csányi, G. Machine-Learning Based Interatomic Potential for Amorphous Carbon. *Phys. Rev. B: Condens. Matter Mater. Phys.* **2017**, *95*, 094203.
- (180) Parsaeifard, B.; Finkler, J. A.; Goedecker, S. Detecting Non-Local Effects in the Electronic Structure of a Simple Covalent System with Machine Learning Methods. *arXiv:2008.11277v1* **2020**.
- (181) Ko, T. W.; Finkler, J. A.; Goedecker, S.; Behler, J. A Fourth-Generation High-Dimensional Neural Network Potential with Accurate Electrostatics Including Non-Local Charge Transfer. *Nat. Commun.* **2020**, *398*.
- (182) Mortier, W. J.; Ghosh, S. K.; Shankar, S. Electronegativity Equalization Method for the Calculation of Atomic Charges in Molecules. *J. Am. Chem. Soc.* **1986**, *108*, 4315.
- (183) Verstraelen, T.; Van Speybroeck, V.; Waroquier, M. The Electronegativity Equalization Method and the Split Charge Equilibration Applied to Organic Systems: Parametrization, Validation, and Comparison. *J. Chem. Phys.* **2009**, *131*, 044127.
- (184) Rappe, A. K.; Goddard, W. A. III Charge Equilibration for Molecular Dynamics Simulations. *J. Phys. Chem.* **1991**, *95*, 3358–3363.
- (185) Wilmer, C. E.; Kim, K. C.; Snurr, R. Q. An Extended Charge Equilibration Method. *J. Phys. Chem. Lett.* **2012**, *3*, 2506–2511.
- (186) Nistor, R. A.; Polihronov, J. G.; Muser, M. H.; Mosey, N. J. A Generalization of the Charge Equilibration Method for Nonmetallic Materials. *J. Chem. Phys.* **2006**, *125*, 094108.
- (187) Zhang, M.; Fournier, R. Self-Consistent Charge Equilibration Method and Its Application to $\text{Au}_{13}\text{Na}_n$ ($n = 1, 10$) Clusters. *J. Phys. Chem. A* **2009**, *113*, 3162–3170.
- (188) Zubatyuk, R.; Smith, J. S.; Leszczynski, J.; Isayev, O. Accurate and Transferable Multitask Prediction of Chemical Properties with an Atoms-in-Molecules Neural Network. *Science Advances* **2019**, *5*, No. eaav6490.
- (189) Metcalf, D. P.; Jiang, A.; Spronk, S. A.; Cheney, D. L.; Sherrill, C. D. Electron-Passing Neural Networks for Atomic Charge Prediction in Systems with Arbitrary Molecular Charge. *ChemRxiv* **2020**, *1*.
- (190) Raza, A.; Sturluson, A.; Simon, C. M.; Fern, X. Message Passing Neural Networks for Partial Charge Assignment to Metal-Organic Frameworks. *J. Phys. Chem. C* **2020**, *124*, 19070–19082.
- (191) Stukowski, A. Visualization and Analysis of Atomistic Simulation Data with OVITO - the Open Visualization Tool. *Modell. Simul. Mater. Sci. Eng.* **2010**, *18*, 015012.
- (192) Blum, V.; Gehrke, R.; Hanke, F.; Havu, P.; Havu, V.; Ren, X.; Reuter, K.; Scheffler, M. Ab Initio Molecular Simulations with Numeric Atom-Centered Orbitals. *Comput. Phys. Commun.* **2009**, *180*, 2175–2196.
- (193) Perdew, J. P.; Burke, K.; Ernzerhof, M. Generalized Gradient Approximation Made Simple. *Phys. Rev. Lett.* **1996**, *77*, 3865–3868.
- (194) Faraji, S.; Ghasemi, S. A.; Rostami, S.; Rasoulkhani, R.; Schaefer, B.; Goedecker, S.; Amsler, M. High Accuracy and Transferability of a Neural Network Potential Through Charge Equilibration for Calcium Fluoride. *Phys. Rev. B: Condens. Matter Mater. Phys.* **2017**, *95*, 104105.
- (195) Faraji, S.; Ghasemi, S. A.; Parsaeifard, B.; Goedecker, S. Surface Reconstructions and Premelting of the (100) CaF_2 Surface. *Phys. Chem. Chem. Phys.* **2019**, *21*, 16270–16281.
- (196) Eivari, H. A.; Ghasemi, S. A.; Tahmasbi, H.; Rostami, S.; Faraji, S.; Rasoulkhani, R.; Goedecker, S.; Amsler, M. Two-Dimensional Hexagonal Sheet of TiO_2 . *Chem. Mater.* **2017**, *29*, 8594–8603.
- (197) Xie, X.; Persson, K. A.; Small, D. W. Incorporating Electronic Information into Machine Learning Potential Energy Surfaces via Approaching the Ground-State Electronic Energy as a Function of Atom-Based Electronic Populations. *J. Chem. Theory Comput.* **2020**, *16*, 4256–4270.
- (198) Becke, A. D. A Multicenter Numerical Integration Scheme for Polyatomic Molecules. *J. Chem. Phys.* **1988**, *88*, 2547.
- (199) Dederichs, P. H.; Blügel, S.; Zeller, R.; Akai, H. Ground States of Constrained Systems: Application to Cerium Impurities. *Phys. Rev. Lett.* **1984**, *53*, 2512.
- (200) Behler, J.; Delley, B.; Reuter, K.; Scheffler, M. Nonadiabatic Potential-Energy Surfaces by Constrained Density-Functional Theory. *Phys. Rev. B: Condens. Matter Mater. Phys.* **2007**, *75*, 115409.
- (201) Kaduk, B.; Kowalczyk, T.; Van Voorhis, T. Constrained Density Functional Theory. *Chem. Rev.* **2012**, *112*, 321–370.
- (202) Rupp, M.; Ramakrishnan, R.; von Lilienfeld, O. A. Machine Learning for Quantum Mechanical Properties of Atoms in Molecules. *J. Phys. Chem. Lett.* **2015**, *6*, 3309–3313.
- (203) Plazinski, W.; Plazinska, A.; Brzyska, A. Efficient Sampling of High-Energy States by Machine Learning Force Fields. *Phys. Chem. Chem. Phys.* **2020**, *22*, 14364–14374.
- (204) Laio, A.; Parrinello, M. Escaping Free-Energy Minima. *Proc. Natl. Acad. Sci. U. S. A.* **2002**, *99*, 12562–12566.
- (205) Seung, H. S.; Opper, M.; Sompolinsky, H. Query by Committee. *Proceedings of the fifth annual workshop on computational learning theory* **1992**, 287–294.
- (206) Artrith, N.; Behler, J. High-Dimensional Neural Network Potentials for Metal Surfaces: A Prototype Study for Copper. *Phys. Rev. B: Condens. Matter Mater. Phys.* **2012**, *85*, 045439.
- (207) Zhang, L.; Lin, D.-Y.; Wang, H.; Car, R.; E, W. Active Learning of Uniformly Accurate Interatomic Potentials for Materials Simulation. *Phys. Rev. Mater.* **2019**, *3*, 023804.
- (208) Podryabinkin, E. V.; Tikhonov, E. V.; Shapeev, A. V.; Oganov, A. R. Accelerating Crystal Structure Prediction by Machine-Learning Interatomic Potentials with Active Learning. *Phys. Rev. B: Condens. Matter Mater. Phys.* **2019**, *99*, 064114.
- (209) Bernstein, N.; Csányi, G.; Deringer, V. L. De Novo Exploration and Self-Guided Learning of Potential-Energy Surfaces. *njp Computational Materials* **2019**, *5*, 99.
- (210) Schran, C.; Brezina, K.; Marsalek, O. Committee Neural Network Potentials Control Generalization Errors and Enable Active Learning. *arXiv:2006.01541v2*, **2020**.
- (211) Schran, C.; Behler, J.; Marx, D. Automated Fitting of Neural Network Potentials at Coupled Cluster Accuracy: Protonated Water Clusters as Testing Ground. *J. Chem. Theory Comput.* **2020**, *16*, 88–99.
- (212) Podryabinkin, E. V.; Shapeev, A. V. Active Learning of Linearly Parametrized Interatomic Potentials. *Comput. Mater. Sci.* **2017**, *140*, 171–180.
- (213) Gastegger, M.; Kauffmann, C.; Behler, J.; Marquetand, P. Comparing the Accuracy of High-Dimensional Neural Network

- Potentials and the Systematic Molecular Fragmentation Method: A Benchmark Study for al-trans Alkanes. *J. Chem. Phys.* **2016**, *144*, 194110.
- (214) Bing Huang, O. A. V. Efficient accurate scalable and transferable quantum machine learning with am-ons. *arXiv:1707.04146v4* 2020.
- (215) Pukrittayakamee, A.; Malshe, M.; Hagan, M.; Raff, L. M.; Narulkar, R.; Bukkapatnum, S.; Komanduri, R. Simultaneous Fitting of a Potential-Energy Surface and its Corresponding Force Fields Using Feedforward Neural Networks. *J. Chem. Phys.* **2009**, *130*, 134101.
- (216) Le, H. M.; Huynh, S.; Raff, L. M. Molecular Dissociation of Hydrogen Peroxide (HOOH) on a Neural Network ab initio Potential Surface with a new Configuration Sampling Method Involving Gradient Fitting. *J. Chem. Phys.* **2009**, *131*, 014107.
- (217) Witkoskie, J. B.; Doren, D. J. Neural Network Models of Potential Energy Surfaces: Prototypical Examples. *J. Chem. Theory Comput.* **2005**, *1*, 14–23.
- (218) Marques, M. R. G.; Wolff, J.; Steigemann, C.; Marques, M. A. L. Neural Network Force Fields for Simple Metals and Semiconductors: Construction and Application to the Calculation of Phonons and Melting Temperatures. *Phys. Chem. Chem. Phys.* **2019**, *21*, 6506–6516.
- (219) Rumelhart, D. E.; Hinton, G. E.; Williams, R. J. Learning Representations by Back-Propagating Errors. *Nature* **1986**, *323*, 533–536.
- (220) Fletcher, R.; Reeves, C. Function Minimization by Conjugate Gradients. *Comput. J.* **1964**, *7*, 149–154.
- (221) Levenberg, K. A Method for the Solution of Certain Non-Linear Problems in Least Squares. *Q. Appl. Math.* **1944**, *2*, 164–168.
- (222) Marquardt, D. W. An Algorithm for Least-Squares Estimation of Nonlinear Parameters. *J. Soc. Ind. Appl. Math.* **1963**, *11*, 431–441.
- (223) Kalman, R. E. A New Approach to Linear Filtering and Prediction Problems. *J. Basic Eng.* **1960**, *82*, 35–45.
- (224) Blank, T. B.; Brown, S. D. Adaptive, Global, Extended Kalman Filters for Training Feed-Forward Neural Networks. *J. Chemom.* **1994**, *8*, 391–407.
- (225) Puskorius, G. V.; Feldkamp, L. A. Multi-Stream Extended Kalman Filter Training for Static and Dynamic Neural Networks. *Systems, Man, and Cybernetics, 1997. Computational Cybernetics and Simulation., 1997 IEEE International Conference on* **1997**, *3*, 2006–2011.
- (226) Singraber, A.; Morawietz, T.; Behler, J.; Dellago, C. Parallel Multi-Stream Training of High-Dimensional Neural Network Potentials. *J. Chem. Theory Comput.* **2019**, *15*, 3075–3092.
- (227) Kingma, D. P.; Ba, J. L. ADAM: A Method for Stochastic Optimization. <https://arxiv.org/abs/1412.6980> 2018.
- (228) Srivastava, N.; Hinton, G.; Krizhevsky, A.; Sutskever, I.; Salakhutdinov, R. Dropout: A Simple Way to Prevent Neural Networks from Overfitting. *J. Mach. Learn. Res.* **2014**, *15*, 1929–1958.
- (229) Nguyen, D.; Widrow, B. Improving the Learning Speed of 2-Layer Neural Networks by Choosing Initial Values of the Adaptive Weights. *Int. Conf. Neur. Netw.* **1990**, *3*, 21–26.
- (230) Glorot, X.; Bengio, Y. Understanding the Difficulty of Training Deep Feedforward Neural Networks. *J. Mach. Learn. Res.* **2010**, *9*, 249–256.
- (231) Siddique, M. N. H.; Tokhi, M. O. Training Neural Networks: Backpropagation vs. Genetic Algorithms. *International Joint Conference on Neural Networks Proceedings* **2001**, *4*, 2673.
- (232) Fischer, T. M.; Petersen, W. P.; Lüthi, H. P. Artificial Neural Networks Applied to Prediction of Force Constants of Large Molecules. *J. Comput. Chem.* **1995**, *16*, 923–936.
- (233) Amari, A.; Fujita, N.; Shinomoto, S. Four Types of Learning Curves. *Neural Comput.* **1992**, *4*, 605–618.
- (234) Lu, D.; Qi, J.; Yang, M.; Behler, J.; Song, H.; Li, J. Mode Specific Dynamics in the $H_2 + SH \rightarrow H + H_2S$ Reaction. *Phys. Chem. Chem. Phys.* **2016**, *18*, 29113–29121.
- (235) Weinreich, J.; Römer, A.; Paleico, M. L.; Behler, J. Properties of α -Brass Nanoparticles. 1. Neural Network Potential Energy Surface. *J. Phys. Chem. C* **2020**, *124*, 12682–12695.
- (236) Paleico, M. L.; Behler, J. Global Optimization of Copper Clusters at the ZnO(1010) Surface Using a DFT-Based Neural Network Potential and Genetic Algorithms. *J. Chem. Phys.* **2020**, *153*, 054704.
- (237) Boes, J. R.; Kitchin, J. R. Modeling Segregation on AuPd(111) Surfaces with Density Functional Theory and Monte Carlo Simulations. *J. Phys. Chem. C* **2017**, *121*, 3479–3487.
- (238) Gabardi, S.; Caravati, S.; Sosso, G. C.; Behler, J.; Bernasconi, M. Microscopic Origin of Resistance Drift in the Amorphous State of the Phase-Change Compound GeTe. *Phys. Rev. B: Condens. Matter Mater. Phys.* **2015**, *92*, 054201.
- (239) Behler, J.; Martoňák, R.; Donadio, D.; Parrinello, M. Metadynamics Simulations of the High-Pressure Phases of Silicon Employing a High-Dimensional Neural Network Potential. *Phys. Rev. Lett.* **2008**, *100*, 185501.
- (240) Senn, H. M.; Thiel, W. QM/MM Methods for Biological Systems. *Top. Curr. Chem.* **2007**, *268*, 173–290.
- (241) Quaranta, V.; Behler, J.; Hellström, M. Structure and Dynamics of the Liquid-Water/Zinc-Oxide Interface from Machine Learning Potential Simulations. *J. Phys. Chem. C* **2019**, *123*, 1293–1304.
- (242) Behler, J.; Martoňák, R.; Donadio, D.; Parrinello, M. Pressure-Induced Phase Transitions in Silicon Studied by Neural Network-Based Metadynamics Simulations. *Phys. Status Solidi B* **2008**, *245*, 2618–2629.
- (243) Khalilullin, R. Z.; Eshet, H.; Kühne, T. D.; Behler, J.; Parrinello, M. Nucleation Mechanism for the Direct Graphite-to-Diamond Phase Transition. *Nat. Mater.* **2011**, *10*, 693–697.
- (244) Mangold, C.; Chen, S.; Barbalinardo, G.; Behler, J.; Pochet, P.; Termentzidis, K.; Han, Y.; Chaput, L.; Lacroix, D.; Donadio, D. Transferability of Neural Network Potentials for Varying Stoichiometry: Phonons and Thermal Conductivity of Mn_xGe_y Compounds. *J. Appl. Phys.* **2020**, *127*, 244901.
- (245) Wang, C.; Tharval, A.; Kitchin, J. R. A Density Functional Theory Parameterised Neural Network Model of Zirconia. *Mol. Simul.* **2018**, *44*, 623–630.
- (246) Artrith, N.; Urban, A. An Implementation of Artificial Neural-Network Potentials for Atomistic Materials Simulations: Performance for TiO_2 . *Comput. Mater. Sci.* **2016**, *114*, 135–150.
- (247) Sosso, G. C.; Miceli, G.; Caravati, S.; Behler, J.; Bernasconi, M. Neural Network Interatomic Potential for the Phase Change Material GeTe. *Phys. Rev. B: Condens. Matter Mater. Phys.* **2012**, *85*, 174103.
- (248) Sosso, G. C.; Donadio, D.; Caravati, S.; Behler, J.; Bernasconi, M. Thermal Transport in Phase-Change Materials from Atomistic Simulations. *Phys. Rev. B: Condens. Matter Mater. Phys.* **2012**, *86*, 104301.
- (249) Sosso, G. C.; Behler, J.; Bernasconi, M. Breakdown of Stokes-Einstein Relation in the Supercooled Liquid State of Phase Change Materials. *Phys. Status Solidi B* **2012**, *249*, 1880–1885.
- (250) Ibarra-Hernández, W.; Hajinazar, S.; Avendano-Franco, G.; Bautista-Hernandez, A.; Kolmogorov, A. N.; Romero, A. H. Structural Search for Stable Mg-Ca Alloys Accelerated with a Neural Network Interatomic Model. *Phys. Chem. Chem. Phys.* **2018**, *20*, 27545–27557.
- (251) Chen, H.-A.; Pao, C.-W. Fast and Accurate Artificial Neural Network Potential Model for $MAPbI_3$ Perovskite Materials. *ACS Omega* **2019**, *4*, 10950–10959.
- (252) Wang, Y.-X.; Chen, H.-A.; Pao, C.-W.; Chang, C.-C. Artificial Neural Network Model for Atomistic Simulations of Sb/MoS₂ van der Waals Heterostructures. *Multiscale Sci. Eng.* **2019**, *1*, 119–129.
- (253) Onat, B.; Cubuk, E. D.; Malone, B. D.; Kaxiras, E. Implanted Neural Network Potentials: Application to Li-Si Alloys. *Phys. Rev. B: Condens. Matter Mater. Phys.* **2018**, *97*, 094106.
- (254) Artrith, N.; Urban, A.; Ceder, G. Constructing First-Principles Phase Diagrams of Amorphous Li_xSi Using Machine-Learning-

- Assisted Sampling with an Evolutionary Algorithm. *J. Chem. Phys.* **2018**, *148*, 241711.
- (255) Liu, M.; Kitchin, J. R. SingleNN: A Modified Behler-Parrinello Neural Network with Shared Weights for Atomistic Simulations with Transferability. *J. Phys. Chem. C* **2020**, *124*, 17811–17818.
- (256) Boes, J. R.; Kitchin, J. R. Neural Network Predictions of Oxygen Interactions on a Dynamic Pd Surface. *Surf. Chem.* **2017**, *43*, 346–354.
- (257) Peterson, A. A. Acceleration of Saddle-Point Searches with Machine Learning. *J. Chem. Phys.* **2016**, *145*, 074106.
- (258) Groenenboom, M. C.; Moffat, T. P.; Schwarz, K. A. Halide-Induced Step Faceting and Dissolution Energetics from Atomistic Machine Learned Potentials on Cu(100). *J. Phys. Chem. C* **2020**, *124*, 12359–12369.
- (259) Kolsbjerg, E. L.; Peterson, A. A.; Hammer, B. Neural-Network-Enhanced Evolutionary Algorithm Applied to Supported Metal Nanoparticles. *Phys. Rev. B: Condens. Matter Mater. Phys.* **2018**, *97*, 195424.
- (260) Elias, J. S.; Artrith, N.; Bugnet, M.; Giordano, L.; Botton, G. A.; Kolpak, A. M.; Shao-Horn, Y. Elucidating the Nature of the Active Phase in Copper/Ceria Catalysts for CO Oxidation. *ACS Catal.* **2016**, *6*, 1675–1679.
- (261) Kolb, B.; Luo, X.; Zhou, X.; Jiang, B.; Guo, H. High-Dimensional Atomistic Neural Network Potentials for Molecule-Surface Interactions: HCl Scattering from Au(111). *J. Phys. Chem. Lett.* **2017**, *8*, 666–672.
- (262) Shakouri, K.; Behler, J.; Meyer, J.; Kroes, G.-J. Accurate Neural Network Description of Surface Phonons in Reactive Gas-Surface Dynamics: N₂+Ru(0001). *J. Phys. Chem. Lett.* **2017**, *8*, 2131–2136.
- (263) Spiering, P.; Shakouri, K.; Behler, J.; Kroes, G.-J.; Meyer, J. Orbital-Dependent Electronic Friction Significantly Effects the Description of Reactive Scattering of N₂ from Ru(0001). *J. Phys. Chem. Lett.* **2019**, *10*, 2957–2962.
- (264) Gastegger, M.; Marquetand, P. High-Dimensional Neural Network Potentials for Organic Reactions and an Improved Training Algorithm. *J. Chem. Theory Comput.* **2015**, *11*, 2187–2198.
- (265) Litman, Y.; Behler, J.; Rossi, M. Temperature Dependence of the Vibrational Spectrum of Porphycene: a Qualitative Failure of Classical-Nuclei Molecular dynamics. *Faraday Discuss.* **2020**, *221*, 526–546.
- (266) Artrith, N.; Kolpak, A. M. Grand Canonical Molecular Dynamics Simulations of Cu-Au Nanoalloys in Thermal Equilibrium Using Reactive ANN Potentials. *Comput. Mater. Sci.* **2015**, *110*, 20–28.
- (267) Thorn, A.; Rojas-Nunez, J.; Hajinazar, S.; Baltazar, S. E.; Kolmogorov, A. N. Toward ab Initio Ground States of Gold Clusters via Neural Network Modeling. *J. Phys. Chem. C* **2019**, *123*, 30088–30098.
- (268) Chiriki, S.; Jindal, S.; Bulusu, S. S. Neural Network Potentials for Dynamics and Thermodynamics of Gold Nanoparticles. *J. Chem. Phys.* **2017**, *146*, 084314.
- (269) Ouyang, R.; Xie, Y.; En Jiang, D. Global Minimization of Gold Clusters by Combining Neural Network Potentials and the Basin-Hopping Method. *Nanoscale* **2015**, *7*, 14817.
- (270) Morawietz, T.; Behler, J. A Density-Functional Theory-Based Neural Network Potential for Water Clusters Including van der Waals Corrections. *J. Phys. Chem. A* **2013**, *117*, 7356–3875.
- (271) Morawietz, T.; Singraber, A.; Dellago, C.; Behler, J. How van der Waals Interactions Determine the Unique Properties of Water. *Proc. Natl. Acad. Sci. U. S. A.* **2016**, *113*, 8368.
- (272) Cheng, B.; Behler, J.; Ceriotti, M. Nuclear Quantum Effects in Water at the Triple Point: Using Theory as a Link Between Experiments. *J. Phys. Chem. Lett.* **2016**, *7*, 2210–2215.
- (273) Hellström, M.; Behler, J. Structure of Aqueous NaOH Solutions: Insights from Neural-Network-Based Molecular Dynamics Simulations. *Phys. Chem. Chem. Phys.* **2017**, *19*, 82–96.
- (274) Hellström, M.; Behler, J. Proton-Transfer-Driven Water Exchange Mechanism in the Na⁺ Solvation Shell. *J. Phys. Chem. B* **2017**, *121*, 4184–4190.
- (275) Natarajan, S. K.; Behler, J. Neural Network Molecular Dynamics Simulations of Solid-Liquid Interfaces: Water at Low-Index Copper Surfaces. *Phys. Chem. Chem. Phys.* **2016**, *18*, 28704–28725.
- (276) Hellström, M.; Quaranta, V.; Behler, J. One-Dimensional vs. Two-Dimensional Proton Transport Processes at Solid-Liquid Zinc-Oxide-Water Interfaces. *Chem. Sci.* **2019**, *10*, 1232–1243.
- (277) Quaranta, V.; Hellström, M.; Behler, J.; Kullgren, J.; Mitev, P.; Hermansson, K. Maximally Resolved Anharmonic OH Vibrational Spectrum of the Water/ZnO(100) Interface from a High-Dimensional Neural Network Potential. *J. Chem. Phys.* **2018**, *148*, 241720.
- (278) Yoo, D.; Lee, K.; Jeong, W.; Lee, D.; Watanabe, S.; Han, S. Atomic Energy Mapping of Neural Network Potential. *Phys. Rev. Materials* **2019**, *3*, 093802.
- (279) Khalilu, R. Z.; Eshet, H.; Kühne, T. D.; Behler, J.; Parrinello, M. Graphite-Diamond Phase Coexistence Study Employing a Neural-Network Mapping of the ab initio Potential Energy Surface. *Phys. Rev. B: Condens. Matter Mater. Phys.* **2010**, *81*, 100103.
- (280) Eshet, H.; Khalilu, R. Z.; Kühne, T. D.; Behler, J.; Parrinello, M. Ab initio Quality Neural-Network Potential for Sodium. *Phys. Rev. B: Condens. Matter Mater. Phys.* **2010**, *81*, 184107.
- (281) Eshet, H.; Khalilu, R. Z.; Kühne, T. D.; Behler, J.; Parrinello, M. Microscopic Origins of the Anomalous Melting Behavior of Sodium under High Pressure. *Phys. Rev. Lett.* **2012**, *108*, 115701.
- (282) Boes, J. R.; Groenenboom, M. C.; Keith, J. A.; Kitchin, J. R. Neural Network and ReaxFF Comparison for Au Properties. *Int. J. Quantum Chem.* **2016**, *116*, 979–987.
- (283) Eckhoff, M.; Lausch, K. N.; Blöchl, P. E.; Behler, J. Predicting Oxidation and Spin States by High-Dimensional Neural Networks: Applications to Lithium Manganese Oxide Spinels. *arXiv:2007.00335v2*, 2020.
- (284) Sosso, G. C.; Miceli, G.; Caravati, S.; Giberti, F.; Behler, J.; Bernasconi, M. Fast Crystallization of the Phase Change Compound GeTe by Large-Scale Molecular Dynamics Simulations. *J. Phys. Chem. Lett.* **2013**, *4*, 4241–4246.
- (285) Hajinazar, S.; Shao, J.; Kolmogorov, A. N. Stratified construction of neural network-based interatomic models for multicomponent materials. *Phys. Rev. B: Condens. Matter Mater. Phys.* **2017**, *95*, 014114.
- (286) Marchand, D.; Jain, A.; Glensk, A.; Curtin, W. A. Machine learning for metallurgy I. A neural-network potential for Al-Cu. *Phys. Rev. Mater.* **2020**, *4*, 103601.
- (287) Lacivita, V.; Artrith, N.; Ceder, G. Structural and Compositional Factors That Control the Li-Ion Conductivity in LiPON Electrolytes. *Chem. Mater.* **2018**, *30*, 7077–7090.
- (288) Hafizi, R.; Ghasemi, S. A.; Hashemifar, S. J.; Akbarzadeh, H. A Neural-Network Potential Through Charge Equilibration for WS₂: From Clusters to Sheets. *J. Chem. Phys.* **2017**, *147*, 234306.
- (289) Morawietz, T.; Behler, J. A Full-Dimensional Neural Network Potential-Energy Surface for Water Clusters up to the Hexamer. *Z. Phys. Chem.* **2013**, *227*, 1559–1581.
- (290) Kondati Natarajan, S.; Morawietz, T.; Behler, J. Representing the Potential-Energy Surface of Protonated Water Clusters by High-Dimensional Neural Network Potentials. *Phys. Chem. Chem. Phys.* **2015**, *17*, 8356–8371.
- (291) Schran, C.; Marx, D. Quantum Nature of the Hydrogen Bond from Ambient Conditions Down to Ultra-Low Temperatures. *Phys. Chem. Chem. Phys.* **2019**, *21*, 24967–24975.
- (292) Schran, C.; Uhl, F.; Behler, J.; Marx, D. High-Dimensional Neural Network Potentials for Solvation: The Case of Protonated Water Clusters in Helium. *J. Chem. Phys.* **2018**, *148*, 102310.
- (293) Schran, C.; Brieuc, F.; Marx, D. Converged Colored Noise Path Integral Molecular Dynamics Study of the Zundel Cation Down to Ultralow Temperatures at Coupled Cluster Accuracy. *J. Chem. Theory Comput.* **2018**, *14*, 5068–5078.

- (294) Cooper, A. M.; Kästner, J.; Urban, A.; Artrith, N. Efficient training of ANN potentials by including atomic forces via Taylor expansion and application to water and a transition-metal oxide. *npg Comput. Mater.* **2020**, *6*, 54.
- (295) Singraber, A.; Morawietz, R.; Behler, J.; Dellago, C. Density Anomaly of Water at Negative Pressures from First Principles. *J. Phys.: Condens. Matter* **2018**, *30*, 254005.
- (296) Monserrat, B.; Brandenburg, J. G.; Engel, E. A.; Cheng, B. Liquid water contains the building blocks of diverse ice phases. *Nat. Commun.* **2020**, *11*, 5757.
- (297) Hellström, M.; Behler, J. Concentration-Dependent Proton Transfer Mechanisms in Aqueous NaOH Solutions: From Acceptor-Driven to Donor-Driven and Back. *J. Phys. Chem. Lett.* **2016**, *7*, 3302–3306.
- (298) Hellström, M.; Ceriotti, M.; Behler, J. Nuclear Quantum Effects in Sodium Hydroxide Solutions from Neural Network Molecular Dynamics Simulations. *J. Phys. Chem. B* **2018**, *122*, 10158–10171.
- (299) Shao, Y.; Hellström, M.; Mitev, P. D.; Knijff, L.; Zhang, C. PiNN: A Python Library for Building Atomic Neural Networks of Molecules and Materials. *J. Chem. Inf. Model.* **2020**, *60*, 1184–1193.
- (300) Kondati Natarajan, S.; Behler, J. Self-Diffusion of Surface Defects at Copper-Water Interfaces. *J. Phys. Chem. C* **2017**, *121*, 4368–4383.
- (301) Quaranta, V.; Hellström, M.; Behler, J. Proton Transfer Mechanisms at the Water-ZnO Interface: The Role of Presolvation. *J. Phys. Chem. Lett.* **2017**, *8*, 1476–1483.
- (302) Wille, S.; Jiang, H.; Bünermann, O.; Wodtke, A. M.; Behler, J.; Kandratsenka, A. An experimentally validated neural-network potential energy surface for H atoms on free-standing graphene in full dimensionality. *Phys. Chem. Chem. Phys.* **2020**, *22*, 26113–26120.
- (303) Boes, J. R.; Kitchin, J. R. Neural Network Predictions of Oxygen Interactions on a Dynamic Pd surface. *Modell. Simul.* **2017**, *43*, 346–354.
- (304) Ulissi, Z. W.; Tang, M. T.; Xiao, J.; Liu, X.; Torelli, D. A.; Karamad, M.; Cummins, K.; Hahn, C.; Lewis, N. S.; Jaramillo, T. F.; Chan, K.; Nørskov, J. K. Machine-Learning Methods Enable Exhaustive Searches for Active Bimetallic Facets and Reveal Active Site Motifs for CO₂ Reduction. *ACS Catal.* **2017**, *7*, 6600–6608.
- (305) Gao, T.; Kitchin, J. R. Modeling Palladium Surfaces with Density Functional Theory, Neural Networks and Molecular Dynamics. *Catal. Today* **2018**, *312*, 132–140.
- (306) Chiriki, S.; Bulusu, S. S. Modeling of DFT Quality Neural Network Potential for Sodium Clusters: Application to Melting of Sodium Clusters (Na₂₀ to Na₄₀). *Chem. Phys. Lett.* **2016**, *652*, 130–135.
- (307) Sun, G.; Sautet, P. Toward Fast and Reliable Potential Energy Surfaces for Metallic Pt Clusters by Hierarchical Delta Neural Networks. *J. Chem. Theory Comput.* **2019**, *15*, 5614–5627.
- (308) Hajinazar, S.; Sandoval, E. D.; Cullo, A. J.; Kolmogorov, A. N. Multitribe Evolutionary Search for Stable Cu-Pd-Ag Nanoparticles Using Neural Network Models. *Phys. Chem. Chem. Phys.* **2019**, *21*, 8729–8742.
- (309) Topolnicki, R.; Brieuc, F.; Schran, C.; Marx, D. Deciphering High-Order Structural Correlations within Fluxional Molecules from Classical and Quantum Configurational Entropy. *J. Chem. Theory Comput.* **2020**, *16*, 6785–6794.
- (310) Pártay, L. B.; Bartók, A. P.; Csányi, G. Efficient Sampling of Atomic Configurational Spaces. *J. Phys. Chem. B* **2010**, *114*, 10502.
- (311) Schaefer, B.; Goedecker, S. Computationally Efficient Characterization of Potential Energy Surfaces Based on Fingerprint Distances. *J. Chem. Phys.* **2016**, *145*, 034101.
- (312) McDonagh, D.; Skylaris, C.-K.; Day, G. M. Machine-Learned Fragment-Based Energies for Crystal Structure Prediction. *J. Chem. Theory Comput.* **2019**, *15*, 2743–2758.
- (313) Jinnouchi, R.; Karsai, F.; Verdi, C.; Asahi, R.; Kresse, G. Descriptors Representing Two- and Three-Body Atomic Distributions and Their Effects on the Accuracy of Machine-Learned Inter-Atomic Potentials. *J. Chem. Phys.* **2020**, *152*, 234102.
- (314) Tkatchenko, A.; DiStasio, R. A., Jr; Car, R.; Scheffler, M. Accurate and Efficient Method for Many-Body van der Waals Interactions. *Phys. Rev. Lett.* **2012**, *108*, 236402.
- (315) Ghasemi, S. A.; Amsler, M.; Hennig, R. G.; Roy, S.; Goedecker, S.; Lenosky, T. J.; Umrigar, C. J.; Genovese, L.; Morishita, T.; Nishio, K. Energy Landscape of Silicon Systems and its Description by Force Fields, Tight Binding Schemes, Density Functional Methods, and Quantum Monte Carlo Methods. *Phys. Rev. B: Condens. Matter Mater. Phys.* **2010**, *81*, 214107.
- (316) Chen, X.; Jørgensen, M. S.; Li, J.; Hammer, B. Atomic Energies from a Convolutional Neural Network. *J. Chem. Theory Comput.* **2018**, *14*, 3933–3942.
- (317) Bernstein, N.; Bhattacharai, B.; Csányi, G.; Drabold, D. A.; Elliott, S. R.; Deringer, V. L. Quantifying Chemical Structure and Atomic Energies in Amorphous Silicon Networks. *Angew. Chem.* **2019**, *131*, 7131–7135.
- (318) Zhang, Y.; Maurer, R. J.; Jiang, B. Symmetry-Adapted High Dimensional Neural Network Representation of Electronic Friction Tensor of Adsorbates on Metals. *J. Phys. Chem. C* **2020**, *124*, 186–195.
- (319) Csányi, G.; Willatt, M. J.; Ceriotti, M. In *Machine Learning Meets Quantum Physics*; Schütt, K. T., Chmiela, S., von Lilienfeld, O. A., Tkatchenko, A., Tsuda, K., Müller, K.-R., Eds.; Springer International Publishing: Cham, 2020; pp 99–127.
- (320) Lubbers, N.; Smith, J. S.; Barros, K. Hierarchical Modeling of Molecular Energies Using a Deep Neural Network. *J. Chem. Phys.* **2018**, *148*, 241715.
- (321) Snyder, J. C.; Rupp, M.; Hansen, K.; Müller, K.-R.; Burke, K. Finding Density Functionals with Machine Learning. *Phys. Rev. Lett.* **2012**, *108*, 253002.
- (322) Brockherde, F.; Vogt, L.; Li, L.; Tuckerman, M. E.; Burke, K.; Müller, K.-R. Bypassing the Kohn-Sham Equations with Machine Learning. *Nat. Commun.* **2017**, *8*, 872.
- (323) Behler, J. *RuNNer - A Program for Constructing High-Dimensional Neural Network Potentials*; Universität Göttingen, 2021.
- (324) Khorshidi, A.; Peterson, A. A. Amp: A Modular Approach to Machine Learning in Atomistic Simulations. *Comput. Phys. Commun.* **2016**, *207*, 310–324.
- (325) Lee, K.; Yoo, D.; Jeong, W.; Han, S. SIMPLE-NN: An Efficient Package for Training and Executing Neural-Network Interatomic Potentials. *Comput. Phys. Commun.* **2019**, *242*, 95–103.
- (326) Huang, S.-D.; Shang, C.; Kang, P.-L.; Zhang, X.-J.; Liu, Z.-P. LASP: Fast Global Potential Energy Surface Exploration. *Wiley Interdiscip. Rev.: Comput. Mol. Sci.* **2019**, *9*, No. e1415.
- (327) Lot, R.; Pellegrini, F.; Shaidu, Y.; Kucukbenli, E. PANNA: Properties from Artificial Neural Network Architectures. *arXiv:1907.03055v1* 2020.
- (328) Kolb, B.; Lentz, L. C.; Kolpak, A. M. Discovering Charge Density Functionals and Structure-Property Relationships with PROPhet: A General Framework for Coupling Machine Learning and First-Principles Methods. *Sci. Rep.* **2017**, *7*, 1192.
- (329) Abadi, M. et al. *TensorFlow: Large-Scale Machine Learning on Heterogeneous Systems*; Tensorflow.org, 2015. <https://www.tensorflow.org/>.